NASA/TP-1998-206543

Robust Flutter Margin Analysis That Incorporates Flight Data

Rick Lind
National Research Council
NASA Dryden Research Associate
Dryden Flight Research Center
Edwards, California

Martin J. Brenner
Dryden Flight Research Center
Edwards, California

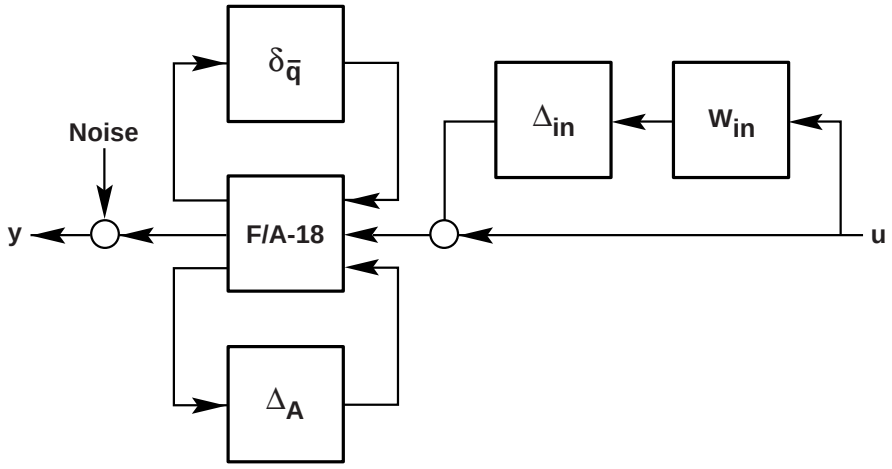

March 1998

The NASA STI Program Office . . . in Profile

Since its founding, NASA has been dedicated to the advancement of aeronautics and space science. The NASA Scientific and Technical Information (STI) Program Office plays a key part in helping NASA maintain this important role.

The NASA STI Program Office is operated by Langley Research Center, the lead center for NASA's scientific and technical information. The NASA STI Program Office provides access to the NASA STI Database, the largest collection of aeronautical and space science STI in the world. The Program Office is also NASA's institutional mechanism for disseminating the results of its research and development activities. These results are published by NASA in the NASA STI Report Series, which includes the following report types:

- TECHNICAL PUBLICATION. Reports of completed research or a major significant phase of research that present the results of NASA programs and include extensive data or theoretical analysis. Includes compilations of significant scientific and technical data and information deemed to be of continuing reference value. NASA's counterpart of peer-reviewed formal professional papers but has less stringent limitations on manuscript length and extent of graphic presentations.

- TECHNICAL MEMORANDUM. Scientific and technical findings that are preliminary or of specialized interest, e.g., quick release reports, working papers, and bibliographies that contain minimal annotation. Does not contain extensive analysis.

- CONTRACTOR REPORT. Scientific and technical findings by NASA-sponsored contractors and grantees.

- CONFERENCE PUBLICATION. Collected papers from scientific and technical conferences, symposia, seminars, or other meetings sponsored or cosponsored by NASA.

- SPECIAL PUBLICATION. Scientific, technical, or historical information from NASA programs, projects, and mission, often concerned with subjects having substantial public interest.

- TECHNICAL TRANSLATION. English-language translations of foreign scientific and technical material pertinent to NASA's mission.

Specialized services that complement the STI Program Office's diverse offerings include creating custom thesauri, building customized databases, organizing and publishing research results . . . even providing videos.

For more information about the NASA STI Program Office, see the following:

- Access the NASA STI Program Home Page at ***http://www.sti.nasa.gov***

- E-mail your question via the Internet to help@sti.nasa.gov

- Fax your question to the NASA Access Help Desk at (301) 621-0134

- Telephone the NASA Access Help Desk at (301) 621-0390

- Write to:
  NASA Access Help Desk
  NASA Center for AeroSpace Information
  800 Elkridge Landing Road
  Linthicum Heights, MD 21090-2934

NASA/TP-1998-206543

Robust Flutter Margin Analysis That Incorporates Flight Data

Rick Lind
National Research Council
NASA Dryden Research Associate
Dryden Flight Research Center
Edwards, California

Martin J. Brenner
Dryden Flight Research Center
Edwards, California

National Aeronautics and
Space Administration

Dryden Flight Research Center
Edwards, California 93523-0273

March 1998

ACKNOWLEDGMENTS

This work was performed while Rick Lind held a National Research Council–NASA Dryden Flight Research Center Postdoctoral Research Associateship.

The authors would like to thank the NASA Dryden employees and associates who voluntarily served on a technical review committee to evaluate and improve this paper. This committee was chaired by Larry Freudinger and staffed by Mark Stephenson and John Carter of the NASA Dryden Controls and Dynamics Branch and visiting professor Rick Howard from the U.S. Navy Postgraduate School. This committee provided an exhaustive review and indicated several improvements that greatly increased the value of this paper. All remaining errors and poor explanations are a direct indication of the authors' inability to sufficiently address the many comments and suggestions.

The authors would also like to thank the NASA Dryden Structural Dynamics group. Leonard Voelker was instrumental in developing the μ method by continuously providing comments and suggestions relating to the physics of flutter and how to interpret μ in terms of this phenomenon. Larry Freudinger helped develop the concepts of uncertainty in aeroelastic models and the introduction of additional uncertainty from signal processing. Dave Voracek was the Chief Engineer for the F/A-18 Systems Research Aircraft (SRA) project during the μ-method development and helped provide the large database of flight data and key information regarding the F/A-18 SRA flight systems and characteristics. Roger Truax and Tim Doyle generated the finite-element model of the F/A-18 SRA and computed theoretical aerodynamic-force matrices for this model. Mike Kehoe oversaw the research program, ensured time and resources were always available, and suggested research avenues to address practical concerns of the aeroelasticity community.

CONTENTS

TABLES

FIGURES

ABSTRACT

An approach for computing worst-case flutter margins has been formulated in a robust stability framework. Uncertainty operators are included with a linear model to describe modeling errors and flight variations. The structured singular value, μ, computes a stability margin that directly accounts for these uncertainties. This approach introduces a new method of computing flutter margins and an associated new parameter for describing these margins. The μ margins are robust margins that indicate worst-case stability estimates with respect to the defined uncertainty. Worst-case flutter margins are computed for the F/A-18 Systems Research Aircraft using uncertainty sets generated by flight data analysis. The robust margins demonstrate flight conditions for flutter may lie closer to the flight envelope than previously estimated by p-k analysis.

NOMENCLATURE

a	arbitrary variable to represent actuator dynamics in figure 2.2
A	state matrix
A_i	i^{th} term in Padé or Roger form of unsteady aerodynamic force matrix
A_P	state matrix of transfer-function operator matrix
A_Q	state matrix of unsteady aerodynamic force matrix
B_P	input matrix of transfer-function operator matrix
B_Q	input matrix of unsteady aerodynamic force matrix
$\bar{c}$	mean aerodynamic chord
c_i	dimension of i^{th} full block of complex uncertainty
C	damping matrix
C_i	dimension of i^{th} scalar block of complex uncertainty
$\mathbf{C}^{n \times m}$	space of complex valued matrices of dimension n by m
C_P	output matrix of transfer-function operator matrix
C_Q	output matrix of unsteady aerodynamic force matrix
D	scaling matrix
D_P	feedthrough matrix of transfer-function operator matrix
D_Q	feedthrough matrix of unsteady aerodynamic force matrix
$\mathcal{D}$	set of scaling matrices
$\bar{\mathcal{D}}$	set of time-invariant and time-varying scaling matrices
e_i	imaginary part of eigenvalue
$\bar{e}_i$	uncertain imaginary part of eigenvalue

e_r	real part of eigenvalue
$\bar{e}_r$	uncertain real part of eigenvalue
$F_l(\cdot,\cdot)$	lower-loop linear fractional transformation in definition 3.1.2
$F_u(\cdot,\cdot)$	upper-loop linear fractional transformation in definition 3.1.1
g	arbitrary operator
G	scaling matrix
$\mathcal{G}$	set of scaling matrices
$\bar{\mathcal{G}}$	set of time-invariant and time-varying scaling matrices
$\mathcal{H}_2$	Hardy space in definition 2.1.8
$\mathcal{H}_\infty$	stable, rational transfer functions in definition 2.2.3
i	a real scalar
in	input
I	identity matrix
I_n	identity matrix of dimension n
j	a real scalar
j	imaginary unit of $\sqrt{-1}$
k	arbitrary variable to represent a feedback controller in figure 2.2
k	reduced frequency
K	stiffness matrix
KEAS	equivalent airspeed, knot
LFT	linear fractional transformation
LMI	linear matrix inequality
LTI	linear time-invariant
LTV	linear time-varying
$\mathcal{L}_\infty$	Lebesgue space of transfer functions in definition 2.2.2
$\mathcal{L}_2$	frequency-domain Lebesgue space in definition 2.1.7
$\mathcal{L}_2(-\infty,\infty)$	time-domain infinite-horizon Lebesgue space in definition 2.1.3
$\mathcal{L}_2[0,\infty)$	time-domain Lebesgue space in definition 2.1.4
m	an integer
M	mass matrix
n	an integer

n_f	number of flight conditions
n_i	number of inputs
n_o	number of outputs
nom	nominal
n_Q	number of states in unsteady aerodynamic force matrix
n_s	number of states
n_w	number of feedback signals from uncertainty to plant
n_z	number of feedback signals from plant to uncertainty
$\mathcal{N}$	nonlinear system
o	a real scalar
p	an integer
p	arbitrary variable to represent plant dynamics in figure 2.2
p-k	method of computing nominal flutter margins
P	transfer-function operator
$\bar{P}$	scaled transfer-function operator
P_{ij}	transfer-function element of P from j^{th} vector input to i^{th} vector output
$\mathcal{P}$	set of system operators
$\bar{q}$	dynamic pressure, lbf
$\bar{q}_{flutter}$	flutter pressure expressing dynamic pressure at which flutter occurs, lbf
$\bar{q}_{nom}$	nominal flutter pressure computed with μ method, lbf
$\bar{q}_o$	nominal value of dynamic pressure, lbf
$\bar{q}_{p\text{-}k}$	nominal flutter pressure computed with p-k method, lbf
$\bar{q}_{rob}$	robust flutter pressure computed with μ method, lbf
Q	unsteady aerodynamic force matrix
Q_{ss}	high-order components of unsteady aerodynamic force matrix
$\mathbf{R}$	space of real scalars
Re	real part
R_i	dimension of i^{th} scalar block of real uncertainty
$\mathbf{R}^n$	space of real vectors of dimension n
$\mathbf{R}^{n \times m}$	space of real-valued matrices of dimension n by m

rob	robust
$\mathcal{RH}_\infty$	stable, rational transfer functions in definition 2.2.4
s	Laplace transform variable
S	state-space system operator
SRA	Systems Research Aircraft
$\mathcal{S}$	space of signals in definition 2.1.1
$\mathcal{S}_{in}$	space of input signals
$\mathcal{S}_{j\omega}$	set of frequency-domain signals in definition 2.1.5
$\mathcal{S}_{out}$	space of output signals
t	time
TI	time-invariant
TV	time-varying
u	input signal
V	velocity
w	feedback signal from uncertainty to plant
w_i	weighting on imaginary part of eigenvalue
w_{lag}	weighting on a lag
w_r	weighting on real part of eigenvalue
W	matrix scaling uncertainty operators
$W_{\bar{q}}$	matrix scaling feedback perturbation to dynamic pressure
x	state vector
$\dot{x}$	derivative of x with respect to time
y	output signal
z	feedback signal from plant to uncertainty
α	real scalar
β	pole in Padé approximation to a lag
Γ	flutter margin expressed as a difference in dynamic pressure, lbf
Γ_{nom}	nominal flutter margin computed with μ method
$\Gamma_{p\text{-}k}$	nominal flutter margin computed with p-k method
Γ_{rob}	robust flutter margin computed with μ method
δ	uncertainty scalar

$\delta_{flutter}$	flutter margin expressed as a difference in dynamic pressure
δ_{lower}	lower bound for real perturbation
$\delta_{\bar{q}}$	uncertainty perturbation on dynamic pressure
δ_{upper}	upper bound for real perturbation
Δ	uncertainty matrix
$\bar{\Delta}$	structured operator containing uncertainty and perturbation to flight condition
$\mathbf{\Delta}$	a set of uncertainty matrix operators
$\bar{\mathbf{\Delta}}$	set of $\bar{\Delta}$
ε	real scalar
ζ	damping
η	state vector
$\dot{\eta}$	derivative of η with respect to time
$\ddot{\eta}$	derivative of $\dot{\eta}$ with respect to time
$\bar{\lambda}$	maximum eigenvalue
μ	structured singular value
Π	flutter margin expressed as percentage of knots of equivalent airspeed
Π_{nom}	nominal flutter margin computed with μ method
$\Pi_{\text{p-k}}$	nominal flutter margin computed with p-k method
Π_{rob}	robust flutter margin computed with μ method
ρ	spectral radius
σ	singular value
$\bar{\sigma}$	maximum singular value
ω	frequency, rad/sec
ω_{nom}	frequency of unstable mode associated with $\bar{q}_{nom}$
$\omega_{\text{p-k}}$	frequency of unstable mode associated with $\bar{q}_{\text{p-k}}$
ω_{rob}	frequency of unstable mode associated with $\bar{q}_{rob}$
Ω	set of frequency points
$\|f(j\omega)\|_2$	2-norm of frequency-domain signal in definition 2.1.6
$\|P\|_\infty$	$\mathcal{H}_\infty$–norm induced by $\mathcal{L}_2$ signals in definition 2.2.1
$\|x(t)\|_2$	2-norm of time-domain signal in definition 2.1.2

CHAPTER 1
INTRODUCTION

Aeroelastic flutter is a potentially destructive instability resulting from an interaction between aerodynamic, inertial, and structural forces.[1] The stability properties of the aeroelastic dynamics must be investigated to determine a flight envelope that is clear of flutter instabilities for new aircraft designs or new configurations of current aircraft. Analytical predictions of the onset of flutter must be accurate to reduce dangers and costs associated with experimental estimation.[2]

Critical flutter conditions are the points closest to the flight envelope at which flutter instabilities occur. This concept of closeness is formally defined here as a flutter pressure that considers the critical dynamic pressure for a constant Mach value. Obviously, different flutter measures such as a flutter speed can be defined because a unique equivalent airspeed is associated with each dynamic pressure for a given Mach number; however, this paper uses definition 1.0.1 for a flutter pressure to describe the critical flutter flight conditions.

Definition 1.0.1: *A flutter pressure is the smallest value of dynamic pressure for which an aircraft at a particular Mach number experiences a flutter instability.*

The flutter pressure is used to compute a stability margin, or flutter margin, that indicates the distance between the flutter pressure and a reference point. A common flutter margin, Γ, considers the difference in dynamic pressure between the flutter pressure and a point on the edge of the flight envelope. Another common flutter margin, Π, considers the percentage difference between equivalent airspeeds at the flutter condition and a point within the flight envelope.

Definition 1.0.2: *A flutter margin relates a measure of distance between the flight condition associated with the flutter pressure and a reference point.*

The traditional p-k method has been extensively used to compute flutter margins for a variety of military and commercial aircraft.[3] This iterative method uses an analytical dynamic model coupled with harmonic motion solutions for the unsteady aerodynamic forces. The p-k method predicts flutter margins entirely from a theoretical model that may not accurately describe the true dynamics of the airplane. The resulting flutter margins do not account for possible variations between the model and the aircraft.

The community studying aeroelasticity has identified the development of improved methods for characterizing flutter margins as a vital research area.[4] Flight testing for envelope expansion incurs dramatic time and cost because stability margins are not computed with a high level of confidence using traditional methods.[2] The flutter dynamics often exhibit an explosive behavior that results in a sudden change in stability for a small change in flight conditions. Thus, small errors in predicted margins could have grave consequences for aircraft and crews operating near the flutter conditions.

Several approaches exist for characterizing accurate flutter margins using flight data generated by the aircraft. These data describe the true dynamics and can be used to generate realistic models and compute confident flutter margins. Parameter estimation algorithms have been developed to directly identify an aeroelastic model from the flight data.[5, 6] The accuracy of the resulting model can deteriorate as the complexity and number of degrees of freedom of the system increase and signal-to-noise ratios decrease from optimal wind-tunnel conditions to realistic flight levels. Modal filtering has been introduced in association with parameter estimation algorithms to simplify analysis by decoupling the system into a set of

first-order responses.[7, 8] This type of filtering does not guarantee robustness and may not perform well for systems with many closely-spaced modal natural frequencies that cross and shift as flight conditions change.

Other approaches toward computing confident flutter margins evaluate the robustness of a stability margin with respect to changes in the model as an indication of the confidence in that margin. A flutter margin robust to perturbations to the model is a confident margin because model inaccuracies do not affect that margin. An algorithm has been developed to compute the most critical flutter margin with respect to first-order perturbations in a model.[9] This method considers only parametric perturbations and can be computationally expensive. A robust control framework has been adopted using a feedback structure to relate the structural model and the aerodynamic model.[10] This approach uses highly conservative robustness conditions with respect to an uncertainty structure that may not be physically meaningful. A similar approach is adopted allowing unmodeled dynamics and high-order parametric perturbations based on series expansion.[11] Statistical approaches are also considered to formulate a flutter probability measure.[12, 13] These approaches will converge to a robustness indicator using Monte Carlo simulations, but the computation time can be prohibitive for complex systems. The robustness measures for these perturbation and statistical approaches are suspect because no global guarantees can be made as to perturbations not explicitly considered by the minimization algorithms or the Monte Carlo simulations.

An approach to computing flutter margins that guarantees a level of robustness and directly accounts for flight data is presented herein.[14] An aeroelastic model is formulated in a formal robust stability framework that uses a set of norm-bounded operators, $\mathbf{\Delta}$, to describe modeling errors and uncertainty. A multivariable robust stability measure known as the structured singular value, μ, computes flutter pressures that are robust to the amount of modeling errors as determined by $\mathbf{\Delta}$.[15] A robust flutter margin problem is posed by questioning what is the largest increase in dynamic pressure for which the plant is stable despite possible modeling errors described by $\mathbf{\Delta}$.

Flight data are easily incorporated into the μ analysis procedure. The modeling errors are determined by comparing transfer functions obtained by flight data with transfer functions predicted by the analytical model. The norm bound on $\mathbf{\Delta}$ is chosen based on these observed errors. A model validation condition is used to ensure the $\mathbf{\Delta}$ is sufficient to account for multiple data sets without being excessively conservative. With respect to $\mathbf{\Delta}$, a worst-case flutter boundary is computed that directly accounts for flight data.

This method is inherently different from traditional algorithms based on p-k methods or parameter identification and robustness approaches. The μ method uses information from both an analytical model and flight data; traditional approaches use only one of these sources (fig. 1.1). Methods that use only an analytical model can be inaccurate, and methods that use only the flight data can fail if the data are of poor quality. The μ method uses the flight data to improve the analytical model by adding uncertainty operators. Poor quality flight data will merely increase the difficulty of obtaining a reasonable uncertainty description resulting in a small $\mathbf{\Delta}$. The robust margins will be similar to the nominal margins in this case, which makes intuitive sense because any information obtained from the data should only enhance the plant model and improve the accuracy of the flutter margin.

The concept of computing robustness in flutter margins has been recognized for its importance and has recently been termed a state-of-the art research area in aeroelasticity.[16] Informal measures of robustness are not necessarily useful because the informal measures provide no guarantee for the system stability. The μ method is based on operator theory and provides a well-defined concept of robustness that has a clear set of guarantees as to the stability properties of the system.

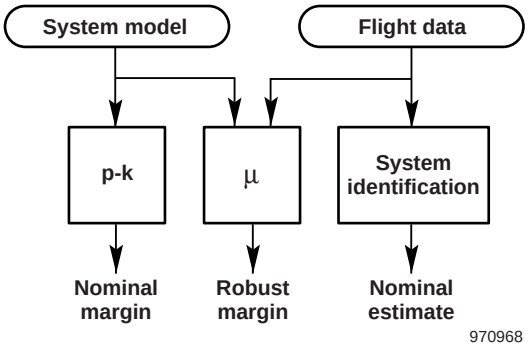

Figure 1.1. Information flowchart for traditional and μ methods to compute flutter margins.

The μ method also allows consideration of a rich set of modeling errors with direct physical interpretations. Traditional techniques compute robustness with respect to a theoretical estimate of modeling errors that can be too conservative or overly optimistic. The μ method is able to use flight data to determine these errors by employing model validation algorithms that are developed specifically for comparing data with uncertain models in the μ framework. Thus, the resulting stability margins directly account for the flight data when determining robust flutter pressures.

Robust, or worst-case, flutter margins are computed for the F/A-18 Systems Research Aircraft (SRA) using the μ method. The flutter results presented represent an improvement to previous flutter results for the F/A-18 SRA computed using the traditional p-k method. Nominal flutter margins computed using the μ method but ignoring all uncertainty operators are shown to closely match the p-k method flutter margins. These results lend validity to the μ method as an accurate indicator of flutter instability. Robust flutter margins are computed with the μ method by directly accounting for modeling uncertainty to represent conservative worst-case stability margins. The computation of the μ method takes only a few minutes on a standard workstation.

CHAPTER 2
ROBUST STABILITY

2.1 Signals

A common definition of a signal is a Lebesgue measurable function that maps the space of real numbers $\mathbf{R}$ into $\mathbf{R}^n$. A space of such signals is denoted $\mathcal{S}$.

Definition 2.1.1: *The space of signals that are Lebesgue measurable functions is* $\mathcal{S}$.

$$\mathcal{S} = \{ f : \mathbf{R} \to \mathbf{R}^n \} \tag{1}$$

Analog measurements x(t) of physical systems are real vector functions of the real parameter t describing time and thus are valid members of the space of signals, $x(t) \in \mathcal{S}$. Values of the time parameter, which are often arbitrarily numbered as a distance from some reference point, actually extend to positive and negative infinity. Stability for physical systems must ensure stability for all values of time. A time-domain 2-norm is defined as a measure of size (or energy) for time-domain signals that considers all time.

Definition 2.1.2: *The 2-norm measures the energy of a signal* $x(t) \in \mathcal{S}$.

$$\|x(t)\|_2 = \left(\int_{-\infty}^{\infty} |x(t)|^2 dt \right)^{\frac{1}{2}} \tag{2}$$

One characteristic of a stable system is only finite-energy output signals are generated in response to finite-energy input signals. Signals with finite energy are known as “square integrable” because the integral of the square of the signal is finite. The Lebesgue space of square integrable signals is defined as $\mathcal{L}_2(-\infty,\infty)$. This space is also referred to as the infinite-horizon Lebesgue 2-space to denote that the norm uses an integral over infinite time.

Definition 2.1.3: *The space* $\mathcal{L}_2(-\infty,\infty)$ *consists of square integrable time-domain signals.*

$$\mathcal{L}_2(-\infty,\infty) = \{ x(t) : x \in \mathcal{S}, \|x(t)\|_2 < \infty \} \tag{3}$$

Signals associated with physical systems are only known for values of time greater than the time at which measurements are started. Stability analysis and norm computations using these signals cannot use properties of the signal before the starting time because no information is known. The traditional method of characterizing these signals is to assume the signal is identically zero for all times before the starting time. The time value at which measurements are started can be chosen without loss of generality and is usually chosen to be t = 0. The space $\mathcal{L}_2[0,\infty)$ is defined as a subset of $\mathcal{L}_2(-\infty,\infty)$ to emphasize such signals.

Definition 2.1.4: *The space* $\mathcal{L}_2[0,\infty) \subset \mathcal{L}_2(-\infty,\infty)$ *consists of square integrable time-domain signals that are identically zero for all* $t < 0$.

$$\mathcal{L}_2[0,\infty) = \left\{ x(t) : \int_0^{\infty} \|x(t)\|^2 dt < \infty, \; x(t) = 0 \; \textit{for all } t < 0 \right\} \tag{4}$$

A similar space $\mathcal{L}_2(-\infty,0] \subset \mathcal{L}_2(-\infty,\infty)$ is defined for signals x(t) that are assumed to begin at $t = -\infty$ and are identically zero for all times t = 0. The integral to compute the energy for elements of this space considers $t = -\infty$ until t > 0.

Frequency-domain signals are often considered in stability analysis but do not fall into the set of signals, $\mathcal{S}$. These signals $f(j\omega)$ are complex-valued functions of the imaginary unit $j = \sqrt{-1}$, and the real frequency variable ω is expressed in rad/sec. The set, $\mathcal{S}_{j\omega}$, is defined for frequency-domain signals.

Definition 2.1.5: *The space of frequency-domain signals is* $\mathcal{S}_{j\omega}$.

$$\mathcal{S}_{j\omega} = \{ f(j\omega) : j\mathbf{R} \to \mathbf{C}^n \text{ and } f^*(j\omega) = f'(-j\omega) \} \tag{5}$$

A frequency-domain 2-norm is formulated to compute a measure of energy.

Definition 2.1.6: *The 2-norm measures the energy of the signal* $f(j\omega) \in \mathcal{S}_{j\omega}$.

$$\| f \|_2 = \left(\frac{1}{2\pi} \int_{-\infty}^{\infty} f^*(j\omega) f(j\omega) d\omega \right)^{\frac{1}{2}} \tag{6}$$

A frequency-domain Lebesgue space, $\mathcal{L}_2$, is defined for finite-energy signals.

Definition 2.1.7: *The space* $\mathcal{L}_2$ *consists of frequency-domain signals with finite energy.*

$$\mathcal{L}_2 = \{ f(j\omega) : f \in \mathcal{S}_{j\omega}, \| f \|_2 < \infty \} \tag{7}$$

The spaces $\mathcal{L}_2(-\infty,\infty)$ and $\mathcal{L}_2$ are isomorphic Hilbert spaces under the appropriate inner products through the Fourier transform, which means the spaces have equivalent algebraic properties. This relationship is used to simplify notation by rarely distinguishing between time-domain and frequency-domain signals except where the context does not make it clear. The notations for the 2-norm of time domain and frequency domain are also not distinguished because the notations are equivalent, as demonstrated by Parseval's identity.[17]

An important subspace of $\mathcal{L}_2$ is the Hardy space, $\mathcal{H}_2$. This space contains the complex variable functions that are analytic in the open right-half of the complex plane and have finite 2-norm.

Definition 2.1.8: *The Hardy space,* $\mathcal{H}_2 \subset \mathcal{L}_2$*, consists of the following functions.*

$$\mathcal{H}_2 = \{ f(s) : f(s) \in \mathcal{L}_2 \text{ and } f(s) \text{ is analytic in } \mathrm{Re}(s) > 0 \} \tag{8}$$

The space $\mathcal{L}_2[0,\infty)$ is isomorphic to $\mathcal{H}_2$ through the Laplace transform. Members of this set can be interpreted as frequency-domain representations of finite-energy time-domain signals that are assumed to be zero at t < 0.

2.2 Systems

A system P is defined as an operator mapping the space of input signals $\mathcal{S}_{in}$ to the space of output signals $\mathcal{S}_{out}$. This definition implies that for any $w \in \mathcal{S}_{in}$ and z = Pw, then $z \in \mathcal{S}_{out}$.

$$P : \mathcal{S}_{in} \rightarrow \mathcal{S}_{out} \tag{9}$$

This paper will consider linear, time-invariant systems defined by state-space equations.

$$\begin{bmatrix} \dot{x}(t) \\ y(t) \end{bmatrix} = \begin{bmatrix} A_P & B_P \\ C_P & D_P \end{bmatrix} \begin{bmatrix} x(t) \\ u(t) \end{bmatrix} \tag{10}$$

The signal $x(t) \in \mathbf{R}^{n_s}$ is the state vector, $u(t) \in \mathbf{R}^{n_i}$ is the input vector, and $y(t) \in \mathbf{R}^{n_o}$ is the output vector. The state update matrix is $A_P \in \mathbf{R}^{n_s \times n_s}$; $B_P \in \mathbf{R}^{n_s \times n_i}$ determines how the input affects the states; $C_P \in \mathbf{R}^{n_o \times n_s}$ computes the outputs as a linear combination of states; and $D_P \in \mathbf{R}^{n_o \times n_i}$ is the direct feedthrough from inputs to outputs. The operator $S = \{A_P, B_P, C_P, D_P\}$ denotes the time-domain state system.

Linear time-invariant state-space systems are commonly represented by transfer-function operators. These functions, P(s), are complex-valued matrices of the complex Laplace transform variable, s. Such a transfer-function matrix exists if and only if the state-space system is linear and time-invariant.

$$P(s) = D_P + C_P(sI_{n_s} - A_P)^{-1}B_P \tag{11}$$

Stability must be considered over the infinite-horizon time lengths so that the operators used map $\mathcal{L}_2(-\infty,\infty)$ into $\mathcal{L}_2(-\infty,\infty)$. Properties of the Fourier transform relating $\mathcal{L}_2(-\infty,\infty)$ and $\mathcal{L}_2$ imply a state-space system, $S : \mathcal{L}_2(-\infty,\infty) \rightarrow \mathcal{L}_2(-\infty,\infty)$, is linear and time-invariant if and only if the associated transfer-function matrix P is such that $y = Pu \in \mathcal{L}_2$ for any $u \in \mathcal{L}_2$. This condition leads to consideration of the gain for these signals.

$$\frac{\|y\|_2}{\|u\|_2} = \frac{\|Pu\|_2}{\|u\|_2} \tag{12}$$

This ratio of 2-norms will be finite if the system is stable. Properties of the 2-norm are used to derive a condition on the system transfer-function operator, P. This condition is referred to as an induced norm because it results from consideration of signal norms associated with the operator. The $\mathcal{L}_2$ induced norm is defined as the $\mathcal{H}_\infty$–norm.

Definition 2.2.1: *Define the $\mathcal{H}_\infty$–norm for transfer-function operators.*

$$\|P\|_\infty = \sup_\omega \bar{\sigma}(P(j\omega)) \tag{13}$$

A space of operators with finite $\mathcal{H}_\infty$–norm is denoted as $\mathcal{L}_\infty$.

Definition 2.2.2: *The space $\mathcal{L}_\infty$ consists of systems with finite $\mathcal{H}_\infty$–norm.*

$$\mathcal{L}_\infty = \{P : \|P\|_\infty < \infty\} \tag{14}$$

Transfer functions of linear time-invariant systems are stable if and only if $z = Pw$ and $w \in \mathcal{H}_2$ implies $z \in \mathcal{H}_2$. This implication results from the Laplace isomorphism between $\mathcal{L}_2[0,\infty)$ and $\mathcal{H}_2$ space. These

transfer functions are shown to be analytic in the open right-half complex plane with finite $\mathcal{H}_\infty$–norm. Define the space $\mathcal{H}_\infty$ to contain these operators.

Definition 2.2.3: *The space $\mathcal{H}_\infty$ consists of transfer functions of stable, linear, time-invariant systems with finite $\mathcal{H}_\infty$–norm.*

$$\mathcal{H}_\infty = \{P : P \text{ is analytic in } \mathrm{Re}(s) > 0 \text{ and } \|P\|_\infty < \infty\} \tag{15}$$

A subspace $\mathcal{RH}_\infty$ is often defined for rational elements.

Definition 2.2.4: *The space, $\mathcal{RH}_\infty \subset \mathcal{H}_\infty$, consists of rational elements of $\mathcal{H}_\infty$.*

$$\mathcal{RH}_\infty = \{P : P \in \mathcal{H}_\infty \text{ and } P \text{ is rational}\} \tag{16}$$

Transfer-function operators of linear, time-invariant state-space systems are rational functions of the Laplace transform variable, s. These transfer functions $P \in \mathcal{RH}_\infty$ if and only if P is stable such that no poles lie in the closed right-half plane. The space $\mathcal{RH}_\infty$, which may appear to be a mathematical abstraction, is thus shown to have a physical interpretation. $\mathcal{RH}_\infty$ is merely the operator theory representation of stable, rational, transfer functions.

2.3 Small Gain Theorem

Stability of a linear time-invariant system is determined by location of all poles in the left-half plane. Robust stability in the $\mathcal{H}_\infty$ and μ frameworks is determined by considering an interconnection of stable operators. The basis for determining stability of these interconnections of operators is the "small gain theorem."

The small gain theorem states that a closed-loop feedback system of stable operators is internally stable if the loop gain of those operators is stable and bounded by unity. Several formulations of the small gain theorem are derived for various signals and systems. Theorem 2.3.1 presents the formulation used for this paper.[17]

Theorem 2.3.1 (Small Gain Theorem): *Given the feedback interconnection structure of figure 2.1 for stable transfer-function operators* $P, \Delta : \mathcal{L}_2 \to \mathcal{L}_2$ *with* $P, \Delta \in \mathcal{RH}_\infty$*; if the $\mathcal{H}_\infty$–norm of the loop gain is bounded by unity such that* $\|P\Delta\|_\infty < 1$*, then:*

1. *the closed-loop system is well-posed and internally stable.*
2. *a unique y, $w \in \mathcal{L}_2$ is associated with each $u \in \mathcal{L}_2$.*

This small gain theorem is overly restrictive in the sense of requiring $P, \Delta \in \mathcal{RH}_\infty$. A more general small gain theorem is formulated for operators not restricted to lie in the subspace $\mathcal{RH}_\infty$; theorem 2.3.1 is a special case of this general theorem.[18] The extended operator space in the general small gain theorem allows consideration of robustness for systems composed of nonlinear and time-varying operators. The requirement of considering stable, rational, transfer-function operators is explicitly stated in the theorem to emphasize that the nominal aeroelastic system considered in this paper is assumed to be stable and the flutter margin is associated with a destabilizing perturbation to that nominal system.

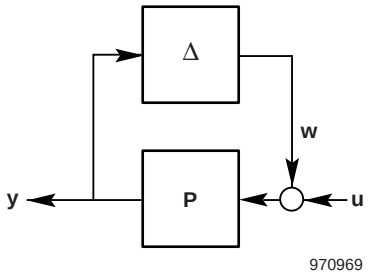

Figure 2.1. Block diagram for the small gain theorem.

The second condition in theorem 2.3.1 is associated with the first condition guaranteeing a well-posed and stable system. This uniqueness condition can be understood by consideration of the solution y for the loop equations shown in figure 2.1.

$$\begin{aligned} y &= P(u + w) \\ &= (I - P\Delta)^{-1} Pu \end{aligned} \tag{17}$$

The inverse term, $(I - P\Delta)^{-1}$, has a magnitude of infinity if the norm of $P\Delta$ is allowed to be unity. Such a condition would allow the norm of signal y to be infinite despite a norm-bounded u input signal. Restricting $\|P\Delta\|_\infty < 1$ ensures the inverse term exists and a unique finite-norm y is generated in response to a finite-norm u. The issue of well-posedness requires this condition to hold at $s = \infty$ and is automatically considered by the $\mathcal{H}_\infty$–norm.

2.4 Robust Stability

The small gain theorem can be directly used to analyze robust stability of a plant model with respect to a set of perturbations.[19] These perturbations are used to describe uncertainty in the analytical plant model caused by errors and unmodeled dynamics. Usually, the exact value of the modeling error is not known, but a norm-bounded, real scalar, $\alpha > 0$, can be placed on the size of that error. Define the $\mathbf{\Delta}$ of norm-bounded operators describing these perturbations that affect the plant P through a feedback relationship.

$$\mathbf{\Delta} = \{\Delta : \|\Delta\|_\infty \le \alpha\} \tag{18}$$

The small gain theorem allows consideration of the entire set of possible modeling uncertainties as described by all $\Delta \in \mathbf{\Delta}$. The $\mathcal{H}_\infty$–norm of the loop gain cannot be explicitly computed for these systems because an infinite number of loop gains $P\Delta$ generated by the $\mathbf{\Delta}$ exists. The triangle inequality of norms can be used to generate a sufficient condition for robust stability of P.

$$\|P\Delta\|_\infty \le \|P\|_\infty \|\Delta\|_\infty \tag{19}$$

A condition for robust stability of the closed-loop system can be stated.

Lemma 2.4.1: *The plant* P *is robustly stable to the set of uncertainty perturbations,* $\mathbf{\Delta}$*, that enter the system as in figure 2.1 with* $\|\Delta\|_\infty \le \alpha$ *for all* $\Delta \in \mathbf{\Delta}$ *if*

$$\|P\|_\infty < \frac{1}{\alpha} \tag{20}$$

Lemma 2.4.1 shows a sufficient, but not necessary, condition for robust stability. The structured singular value, μ, is introduced in the next chapter as a less conservative measure of robust stability that is sufficient and necessary.

An excellent illustrative example has previously been presented[18] to demonstrate the issue of robust stability. This example uses classical arguments to compute a robust stability condition for a simple system that is seen to be identical to the robust stability condition generated using the small gain theorem and lemma 2.4.1. A similar example is given below for the feedback interconnection in figure 2.2.

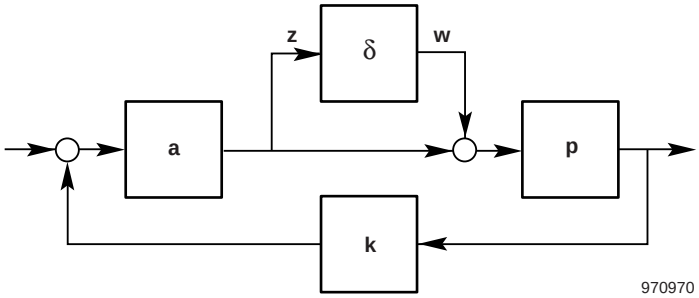

Figure 2.2. Block diagram with uncertainty for the example system.

The single-input and single-output elements in the nominal system model (fig. 2.2) are p, which represents the plant dynamics; a, which represents actuator dynamics; and k, which represents a feedback controller. Each of the nominal system elements are stable transfer functions contained in $\mathcal{RH}_\infty$. A modeling error exists on the output of the actuator that is represented by a multiplicative uncertainty operator, $\delta \in \mathcal{RH}_\infty$, on the output of the element a.

The transfer function from w to z can be computed as follows.

$$z = \left(-(1 + akp)^{-1} akp\right) w \tag{21}$$

Internal stability of the closed-loop feedback system is equivalent to stability of the feedback system shown in figure 2.3 with the operator $g = -(1 + akp)^{-1} akp$.

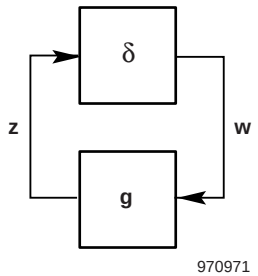

Figure 2.3. Block diagram for robust stability analysis of the example system using the small gain theorem.

Because the operators $\delta, g \in \mathcal{RH}_\infty$ are stable, the Nyquist criterion determines the closed-loop system is stable if and only if the Nyquist plot of δg does not encircle the –1 point. This stability condition is equivalent to the following norm condition.

$$\sup_{\omega} |g(j\omega)\ \delta(j\omega)| < 1 \tag{22}$$

This condition is an $\mathcal{H}_\infty$–norm condition on the loop gain, $g\delta$. Thus, classical Nyquist arguments derive an $\mathcal{H}_\infty$–norm condition that is equivalent to the stability condition immediately formulated by applying the small gain theorem.

$$\text{closed-loop stability} \quad \Leftrightarrow \quad \|g\delta\|_\infty < 1 \tag{23}$$

The error in the actuator command is unknown and possibly time-varying, so the operator δ is used to allow consideration of a range of errors. Assume the actuator is weighted such that the range of errors is described by the set of perturbations, $\|\delta\|_\infty < 1$. Lemma 2.4.1 is used to generate a condition that ensures the system is robustly stable to all actuators errors described by δ.

$$\text{closed-loop stability} \quad \Leftarrow \quad \|g\|_\infty < 1 \tag{24}$$

CHAPTER 3
STRUCTURED SINGULAR VALUE

3.1 Linear Fractional Transformations

The linear fractional transformation (LFT) is a common framework suitable for robust stability analysis using arguments based on the small gain theorem. An LFT is an interconnection of operators arranged in a feedback configuration. These operators can be constant matrices, time-domain state-space systems, or frequency-varying transfer functions. Consider a linear operator $P \in \mathbf{C}^{(o_1 + o_2) \times (i_1 + i_2)}$ that is partitioned into four elements.

$$P = \begin{bmatrix} P_{11} & P_{12} \\ P_{21} & P_{22} \end{bmatrix} \tag{25}$$

The LFT, $F_u(P, \Delta)$, is defined as the interconnection matrix such that the upper loop of P is closed with the operator $\Delta \in \mathbf{C}^{i_1 \times o_1}$.

Definition 3.1.1: *Given* $P \in \mathbf{C}^{(o_1 + o_2) \times (i_1 + i_2)}$ *and* $\Delta \in \mathbf{C}^{i_1 \times o_1}$, *define* $F_u(P, \Delta))$ *as the upper-loop LFT of* P *closed with* Δ *such that* $y = F_u(P, \Delta)\ u$ *as in figure 3.1.*

$$F_u(P, \Delta) = P_{22} + P_{21}\Delta(I - P_{11}\Delta)^{-1}P_{12} \tag{26}$$

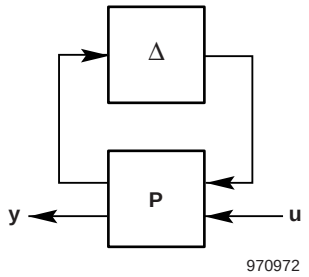

Figure 3.1 Linear fractional transformation $F_u(P, \Delta)$.

A similar LFT is defined as $F_l(P, \Delta)$ to represent the interconnection matrix of the lower loop of P closed with an operator $\Delta \in \mathbf{C}^{i_2 \times o_2}$.

Definition 3.1.2: *Given* $P \in \mathbf{C}^{(o_1 + o_2) \times (i_1 + i_2)}$ *and* $\Delta \in \mathbf{C}^{i_2 \times o_2}$, *define* $F_u(P, \Delta)$ *as the lower-loop LFT of* P *closed with* Δ *such that* $y = F_l(P, \Delta)\ u$ *as in figure 3.2.*

$$F_l(P, \Delta) = P_{11} + P_{12}\Delta(I - P_{22}\Delta)^{-1}P_{21} \tag{27}$$

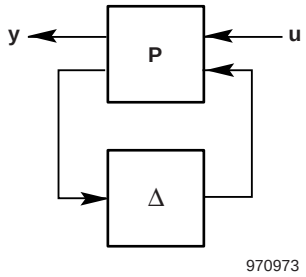

Figure 3.2. Linear fractional transformation $F_l(P, \Delta)$.

An example of an interconnection that is common in stability analysis is the representation of a time-dependent state-space system as a frequency-varying transfer function. Define S as the constant matrix whose entries are the $\{A_P, B_P, C_P, D_P\}$ matrices of a state-space realization. The transfer function can be written as an upper-loop LFT involving S and the Laplace transform variable s where $\frac{1}{s}$ is an integrator.

$$\begin{aligned} \dot{x} &= A_P x + B_p u \\ y &= C_P x + D_P u \end{aligned} \quad \Rightarrow \quad S = \begin{bmatrix} A_P & B_P \\ C_P & D_P \end{bmatrix} \quad \Rightarrow \quad \begin{aligned} P(s) &= D_P + C_P(sI - A_P)^{-1}B_P \\ &= F_u(S, \tfrac{1}{s}) \end{aligned} \tag{28}$$

The LFT is a useful framework for analyzing complex systems with many feedback and series interconnections of operators. Property 3.1.3 shows the main property of LFTs that will be used herein. This property allows complex systems of several interconnected LFTs to be expressed as an equivalent single LFT. The operators of the new LFT are block-structured with blocks composed of the individual operators of the LFTs from the original system.

Property 3.1.3: *Feedback and series interconnections of LFTs can be formulated as a single LFT.*

This issue of stability for LFT systems is associated with the concept of a well-posed interconnection. Stability analysis based on the small gain theorem given in theorem 2.3.1 can be used to guarantee the LFT is stable and well-posed.

3.2 Structured Uncertainty

The concept of uncertainty is formulated as a set of norm-bounded operators, $\mathbf{\Delta}$, associated with a nominal plant, P, through an LFT feedback relationship. A family of plants, $\mathcal{P}$, arises through consideration of $F_u(P, \Delta)$ for every $\Delta \in \mathbf{\Delta}$. The true plant model is assumed to lie within this family of plants.

Modeling the uncertainty as a norm-bounded operator can lead to overly conservative models. The uncertainty description can be made more accurate by including frequency information. Formulating a model of a physical system that is accurate at low frequencies but less accurate for representing the system response at high frequencies is often possible. A frequency-varying transfer function, W, is generally associated with each uncertainty element to describe magnitude and phase uncertainty as it varies with frequency.

Uncertainty can enter a system model in a linear fractional manner in several general ways. Two typical types of uncertainty are termed “multiplicative” and “additive” uncertainty. Multiplicative

uncertainty can be either on the input or output of a system. Systems with these types of uncertainty are easily described in block diagram form. Figure 3.3 shows the LFT for a plant with input multiplicative uncertainty. Figure 3.4 shows the plant with output multiplicative uncertainty. Figure 3.5 shows additive uncertainty.

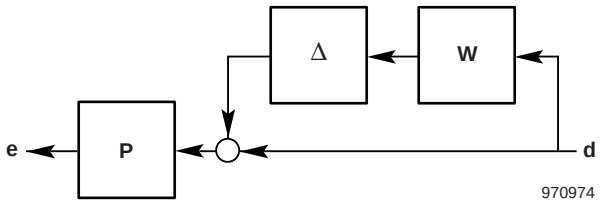

Figure 3.3. Family of plants $\mathcal{P}$ = P(I + Δ W) with input multiplicative uncertainty.

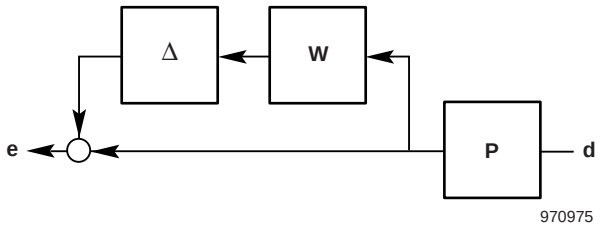

Figure 3.4. Family of Plants $\mathcal{P}$ = (I + Δ W)P with output multiplicative uncertainty.

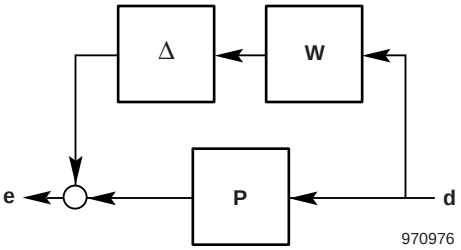

Figure 3.5. Family of plants $\mathcal{P}$ = P + ΔW with additive uncertainty.

Uncertainty can also be associated with specific elements of the system. These parametric uncertainties are usually associated with a system operator in a feedback relationship. The number of input and output signals of the system operator is increased to account for the additional feedback signals associated with the uncertainty operator. This operation can be demonstrated by considering $\mathcal{P}$ generated by a system with an unknown pole.

$$\mathcal{P} = \left\{ \frac{1}{(s+1)(s+x)} : x \in [2, 3] \right\} \tag{29}$$

A norm-bounded, real, scalar, uncertainty parameter δ can be introduced to account for the possible variation in pole value. The set of plants can be written in the LFT framework using this uncertainty operator and definition 3.1.1.

$$\mathcal{P} = \left\{ F_u(P, \delta) : P = \begin{bmatrix} \frac{-1}{s+2.5} & \frac{-1}{s+2.5} \\ \frac{1}{(s+1)(s+2.5)} & \frac{1}{(s+1)(s+2.5)} \end{bmatrix}, \|\delta\|_\infty \le 1, \delta \in \mathbf{R} \right\} \tag{30}$$

A complex system with several uncertainty operators can be expressed as an LFT with a single uncertainty operator using property 3.1.3. This operator is structured as a block-diagonal operator with each block associated with the individual uncertainty operators. Two main types of uncertainty blocks exist. A full-block uncertainty is a matrix with unknown elements. This type of block is used to describe unstructured uncertainty in a group of signals.

Definition 3.2.1: *A full-block uncertainty,* $\Delta \in \mathbf{C}^{n \times m}$*, has unknown elements* Δ_{ij} *for every* $i \in [1, n]$ *and* $j \in [1, m]$.

A repeated-scalar block introduces more structure into the uncertainty description than a full block does. Only the diagonal elements of the matrix contain unknown elements; the remaining elements are zero. Furthermore, the diagonal elements are identical. This type of uncertainty is used to relate input-output signal pairs with the same uncertainty parameter.

Definition 3.2.2: *A repeated-scalar block uncertainty* $\Delta \in \mathbf{C}^{n \times n}$ *has zero-valued elements except an unknown parameter* δ *along the diagonal such that* $\Delta = \delta I_n$. *A scalar block is a repeated-scalar block of dimension* 1.

The single structured uncertainty block used for robust stability analysis is formally defined in terms of these blocks. Let integers m, n, and p define the number of real scalar, complex scalar, and complex full blocks respectively. Define integers $R_1, \ldots, R_m$ such that the i^{th} repeated-scalar block of real, parametric uncertainty is of dimension R_i by R_i. Define similar integers $C_1, \ldots, C_n$ to denote the dimension of the complex repeated-scalar blocks. The structured uncertainty description Δ is assumed to be norm-bounded and belonging to the following set.

$$\mathbf{\Delta} = \left\{ \Delta = \operatorname{diag}\left(\delta_1^R I_{R_1}, \ldots, \delta_m^R I_{R_m}, \delta_1^C I_{C_1}, \ldots, \delta_n^C I_{C_n}, \Delta_1, \ldots, \Delta_p \right) : \delta_i^R \in \mathbf{R}, \delta_i^C \in C, \Delta_i \in \mathbf{C}^{c_i \times c_i} \right\} \tag{31}$$

Real parametric uncertainty is allowed to enter the problem as scalar or repeated-scalar blocks. Complex uncertainty enters the problem as scalar, repeated-scalar, or full blocks. Complex uncertainty parameters allow uncertainty in magnitude and phase to be modeled; uncertainty in physical characteristics can be more accurately modeled with real parameters. The robustness analysis will be less conservative by accounting for this structure to accurately describe the model uncertainty.

3.3 Structured Singular Value

Figure 3.6 shows the general framework for robust stability analysis. The plant operator $P(s) \in \mathcal{RH}_\infty$ is a stable, rational, transfer-function matrix representing the aeroelastic dynamics. A norm-bounded $\mathbf{\Delta} \in \mathcal{RH}_\infty$ is defined such that $\Delta(s) \in \mathbf{\Delta}$ describes the modeling errors in P through a feedback relationship.

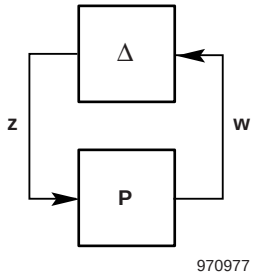

Figure 3.6. Linear fractional transformation system for robust stability analysis using μ.

The robustness of P with respect to the $\mathbf{\Delta}$ can be determined using the small gain theorem as presented in lemma 2.4.1. This condition guarantees stability for any value $\Delta \in \mathbf{\Delta}$ if $\|P\|_\infty < 1$. This robustness condition can be overly conservative because it does not account for structure in the uncertainty operator. The structured singular value, μ, is defined as an alternative measure of robustness.[20]

Definition 3.3.1: *Given the complex transfer-function matrix* $P \in \mathcal{RH}_\infty$ *and associated norm-bounded set of uncertainty operators* $\mathbf{\Delta}$*, define* μ.

$$\mu(P) = \frac{1}{\min\limits_{\Delta \in \mathbf{\Delta}} \{\bar{\sigma}(\Delta) : \det(I - P\Delta) = 0\}} \tag{32}$$

Define $\mu = 0$ *if no* $\Delta \in \mathbf{\Delta}$ *exists such that* $\det(I - P\Delta) = 0$.

The structured singular value is an exact measure of robust stability for systems with structured uncertainty. The value of μ determines the allowable size of uncertainty matrices for which the plant is robustly stable as demonstrated in theorem 3.3.2.[20]

Theorem 3.3.2: *Given the system in figure* 3.6, P *is robustly stable with respect to the* $\mathbf{\Delta}$*, which is norm-bounded by real scalar* α *such that* $\|\Delta\|_\infty \le \alpha$ *for all* $\Delta \in \mathbf{\Delta}$ *if and only if* $\mu(P) < \frac{1}{\alpha}$.

The model P is usually internally weighted such that the range of modeling errors is described by the uncertainty set $\mathbf{\Delta}$, which is norm-bounded by 1.

$$\|\Delta\|_\infty \le 1 \text{ for all } \Delta \in \mathbf{\Delta} \tag{33}$$

Theorem 3.3.3 presents the specific condition for robust stability that will be used in this paper for unity norm-bounded uncertainty sets.

Theorem 3.3.3: *Given the system in figure 3.6,* P *is robustly stable with respect to the* $\mathbf{\Delta}$ *with* $\|\Delta\|_\infty \le 1$ *for all* $\Delta \in \mathbf{\Delta}$ *if and only if* $\mu(P) < 1$.

A value of $\mu < 1$ implies no perturbation within $\mathbf{\Delta}$ exists that will destabilize the feedback system. This condition can also be interpreted as saying the true plant dynamics are stable, assuming these dynamics lie within the range generated by the nominal model dynamics coupled with the set of modeling errors.

Obviously, μ is dependent on the block structure of $\mathbf{\Delta}$. The robust stability properties computed by μ will only be accurate if a realistic uncertainty operator is chosen. The structured singular value may be arbitrarily greater when computed with respect to an unstructured uncertainty operator as compared to a highly structured uncertainty operator. Definition 3.3.1 demonstrates the μ condition of theorem 3.3.3 is equivalent to the small gain condition of lemma 2.4.1 when the uncertainty is unstructured.

Unfortunately, μ is a difficult quantity to compute. Closed-form solutions exist to exactly compute μ for only a small number of block structures for $\mathbf{\Delta}$. Upper and lower bounds are used to compute μ for generalized uncertainty block structures. Appendix A shows a derivation of the upper bound, which represents a limit on the worst-case robustness properties.

CHAPTER 4
ROBUST FLUTTER MARGINS

4.1 Nominal Aeroelastic Model

Consider the generalized equation of motion for the structural response of the aircraft.[21]

$$M\ddot{\eta} + C\dot{\eta} + K\eta + \bar{q}Q(s)\eta = 0 \tag{34}$$

For a system with n modes, define $M \in \mathbf{R}^{n \times n}$ as the mass matrix, $C \in \mathbf{R}^{n \times n}$ as the damping matrix, and $K \in \mathbf{R}^{n \times n}$ as the stiffness matrix. Define $\bar{q} \in \mathbf{R}$ as a scalar representing the dynamic pressure, and $Q(s) \in \mathbf{C}^{n \times n}$ as the matrix of unsteady aerodynamic forces. This equation is valid for a particular Mach number, with a different Q(s) describing the unsteady aerodynamic forces at a different Mach number.

Values of the aerodynamic force matrix at distinct frequencies can be derived using finite-element models of the aircraft and panel methods for unsteady force calculations. This research uses a computer program developed for NASA known as STARS.[22, 23] This code solves the subsonic aerodynamic equations using the doublet-lattice method.[24, 25] The supersonic forces are generated using a different approach known as the constant panel method.[26]

Formulating a linear time-invariant representation of the aerodynamic forces to incorporate them into the robust stability framework is desired. Padé approximations can be used to compute a rational function approximation to the transfer-function matrix.

$$Q(s) = A_0 + sA_1 + s^2A_2 + \frac{s}{s + \beta_1}A_3 + \frac{s}{s + \beta_2}A_4 \tag{35}$$

This form is often referred to as Roger's form.[27] The equation presented here includes only two lag terms, although more terms can be included. The poles of the lag terms, β_1 and β_2, are restricted to be real and positive to maintain system stability. The matrix elements of Roger's form can be computed using a least-squares algorithm to fit the frequency-varying aerodynamic data.

The aerodynamic lag terms can be replaced in the formulation with a finite-dimensional state-space system represented by a transfer-function matrix using Karpel's method.[28]

$$Q(s) = A_0 + sA_1 + s^2A_2 + C_Q(sI - A_Q)^{-1}B_Qs \tag{36}$$

Standard system identification algorithms, including curve-fitting or least-squares approaches, can be used to compute the elements in the state-space portion of the formulation. The A_i matrices are assumed to be known from the low-frequency aerodynamic force data or from experimental wind-tunnel data.

A matrix fraction approach is also formulated to represent the aerodynamic forces as a linear time-invariant system.[29, 30] This generalized form computes rational matrix polynomials in a fractional form using a least-squares algorithm. Roger's form and Karpel's form can be shown to be subsets of the matrix fractional form.

The approach taken in this paper is to fit the aerodynamic force matrices to a single, finite-dimensional, state-space system. This form is most similar to Karpel's form, except the additional A_i matrices are not explicitly accounted for in the formulation.

$$Q(s) = \begin{bmatrix} A_Q & B_Q \\ C_Q & D_Q \end{bmatrix} = D_Q + C_Q(sI - A_Q)^{-1}B_Q \tag{37}$$

Given the number of generalized states, n, and the number of aerodynamic states, n_Q, define $A_Q \in \mathbf{R}^{n_Q \times n_Q}$, $B_Q \in \mathbf{R}^{n_Q \times n}$, $C_Q \in \mathbf{R}^{n \times n_Q}$, and $D_Q \in \mathbf{R}^{n \times n}$ as the elements of the state-space system approximating Q(s).

Fitting the aerodynamic data to a finite-dimensional state-space system is equivalent to fitting each term in the matrix to a real, rational, proper, transfer function. This method seems to contradict the methods of Roger and Karpel, which form nonproper transfer functions caused by the terms in s and s^2. An approximation to these forms allows them to fall within the framework of the method used in this paper. Including a high-frequency pole in the nonproper term, such as replacing s with $\frac{s}{s + 10000}$, would not affect the low-frequency region of interest while ensuring stable and proper functions. With the approximation, the forms of Roger and Karpel can be shown to be subsets of this method.

Standard frequency-domain system identification algorithms can generate a system with an arbitrarily large number of states. This state dimension does not greatly affect the computational cost of the robust stability analysis. Extending the robustness analysis to controller synthesis, however, places an emphasis on limiting the state dimension.[31] Limiting the number of states in the identification process is not directly considered here, although standard model reduction techniques can be used on the state-space system to lower the state dimension.[15]

Generating a state-space representation of the aeroelastic system, including the state-space form of the unsteady aerodynamic forces, is straightforward. Consider the force vector, y, generated by the state vector, η. Define $x \in \mathbf{R}^{n_Q}$ as the vector of aerodynamic states.

$$y = Q(s)\eta \quad \Leftrightarrow \quad \begin{bmatrix} \dot{x} \\ y \end{bmatrix} = \begin{bmatrix} A_Q & B_Q \\ C_Q & D_Q \end{bmatrix} \begin{bmatrix} x \\ \eta \end{bmatrix} \tag{38}$$

Using x, formulate the aeroelastic differential equation.

$$\begin{aligned} 0 &= M\ddot{\eta} + C\dot{\eta} + K\eta + \bar{q}Q(s)\eta \\ &= M\ddot{\eta} + C\dot{\eta} + K\eta + \bar{q}y \\ &= M\ddot{\eta} + C\dot{\eta} + K\eta + \bar{q}(C_Q x + D_Q \eta) \\ &= M\ddot{\eta} + C\dot{\eta} + (K + \bar{q}D_Q)\eta + \bar{q}C_Q x \end{aligned} \tag{39}$$

A state-space system is formulated using the generalized states, η and $\dot{\eta}$, and the unsteady aerodynamic states, x. The state-update matrix is determined by the following three differential equations.

$$\begin{bmatrix} \dot{\eta} \\ \ddot{\eta} \\ \dot{x} \end{bmatrix} = \begin{bmatrix} 0 & I & 0 \\ -M^{-1}(K + \bar{q}D_Q) & -M^{-1}C & -\bar{q}M^{-1}C_Q \\ B_Q & 0 & A_Q \end{bmatrix} \begin{bmatrix} \eta \\ \dot{\eta} \\ x \end{bmatrix} \tag{40}$$

4.2 Nominal Aeroelastic Model in the Structured Singular Value Framework

The generalized equation of motion for the nominal aeroelastic system can be expressed in a form suitable for using μ analysis to compute a flutter margin. The flutter margin is dependent on the flight condition parameters that result in a flutter instability, and μ is defined to be the smallest perturbation among the $\mathbf{\Delta}$ that causes an instability. The obvious approach to formulating flutter analysis in the μ framework is to introduce a perturbation to a flight condition parameter and find the smallest perturbation that causes an instability.

Essentially, the two subsystems in the nominal aeroelastic model are composed of the structural dynamics, involving mass, damping, and stiffness matrices; and the unsteady aerodynamics scaled by the dynamic pressure. The generalized equation of motion demonstrates the dynamic pressure linearly affects the dynamics at a constant Mach condition. Perturbations to dynamic pressure can thus enter the system through a feedback operator in a linear fractional manner that is perfectly suited to μ analysis.

Consider an additive perturbation, $\delta_{\bar{q}} \in \mathbf{R}$, on the nominal dynamic pressure, $\bar{q}_o$.

$$\bar{q} = \bar{q}_o + \delta_{\bar{q}} \tag{41}$$

Separate terms in the system dynamics that involve $\delta_{\bar{q}}$.

$$\begin{aligned} 0 &= M\ddot{\eta} + C\dot{\eta} + (K + \bar{q}D_Q)\eta + \bar{q}C_Q x \\ &= M\ddot{\eta} + [C\dot{\eta} + (K + \bar{q}_o D_Q)\eta + \bar{q}_o C_Q x] + \delta_{\bar{q}}[D_Q\eta + C_Q x] \\ &= \ddot{\eta} + [M^{-1}C\dot{\eta} + M^{-1}(K + \bar{q}_o D_Q)\eta + \bar{q}_o M^{-1}C_Q x] \\ &\qquad + \delta_{\bar{q}}[M^{-1}D_Q\eta + M^{-1}C_Q x] \\ &= \ddot{\eta} + [M^{-1}C\dot{\eta} + M^{-1}(K + \bar{q}_o D_Q)\eta + \bar{q}_o M^{-1}C_Q x] + \delta_{\bar{q}} z \\ &= \ddot{\eta} + [M^{-1}C\dot{\eta} + M^{-1}(K + \bar{q}_o D_Q)\eta + \bar{q}_o M^{-1}C_Q x] + w \end{aligned} \tag{42}$$

The signals z and w are introduced into this formulation to associate the perturbation in dynamic pressure to the nominal dynamics in a feedback manner. The signal z can be generated as an output of the plant because z is a linear combination of states.

$$z = M^{-1}D_Q\eta + M^{-1}C_Q x \tag{43}$$

The signal w is related to z by the dynamic pressure perturbation.

$$w = \delta_{\bar{q}}\, z \tag{44}$$

The state-space aeroelastic model for nominal stability analysis in the μ framework is formulated using the state-update matrix. This matrix is determined by the dynamics at the nominal dynamic pressure, and the additional input and output signals that introduce perturbations to the dynamic pressure. That perturbation, $\delta_{\bar{q}}$, is not an explicit parameter in the state-space model because $\delta_{\bar{q}}$ only affects the plant through a feedback relationship as determined by the signals z and w. Define the transfer function P(s) generated by state-space matrices such that z = P(s)w.

$$\begin{bmatrix} \dot{\eta} \\ \ddot{\eta} \\ x \\ \hline z \end{bmatrix} = \left[\begin{array}{ccc|c} 0 & I & 0 & 0 \\ -M^{-1}(K + \bar{q}_o D_Q) & -M^{-1}C & -\bar{q}M^{-1}C_Q & -I \\ B_Q & 0 & A_Q & 0 \\ \hline M^{-1}D_Q & 0 & M^{-1}C_Q & 0 \end{array}\right] \begin{bmatrix} \eta \\ \dot{\eta} \\ x \\ \hline w \end{bmatrix} \tag{45}$$

Figure 4.1 shows the feedback interconnection between the perturbation in dynamic pressure and the nominal plant model parameterized around that perturbation. This interconnection is an LFT, and the small gain condition of lemma 2.4.1 or the μ condition of theorem 3.3.3 can be directly applied to analyze stability with respect to a variation in the flight condition $\bar{q}$.

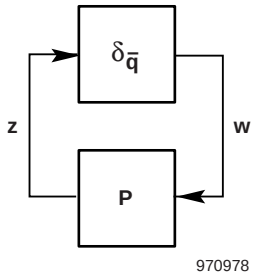

Figure 4.1. Linear fractional transformation system for nominal stability analysis in the μ framework with parameterization around perturbation in dynamic pressure.

Formulating the nominal aeroelastic dynamics in the μ framework immediately demonstrates the procedure used in computing a flutter margin. Traditional flutter analysis algorithms such as the p-k method and the μ method as applied to figure 4.1 are searching for a value of dynamic pressure that results in a flutter instability. The nominal flutter margin question may be posed, which is answered by these methods.

Question 4.2.1 (nominal flutter margin): *What is the largest perturbation to dynamic pressure for which the nominal aeroelastic dynamics are stable?*

The dimension of the uncertainty block is the dimension of the signal z. The state-space equations for P(s) demonstrate this dimension is the number of modes in the system, n. The number of free variables in the μ upper-bound optimization, and consequently the computational cost of μ, is a function of the

uncertainty dimension. In this way, the number of aerodynamic states, n_Q, does not directly affect the cost of the flutter estimation. The only cost increase caused by these additional states is computing the frequency response of the state-space matrix, which is generally much lower than the cost of computing μ.

Demonstrating the aeroelastic system formulated in the μ framework in figure 4.1 is straightforward. The dynamic pressure parameterization is equivalent to the nominal state-space system given in the previous section. Simply compute the closed-loop transfer function with no uncertainty, $\delta_{\bar{q}} = 0$, and the nominal system is recovered.

Wind-tunnel and ground vibration testing can experimentally determine aerodynamic stiffness and damping matrices that are more accurate than the matrices approximated by a finite-element model. These matrices can be incorporated into a nominal state-space model in the μ framework using the derivation in Appendix B.

This procedure considers variations in dynamic pressure for an aeroelastic model at constant Mach number. The unsteady aerodynamics are highly nonlinear with variation in Mach number, and attempts to model Mach variations in an LFT may produce highly conservative flutter margins.[32, 33] The μ method presented herein is considering flutter margins in terms of dynamic pressure as measured along lines of constant Mach. Flutter is a function of the two variables, dynamic pressure and Mach, so computing the dynamic pressure causing flutter for a dense set of discrete Mach values will generate an accurate portrait of the flutter margins.

4.3 Robust Aeroelastic Model in the Structured Singular Value Framework

A robust aeroelastic model in the μ framework can be generated by associating uncertainty operators, Δ, with the nominal model and including the parameterization around a perturbation in dynamic pressure. These uncertainty operators can resemble any of the forms presented in section 3.2, including parametric uncertainty and additive and multiplicative representations of dynamic uncertainty.

Choosing a reasonable uncertainty description is crucial for determining a valid robust flutter margin. This choice can arise logically from consideration of weaknesses in the modeling process, previous experience with aeroelastic analysis, and comparison with observed flight dynamics. Chapter 5 gives a noncomprehensive examination of several obvious uncertainty descriptions that may be associated with an aeroelastic model.

The LFT is a valuable framework for formulating the robust aeroelastic model so that the model is suitable for μ analysis. The various system blocks composed of the nominal state-space model with associated uncertainties and any additional subsystem blocks and their associated uncertainties can be expressed as a single model and uncertainty operator.

Figure 4.2 shows the block structure used for μ analysis of the uncertain aeroelastic system. The structured singular value is computed with respect to a single, block-diagonal, structured operator that contains the perturbation to dynamic pressure and the structured uncertainty operator along the diagonal. The perturbation to dynamic pressure is explicitly shown to distinguish $\delta_{\bar{q}}$ from the modeling uncertainty and emphasize $\delta_{\bar{q}}$ as a special operator used to describe a range of flight conditions.

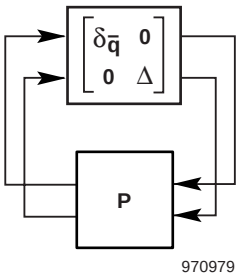

Figure 4.2. Linear fractional transformation system for robust stability analysis in the μ framework with parameterization around perturbation in dynamic pressure and structured uncertainty.

The flutter margin computed for the uncertain system (fig. 4.2) is a more accurate margin than one computed with traditional methods such as p-k. These traditional methods address the nominal flutter problem in question 4.2.1; the robust flutter margin must consider the effect of the modeling uncertainty. The robust flutter margin actually finds the smallest perturbation to dynamic pressure for the entire set of plants formulated by the interconnection of the nominal dynamics and all elements $\Delta \in \mathbf{\Delta}$. Question 4.3.1 poses how to compute these margins.

Question 4.3.1 (robust flutter margin): *What is the largest perturbation to dynamic pressure for which the nominal aeroelastic dynamics are robustly stable to the entire range of modeling errors as described by the norm-bounded* $\mathbf{\Delta}$*?*

This question can be answered by computing μ for the system in figure 4.2.

4.4 Computing a Flutter Margin with the Structured Singular Value

The nominal flutter problem posed by question 4.2.1 and the robust flutter problem posed by question 4.3.1 can be solved as a μ computation. The value of μ is a sufficient direct indication of the flutter margin for the nominal system; additional information regarding the norm bound on the uncertainty is required to derive the robust flutter margin.

The nominal aeroelastic model is formulated for stability analysis in the μ framework in section 4.2 by introducing a perturbation, $\delta_{\bar{q}}$, to dynamic pressure. A nominal flutter margin is computed to answer question 4.2.1 by considering the smallest value of this perturbation that destabilizes the model. The nominal flutter pressure can be directly calculated by computing μ with respect to the perturbation operator $\delta_{\bar{q}}$.

The exact value of μ can be analytically formulated to compute a nominal flutter pressure because a closed-form solution for μ with respect to a single, real, scalar operator is known. This solution is the spectral radius of the frequency-varying transfer-function matrix.

$$\mu(\mathrm{P}) = \max_{\omega \in \mathbf{R}} \rho(\mathrm{P}(j\omega)) \tag{46}$$

The spectral radius of $\mathrm{P}(j\omega)$ is a discontinuous function of frequency, so computational algorithms based on searches over a finite set of frequency points may not guarantee the correct computation of robustness values. A small amount of complex uncertainty can be added to the real uncertainty that allows a continuous μ function to be analyzed but introduces unrealistic conservatism. An heuristic

robustness indicator can be substituted for μ that considers stability over a frequency segment but is not considered here.[34, 35]

A relatively simple approach can be used to compute μ with respect to a single real parameter by considering the destabilizing value of the parameter. A search over the parameter space will result in computation of μ and the desired flutter margin. Lemma 4.4.1 presents the principle of this approach.

Lemma 4.4.1: *Given the plant,* P, *derived at nominal dynamic pressure,* $\bar{q}_o$, *with a perturbation to dynamic pressure,* $\delta_{\bar{q}}$, *arranged in the feedback relationship of figure 4.2, define* δ.

$$\delta = \min_{\delta_{\bar{q}} > 0} \{ \delta_{\bar{q}} \ : \ F_u(P, \delta_{\bar{q}}) \ \textit{is unstable} \}$$

Then $\mu(P) = \frac{1}{\delta}$ *such that* $\bar{q}^{nom}_{flutter} = \bar{q}_o + \delta$ *is the nominal flutter pressure and*

$$\Gamma_{nom} = \delta$$

represents the nominal flutter margin answering question 4.2.1.

Proof:

This result is immediately obvious using definition 3.3.1 for μ with respect to a scalar uncertainty parameter $\delta_{\bar{q}}$. The μ is the inverse of the smallest destabilizing perturbation, and δ is computed as the smallest value of $\delta_{\bar{q}}$ that destabilizes P; thus $\mu(P) = \frac{1}{\delta}$.

□

Lemma 4.4.1 indicates a computational strategy to compute a nominal flutter margin that does not require a search over a set of frequency points. The flutter pressure is found by increasing values of $\delta_{\bar{q}}$ until an eigenvalue of the state matrix of $F_u(P, \delta_{\bar{q}})$ has a negative real part indicating $F_u(P, \delta_{\bar{q}})$ is unstable. Algorithm 4.4.2 demonstrates a bisection search implementation that efficiently computes upper and lower bounds on the minimum destabilizing $\delta_{\bar{q}}$ perturbation to within a desired level of accuracy.

Algorithm 4.4.2 (nominal flutter margin):

Given plant P *at nominal dynamic pressure,* $\bar{q}_o$, *affected by perturbation* $\delta_{\bar{q}}$ *as in figure 4.1:*
Define scalars $\delta_{upper} > \delta_{lower} > 0$ *as bounds on the smallest destabilizing* $\delta_{\bar{q}}$.
Define scalar $\varepsilon > 0$ *for accuracy.*

while $(\delta_{upper} - \delta_{lower} > \varepsilon)$ {

$\delta_{\bar{q}} = \frac{1}{2}(\delta_{upper} + \delta_{lower})$

if $F_u(P, \delta_{\bar{q}})$ *has an unstable pole), then* $\delta_{upper} = \delta_{\bar{q}}$

else $\delta_{lower} = \delta_{\bar{q}}$

}

$\bar{q}^{nom}_{flutter} = \bar{q}_o + \delta_{upper}$

$\Gamma_{nom} = \delta_{upper}$

Robust flutter margins that address question 4.3.1 cannot be computed using algorithm 4.4.2 because an additional search over the set of uncertainty operators $\mathbf{\Delta}$ must be included. These margins must be computed using the augmented plant P, which includes feedback signals relating the perturbation to dynamic pressure and the uncertainty description as shown in figure 4.2. Define the block-structured set of operators, $\bar{\Delta}_{\delta_{\bar{q}}}$, which considers a particular perturbation $\delta_{\bar{q}}$ and set of operators $\mathbf{\Delta}$ describing model uncertainty.

$$\bar{\mathbf{\Delta}}_{\delta_{\bar{q}}} = \left\{ \bar{\Delta}_{\delta_{\bar{q}}} : \bar{\Delta}_{\delta_{\bar{q}}} = \begin{bmatrix} \delta_{\bar{q}} & 0 \\ 0 & \Delta \end{bmatrix}, \Delta \in \mathbf{\Delta}, \|\Delta\|_\infty \le 1 \right\} \tag{47}$$

A set of plant models, $F_u(P,\bar{\mathbf{\Delta}}_{\delta_{\bar{q}}})$, exists for each value of $\delta_{\bar{q}}$ that defines the nominal plant at dynamic pressure $\bar{q} = \bar{q}_o + \delta_{\bar{q}}$ and variations to that plant caused by the set of uncertainties $\mathbf{\Delta}$. The robust flutter margin corresponds to the smallest perturbation $\delta_{\bar{q}}$ for which an unstable plant, $F_u(P,\bar{\Delta}_{\delta_{\bar{q}}})$, exists with $\bar{\Delta}_{\delta_{\bar{q}}} \in \bar{\mathbf{\Delta}}_{\delta_{\bar{q}}}$. If every member of the set of plants $F_u(P,\bar{\mathbf{\Delta}}_{\delta_{\bar{q}}})$ is stable, then $\bar{q} = \bar{q}_o + \delta_{\bar{q}}$ is not a flutter pressure and P formulated at $\bar{q}$ is robustly stable to the uncertainty description $\mathbf{\Delta}$.

The smallest destabilizing perturbation $\delta_{\bar{q}}$ corresponding to a robust flutter margin can be computed by a μ computation. The μ framework analyzes robustness with respect to a single, structured operator, so the operator set used to compute a robust flutter margin must contain the set of uncertainty operators $\mathbf{\Delta}$ along with a range of dynamic pressure perturbations. The μ will compute the robustness of P with respect to this operator set to find the smallest destabilizing perturbation to dynamic pressure and the smallest destabilizing uncertainty operator. Define the $\bar{\mathbf{\Delta}}$ that contains $\bar{\Delta}_{\delta_{\bar{q}}}$ sets for a norm-bounded set of $\delta_{\bar{q}}$ operators.

$$\bar{\mathbf{\Delta}} = \left\{ \bar{\Delta} : \bar{\Delta} = \begin{bmatrix} \delta_{\bar{q}} & 0 \\ 0 & \Delta \end{bmatrix}, \Delta \in \mathbf{\Delta}, \|\Delta\|_\infty \le 1, \|\delta_{\bar{q}}\|_\infty \le 1 \right\} \tag{48}$$

Imposing the norm bound for $\delta_{\bar{q}}$ operators as $\|\delta_{\bar{q}}\|_\infty \le 1$ may seem overly restrictive because the units of $\delta_{\bar{q}}$ are the same as the units of $\bar{q}$ in the model. This condition implies the $\bar{\mathbf{\Delta}}$ considers the range of flight conditions $\bar{q} = \bar{q}_o \pm 1$ lbf/ft^2 for plants formulated by dynamic pressure in units of lbf/ft^2. Such a small range of flight conditions is not useful for stability analysis unless $\bar{q}_o$ is extremely close to the flutter pressure. This limitation is avoided by introducing a weighting function, $W_{\bar{q}}$, to the computation of $\bar{q}$.

$$\bar{q} = \bar{q}_o + W_{\bar{q}}\,\delta_{\bar{q}} \tag{49}$$

A $W_{\bar{q}} > 1$ allows a large range of flight conditions to be considered despite the unity norm-bound constraint on $\delta_{\bar{q}}$. This weighting is incorporated into the stability analysis by scaling the feedback signals between the $\delta_{\bar{q}}$ operator and the plant P to form the scaled plant, $\bar{P}$.

$$\bar{P} = P\begin{bmatrix} W_{\bar{q}} & 0 \\ 0 & I \end{bmatrix} \tag{50}$$

A robust flutter margin is computed by analyzing $\mu(\bar{P})$ with respect to the $\bar{\mathbf{\Delta}}$. The robust flutter pressure is determined by iterating over scalings $W_{\bar{q}}$ until the smallest pressure $\bar{q} = \bar{q}_o + W_{\bar{q}}$ is found for which the $\bar{P}$ is robustly stable to the set of uncertainties $\mathbf{\Delta}$. Theorem 4.4.3 formally demonstrates this concept.

Theorem 4.4.3: *Given the plant* P *derived at nominal dynamic pressure* $\bar{q}_o$ *with a perturbation to dynamic pressure* $\delta_{\bar{q}}$ *and set of uncertainty operators* $\mathbf{\Delta}$ *norm-bounded by one arranged in the feedback relationship of figure 4.2, define the plant* $\bar{P}$ *with real diagonal matrix* $W_{\bar{q}}$ *scaling the feedback signals relating* $\delta_{\bar{q}}$ *and* P.

$$\bar{P} = P\begin{bmatrix} W_{\bar{q}} & 0 \\ 0 & I \end{bmatrix} \tag{51}$$

Then $\bar{q}^{rob}_{flutter} = \bar{q}_o + W_{\bar{q}}$ *is the robust flutter pressure if and only if* $\mu(\bar{P}) = 1$. *Also,*

$$\Gamma_{rob} = W_{\bar{q}} \tag{52}$$

represents the least conservative robust flutter margin answering question 4.3.1.

Proof

$\Leftarrow$ (necessary)

The condition $\mu(\bar{P}) = 1$ implies that the smallest destabilizing perturbation to $\bar{P}$ is described by some $\bar{\Delta} \in \bar{\mathbf{\Delta}}$ with $\|\bar{\Delta}\|_\infty = 1$, so no destabilizing $\Delta \in \mathbf{\Delta}$ exists and the smallest positive destabilizing perturbation to dynamic pressure is at least $\delta_{\bar{q}} = 1$, which corresponds to dynamic pressure $\bar{q} = \bar{q}_o + W_{\bar{q}}\,\delta_{\bar{q}} = \bar{q}_o + W_{\bar{q}}$. Thus, $\bar{P}$ is guaranteed to be robustly stable to the uncertainty set $\mathbf{\Delta}$ for any perturbation to dynamic pressure less than $W_{\bar{q}}$, so $W_{\bar{q}}$ is a robust flutter margin.

$\Rightarrow$ (sufficient)

Assume $\mu(\bar{P}) > 1$. Define real, scalar $\alpha < 1$ such that $\mu(\bar{P}) = \frac{1}{\alpha}$, which implies, from theorem 3.3.2, that $\bar{P}$ is robustly stable to all uncertainties $\bar{\Delta} \in \bar{\mathbf{\Delta}}$ with $\|\bar{\Delta}\|_\infty < \alpha < 1$. Thus, $\bar{P}$ is not guaranteed to be stable over the entire range of modeling uncertainty defined by the unity norm-bounded set $\bar{\mathbf{\Delta}}$, so this perturbation is not a valid robust flutter margin and does not answer question 4.3.1.

Assume $\mu(\bar{P}) < 1$. Define real, scalar $\alpha > 1$ such that $\mu(\bar{P}) = \frac{1}{\alpha}$, which implies, from theorem 3.3.2, that $\bar{P}$ is robustly stable to all uncertainties $\bar{\Delta} \in \bar{\mathbf{\Delta}}$ with $\|\bar{\Delta}\|_\infty < \alpha$. Thus, $\bar{P}$ is robustly stable to an uncertainty description larger than that defined by the unity norm-bounded set $\bar{\mathbf{\Delta}}$, so this condition

defines a valid flutter margin but is not the least conservative robust flutter margin and does not answer question 4.3.1.

□

The only difference between models $\bar{P}$ and P results from the scaling $W_{\bar{q}}$, which scales the feedback signals between $\bar{P}$ and $\delta_{\bar{q}}$. No external scaling matrix is allowed to affect the feedback signals between $\bar{P}$ and Δ because Δ is defined with a unity norm bound. Computing μ of the plant $\bar{P}$ with an additional scaling on the lower-loop signals would consider a scaled set of operators $\mathbf{\Delta}$ that does not accurately represent the uncertainty description. Therefore, $\bar{P}$ only scales the $\delta_{\bar{q}}$ feedback signals.

Theorem 4.4.3 can be modified to compute a nominal flutter margin by changing the identity matrix in the scaling used to compute $\bar{P}$ to a zero matrix. This modification eliminates the feedback interconnection between the model and the uncertainty description $\mathbf{\Delta}$, so μ considers only the nominal dynamics and computes the smallest destabilizing perturbation to dynamic pressure and $\Gamma_{rob} = \Gamma_{nom}$.

Including the uncertainty description $\mathbf{\Delta}$ ensures the robust flutter margin will be no greater than the nominal flutter margin. The robust flutter margin considers the model used to compute the nominal flutter margin that corresponds to the uncertainty operator $\Delta = 0 \in \mathbf{\Delta}$ and the models that correspond to the remaining operators $\Delta \in \mathbf{\Delta}$. The conservatism in the robust flutter margin makes intuitive sense because the nominal flutter margin is the worst-case stability boundary for a single model and the robust flutter margin is the worst-case stability boundary for a family of models.

$$\Gamma_{rob} \leq \Gamma_{nom} \tag{53}$$

The proof demonstrating the necessary and sufficient condition $\mu(\bar{P}) = 1$ also makes intuitive sense because the equality sign is needed to ensure the flutter margin is valid without being overly conservative. If $\mu(\bar{P}) < 1$, then no $\Delta \in \mathbf{\Delta}$ causes an instability and the flutter margin is too conservative. If $\mu(\bar{P}) > 1$, then the system is not robust to all modeling errors $\Delta \in \mathbf{\Delta}$ and the flutter margin is not a valid robust flutter margin.

Theorem 4.4.3 demonstrates a robust flutter margin can be computed by determining a scaling matrix $W_{\bar{q}}$ for which $\mu(\bar{P}) = 1$. Algorithm 4.4.4 implements an iterative approach to compute a scaling matrix for which $\mu(\bar{P}) \in (1 \pm \varepsilon)$ for some desired level of accuracy ε.

Algorithm 4.4.4 (robust flutter margin):

Given plant P *at nominal dynamic pressure* $\bar{q}_o$ *affected by unity norm-bounded* $\delta_{\bar{q}}$ *and* $\mathbf{\Delta}$ *as in figure 4.2:*
Define initial weighting $W_{\bar{q}}$.
Define scalar $\varepsilon > 0$ *for accuracy.*

$$\bar{P} = P \begin{bmatrix} W_{\bar{q}} & 0 \\ 0 & I \end{bmatrix}$$

while $(\mu(\bar{P}) > 1 + \varepsilon)$ OR $(\mu(\bar{P}) < 1 - \varepsilon)$ {

$$W_{\bar{q}} = \frac{W_{\bar{q}}}{\mu(\bar{P})}$$

$$\bar{P} = P\begin{bmatrix} W_{\bar{q}} & 0 \\ 0 & I \end{bmatrix}$$

}

$$\bar{q}^{rob}_{flutter} = \bar{q}_o + W_{\bar{q}}$$

$$\Gamma_{rob} = W_{\bar{q}}$$

The dynamic pressure $\bar{q}_o$ defining the flight condition for the nominal plant dynamics must be chosen carefully to ensure the robust flutter margin computed with algorithm 4.4.4 is valid. The nature of μ and the upper bound is such that all norm-bounded operators centered around the origin are assumed to be valid perturbations to the plant dynamics, so positive and negative perturbations to dynamic pressure are considered by the robust stability analysis. Thus, the robust flutter margin computed by $\mu(\bar{P}) = 1$ could correspond to either perturbation $\delta_{\bar{q}} = 1$ or $\delta_{\bar{q}} = -1$.

The actual dynamic pressure at the flutter instability is $\bar{q}^{rob}_{flutter} = \bar{q}_o - W_{\bar{q}}$ if $\delta_{\bar{q}} = -1$. A large weighting of $W_{\bar{q}} > \bar{q}_o$ indicates the flutter occurs at a negative dynamic pressure that may be unrealistic for classical flutter analysis. The value of the nominal dynamic pressure $\bar{q}_o$ can slide along the real axis to a large value without loss of generality in the μ analysis because this parameter linearly affects the nominal dynamics. A simple approach to ensure that the robust flutter pressure is a positive dynamic pressure is demonstrated in algorithm 4.4.5, which iterates over increasing values of $\bar{q}_o$ until the scaling associated with the robust flutter margin satisfies $W_{\bar{q}} < \bar{q}_o$.

Algorithm 4.4.5 (robust flutter margin with $\bar{q}_o$ iteration):

Given parameters as in algorithm 4.4.4:
Given initial value of nominal dynamic pressure $\bar{q}_o$:

valid_margin = FALSE
while (valid_margin == FALSE*)* {
    compute plant P *at nominal dynamic pressure* $\bar{q}_o$
    compute $\bar{q}^{rob}_{flutter}$ *and associated* $W_{\bar{q}}$ *from algorithm 4.4.4*
    if ($W_{\bar{q}} > \bar{q}_o$*), then* $\bar{q}_o = 1.1\ W_{\bar{q}}$
    else *valid_margin* = TRUE
}

The exclusion of low and negative dynamic pressures for stability analysis may not be desirable for all applications related to aeroelasticity. An example of such an application is the analysis of aeroservoelastic dynamics for a high-angle-of-attack aircraft that concerns instabilities at low dynamic pressures.[36] The procedure for these types of analysis chooses a low value of $\bar{q}_o$ and finds the scaling

$W_{\bar{q}}$ corresponding to $\delta_{\bar{q}} = -1$, which computes the low dynamic pressure instability. Algorithm 4.4.5 can be modified for these applications.

The flutter margin computation must allow for an arbitrary structure of operators $\bar{\mathbf{\Delta}}$, so an upper bound such as the function derived in appendix A must be used. Algorithms 4.4.4 and 4.4.5 can be adapted by replacing the μ calculation with a μ upper-bound calculation to compute flutter margins. A search over frequency points is required when using the upper bound (appendix A), so the accuracy of the robust flutter margin requires a dense grid of frequencies associated with the natural frequencies of the worst-case dynamics to be considered.

A simple approach can be implemented if the natural frequency of the unstable dynamics at the nominal flutter pressure can be assumed to be similar to the natural frequency of the unstable dynamics at the robust flutter pressure. This assumption can be justified if the uncertainty does not change the critical flutter mode between the nominal and robust flutter pressures, which is often true for systems that have relatively small levels of uncertainty and clear separation between critical and subcritical modal frequencies. Algorithm 4.4.6 presents this approach, which first computes the frequency of the nominal flutter mode and then computes a robust flutter margin from the μ upper bound evaluated near that frequency.

Algorithm 4.4.6 (robust flutter margin with reduced frequency grid):

Given the system in figure 4.2:
Compute frequency ω associated with nominal flutter dynamics using algorithm 4.4.2.
Define dense frequency grid Ω centered around ω.
Compute robust flutter margin from μ upper bound evaluated at Ω using algorithm 4.4.5.

A large and dense frequency grid increases the confidence that computed robustness measure is actually an upper bound for μ. Algorithm 4.4.6 must be used with caution because the assumptions behind its use may not be satisfied. Computing a robust flutter margin with a dense frequency grid for a particular aircraft at several Mach numbers and then comparing the frequencies of the flutter dynamics to those of the nominal flutter dynamics is recommended. If these frequencies are similar, then algorithm 4.4.6 can be considered for further analysis at different Mach numbers.

4.5 Properties of the Structured Singular Value as a Flutter Margin

The flutter computation method described herein uses μ as the worst-case flutter parameter. The structured singular value is a much more informative flutter margin than traditional parameters such as pole location and modal damping, so μ presents several advantages as a flutter parameter.

The conservatism introduced by considering the worst-case uncertainty perturbation can be interpreted as a measure of sensitivity. Robust μ values that are significantly different than the nominal flutter margins indicate the plant is highly sensitive to modeling errors and changes in flight condition. A small perturbation to the system can drastically alter the flutter stability properties. Conversely, similarity between the robust and nominal flutter margins indicates the aircraft is not highly sensitive to small perturbations.

Robustness analysis determines not only the norm of the smallest destabilizing perturbation but also the direction. This information relates exact perturbations for which the system is particularly sensitive. Thus, μ can indicate the worst-case flutter mechanism, which may naturally extend to indicate active and passive control strategies for flutter suppression.

Damping is only truly informative at the point of instability because stable damping at a given flight condition does not necessarily indicate an increase in dynamic pressure will be a stable flight condition.[37] The structured singular value computes the smallest destabilizing perturbation, which indicates the nearest flight conditions that will cause a flutter instability. In this respect, μ is a stability predictor and damping is merely a stability indicator.

These characteristics of μ make the worst-case flutter algorithm especially valuable for flight test programs. Aeroelastic flight data can be measured at a stable flight condition and used to evaluate uncertainty operators. Unlike damping estimation, the μ method does not require the aircraft to approach instability for accurate prediction. The μ can be computed to update the stability margins with respect to the new uncertainty levels. The worst-case stability margin then indicates what flight conditions can be safely considered.

Safe and efficient expansion of the flight envelope can be performed using an on-line implementation of the worst-case stability estimation algorithm. Computing μ does not introduce an excessive computational burden because each F/A-18 flutter margin presented herein was derived in less than 2 min using standard off-the-shelf hardware and software packages. The predictive nature of μ and the computational efficiency allow a flutterometer tool to be developed that tracks the flutter margin during a flight test.[38]

CHAPTER 5
UNCERTAINTY DESCRIPTIONS IN AEROELASTIC MODELS

5.1 Parametric Uncertainty in Structural Models

Parametric uncertainty denotes operators that describe errors and unmodeled variations in specific elements and coefficients in dynamic system equations. Recall the generalized aeroelastic equation of motion for state vector $\eta \in \mathbf{R}^n$.[21]

$$M\ddot{\eta} + C\dot{\eta} + K\eta + \bar{q}Q(s)\eta = 0 \tag{54}$$

Robust flutter margins computed with the μ method are strongly affected by the choice of uncertainty descriptions associated with these dynamics, so this uncertainty must be a reasonable indicator of potential modeling errors. Parametric uncertainty can be directly associated with the structural matrices to indicate specific errors in the finite-element model.

Define an operator, $\Delta_K \in \mathbf{R}^{n \times n}$, that describes additive uncertainty of a nominal stiffness matrix K_o. Associate a weighting matrix, $W_K \in \mathbf{R}^{n \times n}$, with this uncertainty such that a stability analysis should consider a range of stiffness matrices described by all Δ_K with $\|\Delta_K\|_\infty \leq 1$.

$$K = K_o + W_K \Delta_K \tag{55}$$

Parametric uncertainty can also be associated with structural elements in a multiplicative relationship. Define an operator, $\Delta_C \in \mathbf{R}^{n \times n}$, that describes multiplicative uncertainty of the nominal damping matrix C_o. A weighting $W_C \in \mathbf{R}^{n \times n}$ is again associated with the uncertainty such that the anticipated range of damping matrices for robust stability analysis is described by all Δ_C with $\|\Delta_C\|_\infty \leq 1$.

$$C = C_o(I + W_C\Delta_C) \tag{56}$$

The choice of additive uncertainty for Δ_K and multiplicative uncertainty for Δ_C does not reflect any generalized assumptions regarding the proper way to model errors in stiffness and damping; rather, each type is included to demonstrate the different mathematical derivations. Additive and multiplicative operators are common types of uncertainty models, so demonstrating how these types of uncertainty are associated with a structural model is instructive. The actual choice of Δ_K and Δ_C is problem-dependent and can vary with different aircraft and different finite-element modeling procedures.

The uncertainty operators are described in this section as $\Delta_K, \Delta_C \in \mathbf{R}^{n \times n}$ with real elements because the operators describe perturbations to the generalized stiffness and damping matrices that are usually real. These operators are often additionally constrained to be diagonal operators with n independent parameters because the generalized stiffness and damping are often computed as real diagonal matrices. The real and diagonal nature of these uncertainties is not required for μ analysis, so full-block complex uncertainties can be used if they better describe the nature of the modeling errors.

Also, the weighting functions $W_K, W_C \in \mathbf{R}^{n \times n}$ are presented as constant and real matrices because the functions are associated with constant and real stiffness and damping matrices. These constraints on

the weightings can be relaxed if the nature of the uncertainty is best described by complex and frequency-varying weighting functions.

Substitute the uncertain K and C into the equation of motion, including the state-space representation of the unsteady aerodynamic forces Q(s) presented in section 4.1. Introduce a perturbation, $\delta_{\bar{q}}$, to dynamic pressure, and separate the nominal dynamics from the unknown terms.

$$\begin{aligned}
0 &= M\ddot{\eta} + C\dot{\eta}(K + \bar{q}D_Q)\eta + \bar{q}C_Q x \\
&= M\ddot{\eta} + C_o(I + W_C\Delta_C)\dot{\eta} + (K_o + W_K\Delta_K + (\bar{q}_o + \delta_{\bar{q}})D_Q)\eta + (\bar{q}_o + \delta_{\bar{q}})C_Q x \\
&= \ddot{\eta} + [M^{-1}C_o\dot{\eta} + M^{-1}(K_o + \bar{q}_o D_Q)\eta + \bar{q}_o M^{-1}C_Q x] \\
&\quad + \delta_{\bar{q}}[M^{-1}D_Q\eta + M^{-1}C_Q x] + \Delta_K[M^{-1}W_K\eta] + \Delta_C[M^{-1}C_o W_C\dot{\eta}] \\
&= \ddot{\eta} + [M^{-1}C_o\dot{\eta} + M^{-1}(K_o + \bar{q}_o D_Q)\eta + \bar{q}_o M^{-1}C_Q x] + \delta_{\bar{q}} z_{\bar{q}} + \Delta_K z_K + \Delta_C z_C \\
&= \ddot{\eta} + [M^{-1}C_o\dot{\eta} + M^{-1}(K_o + \bar{q}_o D_Q)\eta + \bar{q}_o M^{-1}C_Q x] + w_{\bar{q}} + w_K + w_C
\end{aligned} \tag{57}$$

The signals $z_{\bar{q}}$ and $w_{\bar{q}}$ are introduced in section 4.2 to relate the perturbation in dynamic pressure to the nominal plant through a feedback relationship. The feedback operation $w_{\bar{q}} = \delta_{\bar{q}} z_{\bar{q}}$ is used where $z_{\bar{q}}$ is a linear combination of the states of the plant.

$$z_{\bar{q}} = M^{-1}D_Q\eta + M^{-1}C_Q x \tag{58}$$

Additional signals are introduced to the plant formulation, where z_K and w_K are associated with the uncertainty in the stiffness matrix, and z_C and w_C are associated with the uncertainty in the damping matrix. The outputs of the plant z_K and z_C are formulated as linear combinations of the states.

$$\begin{aligned}
z_K &= M^{-1}W_K\eta \\
z_C &= M^{-1}W_C C_o\dot{\eta}
\end{aligned} \tag{59}$$

The feedback mechanism to describe the modeling uncertainty uses a relationship between these output signals and the w_K and w_C input signals.

$$\begin{aligned}
w_K &= \Delta_K z_K \\
w_C &= \Delta_C z_C
\end{aligned} \tag{60}$$

The state-space plant matrix can be formulated using these additional input and output signals.

$$\left[\begin{array}{c} \dot{\eta} \\ \ddot{\eta} \\ \dot{x} \\ \hline z_{\bar{q}} \\ z_K \\ z_C \end{array}\right] = \left[\begin{array}{ccc|ccc} 0 & I & 0 & 0 & 0 & 0 \\ -M^{-1}(K_o + \bar{q}_o D_Q) & -M^{-1}C & -\bar{q}M^{-1}C_Q & -I & -I & -I \\ B_Q & 0 & A_Q & 0 & 0 & 0 \\ \hline M^{-1}D_Q & 0 & M^{-1}C_Q & 0 & 0 & 0 \\ M^{-1}W_K & 0 & 0 & 0 & 0 & 0 \\ 0 & M^{-1}C_o W_C & 0 & 0 & 0 & 0 \end{array}\right] \left[\begin{array}{c} \eta \\ \dot{\eta} \\ x \\ \hline w_{\bar{q}} \\ w_K \\ w_C \end{array}\right] \tag{61}$$

Figure 5.1 shows how the uncertainty operators and perturbation to dynamic pressure affect this plant formulation in a feedback manner.

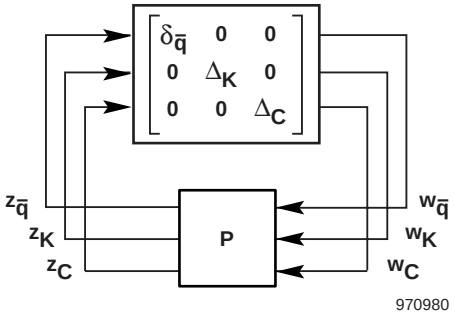

Figure 5.1. Linear fractional transformation system for robust stability analysis in the μ framework with parameterization around perturbation in dynamic pressure and uncertainty in structural stiffness and damping matrices.

The formulation does not directly allow uncertainty in mass to be described by a feedback operator. The LFT and μ frameworks require uncertainty operators to affect the nominal dynamics in a linear manner, and this requirement precludes introducing mass uncertainty. The inverse of the mass matrix scales most terms in the state matrix of P(s), including terms involving $\bar{q}$. Associating a mass uncertainty operator Δ_M with the mass matrix scaling $\bar{q}$ would introduce terms of $\Delta_M \delta_{\bar{q}}$, which is a nonlinear function of uncertainty operators and cannot be directly considered by the μ method.

5.2 Parametric Uncertainty in Aerodynamic Models

The unsteady aerodynamic forces $Q(s) \in \mathbf{C}^{n \times n}$ can be represented as a state-space model with n_Q states.

$$Q(s) = D_Q + C_Q (sI - A_Q)^{-1} B_Q \tag{62}$$

Parametric uncertainty can be associated with the matrix elements of this state-space representation to describe errors. These errors can result from several sources in the modeling procedure, including computational fluid dynamic algorithms that determine the frequency-varying forces and the system identification algorithms that represent the computational values as a state-space system.

Define an operator $\Delta_{A_Q} \in \mathbf{R}^{n_Q \times n_Q}$ to describe uncertainty in the state matrix of Q(s). This operator directly affects a nominal A_{Q_o} and describes errors and variations in the poles of the state-space representation of the unsteady aerodynamic forces. Include a weighting function $W_{A_Q} \in \mathbf{R}^{n \times n}$ such that the range of state matrices to be considered by robust stability analysis is described by all Δ_{A_Q} with $\left\|\Delta_{A_Q}\right\|_\infty \le 1$.

$$A_Q = A_{Q_o} + W_{A_Q}\Delta_{A_Q} \tag{63}$$

Define also an operator $\Delta_{B_Q} \in \mathbf{R}^{n_Q \times n}$ to describe multiplicative uncertainty in a nominal B_{Q_o} matrix of Q(s). A weighting function $W_{B_Q} \in \mathbf{R}^{n_Q \times n}$ is associated with this uncertainty such that the range of possible B_Q matrices is described by all Δ_{B_Q} with $\left\|\Delta_{B_Q}\right\|_\infty \le 1$.

$$B_Q = B_{Q_o}(I + W_{B_Q}\Delta_{B_Q}) \tag{64}$$

The choice of additive and multiplicative operators is made for reasons similar to those presented in section 5.1. One of each type of uncertainty is included to demonstrate the derivation procedures of how each uncertainty is associated with the nominal aeroelastic dynamics in a feedback relationship. The actual choice of which type of uncertainty is most suitable to describe errors in A_Q and B_Q is problem-dependent.

Also, defining the uncertainty operators as real and weightings that are real and constant is not a requirement. This section presents the problem formulation with these definitions because associating these types of uncertainties and weightings with the constant real A_Q and B_Q matrices makes intuitive sense. Certainly μ can also compute robust flutter margins with respect to complex frequency-varying weighted uncertainties.

The nominal aeroelastic model in section 4.2 defined the vector x as the states associated with the state-space model Q(s). The matrices A_Q and B_Q directly affect the aeroelastic dynamics only through the state derivative equation for x and do not appear in the other state derivative equations. The aeroelastic plant can be formulated in the μ framework by substituting the uncertain values of A_Q and B_Q into this state derivative equation without considering changes in the derivative equations for the remaining states η and $\dot{\eta}$.

$$\begin{aligned}
\dot{x} &= A_Q x + B_Q \eta \\
&= (A_{Q_o} + W_{A_Q}\Delta_{A_Q})x + B_{Q_o}(I + W_{B_Q}\Delta_{B_Q})\eta \\
&= A_{Q_o}x + B_{Q_o}\eta + \Delta_{A_Q}W_{A_Q}x + \Delta_{B_Q}W_{B_Q}B_{Q_o}\eta \\
&= A_{Q_o}x + B_{Q_o}\eta + \Delta_{A_Q}z_{A_Q} + \Delta_{B_Q}z_{B_Q} \\
&= A_{Q_o}x + B_{Q_o}\eta + w_{A_Q} + w_{B_Q}
\end{aligned} \tag{65}$$

Several signals are introduced to this equation, where z_{A_Q} and w_{A_Q} are associated with the uncertainty in A_Q and z_{B_Q}, and w_{B_Q} is associated with the uncertainty in B_Q. The signals z_{A_Q} and z_{B_Q} are output from the plant matrix as linear combinations of the states.

$$\begin{aligned} z_{A_Q} &= W_{A_Q} x \\ z_{B_Q} &= W_{B_Q} B_{Q_o} \eta \end{aligned} \tag{66}$$

The feedback mechanism to describe the modeling uncertainty uses a relationship between these output signals and the w_K and w_C input signals.

$$\begin{aligned} w_{A_Q} &= \Delta_{A_Q} z_{A_Q} \\ w_{B_Q} &= \Delta_{B_Q} z_{B_Q} \end{aligned} \tag{67}$$

The state-space plant matrix can be formulated using these additional input and output signals.

$$\left[\begin{array}{c} \dot{\eta} \\ \ddot{\eta} \\ \dot{x} \\ \hline z_{\bar{q}} \\ z_{A_Q} \\ z_{B_Q} \end{array}\right] = \left[\begin{array}{ccc|ccc} 0 & I & 0 & 0 & 0 & 0 \\ -M^{-1}(K_o + \bar{q}_o D_Q) & -M^{-1}C_o & -\bar{q}M^{-1}C_Q & -I & 0 & 0 \\ B_{Q_o} & 0 & A_{Q_o} & 0 & I & I \\ \hline M^{-1}D_Q & 0 & M^{-1}C_Q & 0 & 0 & 0 \\ 0 & 0 & W_{A_Q} & 0 & 0 & 0 \\ W_{B_Q}B_{Q_o} & 0 & 0 & 0 & 0 & 0 \end{array}\right] \left[\begin{array}{c} \eta \\ \dot{\eta} \\ x \\ \hline w_{\bar{q}} \\ w_{A_Q} \\ w_{B_Q} \end{array}\right] \tag{68}$$

Figure 5.2 shows how the uncertainty operators and perturbation to dynamic pressure affect this plant formulation in a feedback manner.

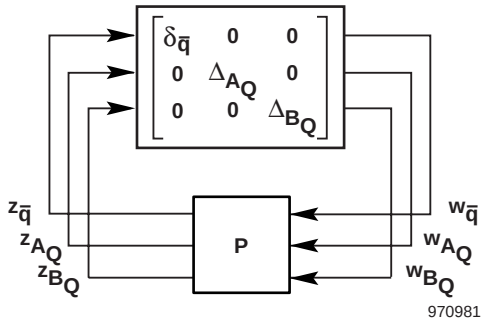

Figure 5.2. Linear fractional transformation system for robust stability analysis in the μ framework with parameterization around perturbation in dynamic pressure and uncertainty in A_Q and B_Q matrices of the state-space Q(s) model.

Associating a Δ_{B_Q} uncertainty operator with the B_Q matrix may not seem immediately useful because considering errors in the poles determined by the A_Q matrix is often intuited. This Δ_{B_Q} uncertainty can be essential to accurately describe the modeling errors because errors in terms common to both A_Q and B_Q may exist. Such a situation arises for certain modeling representations of aerodynamic lags. Consider a simplified Roger's form Q(s) matrix that uses two Padé approximations to represent lag terms.

$$Q(s) = \frac{s}{s+\beta_1} + \frac{s}{s+\beta_2} = \left[\begin{array}{cc|c} -\beta_1 & 0 & -\beta_1 \\ 0 & -\beta_2 & -\beta_2 \\ \hline 1 & 1 & 2 \end{array}\right] \tag{69}$$

The poles of this system are determined entirely by the A_Q matrix, so uncertainty in the poles can be entirely described by a Δ_{A_Q} operator associated with the A_Q matrix. A similar uncertainty Δ_{B_Q} should also be associated with the B_Q matrix in this case because the β_1 and β_2 terms appear in both A_Q and B_Q. Allowing variation in A_Q but not in B_Q will introduce unwanted zeros to the system, so the proper way to model pole uncertainty for this formulation is to include both Δ_{A_Q} and Δ_{B_Q} operators.

The Padé approximation appears often in aeroelastic models, so demonstrating the LFT formulation of Q(s), which includes the uncertainties in poles β_1 and β_2 in a feedback relationship, may be useful. The uncertainties in Q(s) can be developed distinctly from the structural uncertainties because LFT operations allow the structural and aerodynamic models to be combined into a single plant model with a structured uncertainty description.[10]

Define real scalar operators Δ_{B_1} and Δ_{B_2} to describe uncertainty associated with nominal values of the poles β_{1_o} and β_{2_o}. Real scalar weightings W_{β_1} and W_{β_2} normalize the uncertainty such that the range of poles to be considered by robust stability analysis is described by all Δ_{B_1} with $\|\Delta_{B_1}\|_\infty \le 1$ and all Δ_{β_2} with $\|\Delta_{\beta_2}\|_\infty \le 1$.

$$\begin{aligned} \beta_1 &= \beta_{1_o} + W_{\beta_1}\Delta_{\beta_1} \\ \beta_2 &= \beta_{2_o} + W_{\beta_2}\Delta_{\beta_2} \end{aligned} \tag{70}$$

Define states x_1 and x_2 of Q(s), and consider an input signal u_Q that generates the output signal y_Q by the relationship $y_Q = Qu_Q$. Substitute the uncertain β_1 into the state equation of x_1.

$$\begin{aligned} \dot{x}_1 &= -\beta_1 x_1 - \beta_1 u_Q \\ &= -(\beta_{1_o} + W_{\beta_1}\Delta_{\beta_1})x_1 - (\beta_{1_o} + W_{\beta_1}\Delta_{\beta_1})u_Q \\ &= -\beta_{1_o}x_1 - \beta_{1_o}u_Q - \Delta_{\beta_1}(W_{\beta_1}x_1 + W_{\beta_1}u_Q) \\ &= -\beta_{1_o}x_1 - \beta_{1_o}u_Q - \Delta_{\beta_1}z_{\beta_1} \\ &= -\beta_{1_o}x_1 - \beta_{1_o}u_Q - w_{\beta_1} \end{aligned} \tag{71}$$

Perform a similar derivation for the state equation of x_2.

$$\begin{aligned}
\dot{x}_2 &= -\beta_2 x_2 - \beta_2 u_Q \\
&= -(\beta_{2_o} + W_{\beta_2}\Delta_{\beta_2})x_2 - (\beta_{2_o} + W_{\beta_2}\Delta_{\beta_2})u_Q \\
&= -\beta_{2_o} x_2 - \beta_{2_o} u_Q - \Delta_{\beta_2}(W_{\beta_2} x_2 + W_{\beta_2} u_Q) \\
&= -\beta_{2_o} x_2 - \beta_{2_o} u_Q - \Delta_{\beta_2} z_{\beta_2} \\
&= -\beta_{2_o} x_2 - \beta_{2_o} u_Q - w_{\beta_2}
\end{aligned} \tag{72}$$

The signals z_{β_1} and w_{β_1} are introduced as plant output and input signals to related the uncertainty Δ_{B_1} in a feedback manner. The signals z_{β_1} and w_{β_1} are similarly introduced to relate the uncertainty Δ_{B_2} in a feedback manner. The state-space matrix can be formulated to describe the nominal $Q_o(s)$ with these additional input and output signals.

$$\begin{bmatrix} \dot{x}_1 \\ \dot{x}_2 \\ \hline z_{\beta_1} \\ z_{\beta_2} \\ y_Q \end{bmatrix} = \left[\begin{array}{cc|ccc} -\beta_{1_o} & 0 & -1 & 0 & -\beta_{1_o} \\ 0 & -\beta_{2_o} & 0 & -1 & -\beta_{2_o} \\ \hline W_{\beta_1} & 0 & 0 & 0 & W_{\beta_1} \\ 0 & W_{\beta_2} & 0 & 0 & W_{\beta_2} \\ 1 & 1 & 0 & 0 & 2 \end{array}\right] \begin{bmatrix} x_1 \\ x_2 \\ \hline w_{\beta_1} \\ w_{\beta_2} \\ u_Q \end{bmatrix} \tag{73}$$

Figure 5.3 shows the block diagram for Q(s) and the uncertainties.

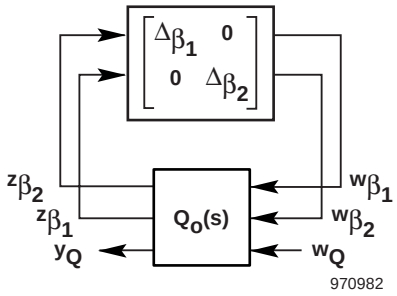

Figure 5.3. Linear fractional transformation system describing Padé approximation to represent unsteady aerodynamic force matrix in the μ framework with uncertainty in lag terms.

5.3 Dynamic Uncertainty

Dynamic uncertainty operators are often associated with aeroelastic models to account for modeling errors that are not efficiently described by parametric uncertainty. Unmodeled dynamics and inaccurate mode shapes are examples of modeling errors that can be described with less conservatism by dynamic

uncertainties than with parametric uncertainties. These dynamic uncertainties are typically complex in order to represent errors in both magnitude and phase of signals.

Consider a system P having two modes with natural frequencies at 4 rad/sec and 30 rad/sec.

$$P = \left(\frac{16}{s^2 + 0.4s + 16}\right)\left(\frac{900}{s^2 + 0.6 + 900}\right) \tag{74}$$

Define a nominal model P_o, which will be used for stability analysis of the system but does not model the high-frequency mode of P.

$$P_o = \left(\frac{16}{s^2 + 0.4s + 16}\right) \tag{75}$$

The large difference in natural frequency between the high- and low-frequency modes of P precludes parametric uncertainty associated with the low-frequency mode of P_o from being a reasonable description of the modeling errors in P_o. The magnitude of any parametric uncertainty associated with the low-frequency mode would need to be extremely large to account for the unmodeled high-frequency dynamics, so the stability analysis would be relatively meaningless because the large uncertainty would imply the plant is not accurate at any frequencies.

A multiplicative uncertainty operator, $\Delta \in \mathbf{C}$, can be used to describe the high-frequency modeling error without introducing the excessive conservatism resulting from a parametric uncertainty description. Associate a complex, scalar, weighting function $W(s) \in \mathbf{C}$ with this uncertainty to reflect the frequency-varying levels of modeling errors.

$$W = 100\frac{s + 0.5}{s + 500} \tag{76}$$

The set of plants $\mathcal{P}$ used for robust stability analysis is formulated to account for the range of dynamics as described by the norm-bounded multiplicative uncertainty Δ.

$$\mathcal{P} = \{P_o (I + W\Delta) \ : \ \|\Delta\|_\infty \leq 1\} \tag{77}$$

Figure 5.4 shows the block diagram for robust stability analysis of $\mathcal{P}$.

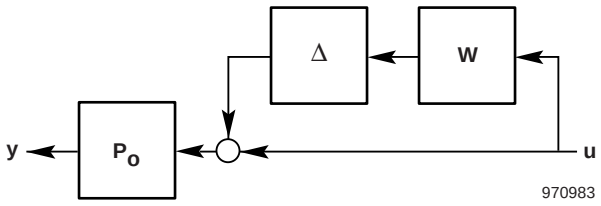

Figure 5.4. Family of plants $\mathcal{P} = P_o (I + \Delta W)$ with input multiplicative uncertainty.

Figure 5.5 shows the magnitude of the transfer function from input to output for P and P_o, and the maximum magnitude of $|P_o (I + W\Delta)|$, which is an upper bound for the output of P at each frequency. The multiplicative uncertainty is able to bound the modeling error at the high-frequency mode without introducing excessive conservatism from large uncertainty associated with the low-frequency mode.

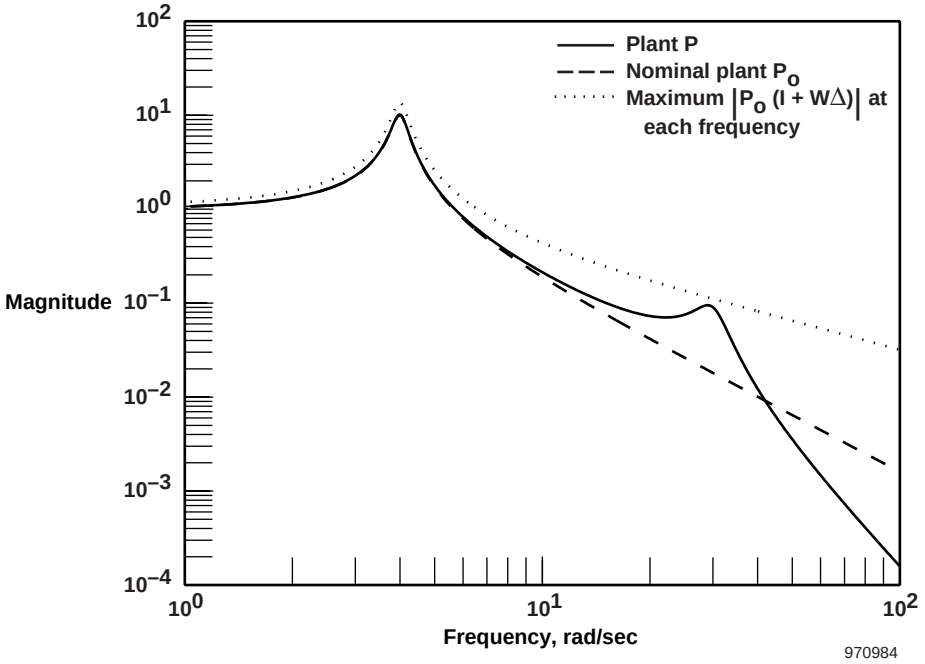

Figure 5.5. Transfer functions for example system with multiplicative uncertainty.

Dynamic additive operators may also be required in the uncertainty description to account for errors that are not efficiently described by either multiplicative and parametric uncertainties. Modeling errors associated with a zero of the system dynamics are an example of an error that is best described by additive uncertainty. Multiplicative operators are not useful in this case because $P_o(j\omega) = 0$ at the frequency ω associated with the zero of nominal model and, correspondingly, every member of the set of plants $P_o(j\omega)(I + W\Delta) = 0$ at this frequency. Additive uncertainty allows the system output for some member of the set of plants to be nonzero even at frequencies of the zeros of the nominal plant.

Consider a plant P with several poles and zeros.

$$P = \frac{16}{64}\left(\frac{s^2 + 0.48s + 64}{s^2 + 0.48s + 16}\right)\left(\frac{900}{s^2 + 0.6s + 900}\right) \tag{78}$$

Assume the nominal plant P_o of this plant is similar to P and has the correct number of poles and zeros, but the coefficients of the system equations are incorrect.

$$P_o = \frac{16}{36}\left(\frac{s^2 + 0.36s + 36}{0s^2 + 0.4s + 16}\right)\left(\frac{900}{s^2 + 0.6s + 900}\right) \tag{79}$$

Define an additive uncertainty operator $\Delta \in \mathbf{C}$ that is normalized by a complex, scalar function W to reflect the frequency-varying levels of the modeling errors.

$$W = 0.1 \frac{s + 50}{s + 5} \tag{80}$$

The set of plants $\mathcal{P}$ used for robust stability analysis is formulated to account for the range of dynamics as described by the norm-bounded additive uncertainty Δ.

$$\mathcal{P} = \{ P_o + W\Delta \ : \ \|\Delta\|_\infty \leq 1 \} \tag{81}$$

Figure 5.6 shows the block diagram for robust stability analysis of $\mathcal{P}$.

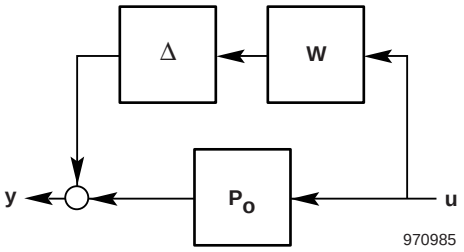

Figure 5.6. Family of plants $\mathcal{P} = P_o + W\Delta$ with additive uncertainty.

Figure 5.7 shows the magnitude of the transfer function from input to output for P and P_o, and the maximum magnitude of $|P_o + W\Delta|$ at each frequency. The additive uncertainty bounds the modeling error at each frequency, including the frequencies near the zero of the nominal plant, because the output of P is bounded above by the maximum magnitude of the members of the set $\mathcal{P}$.

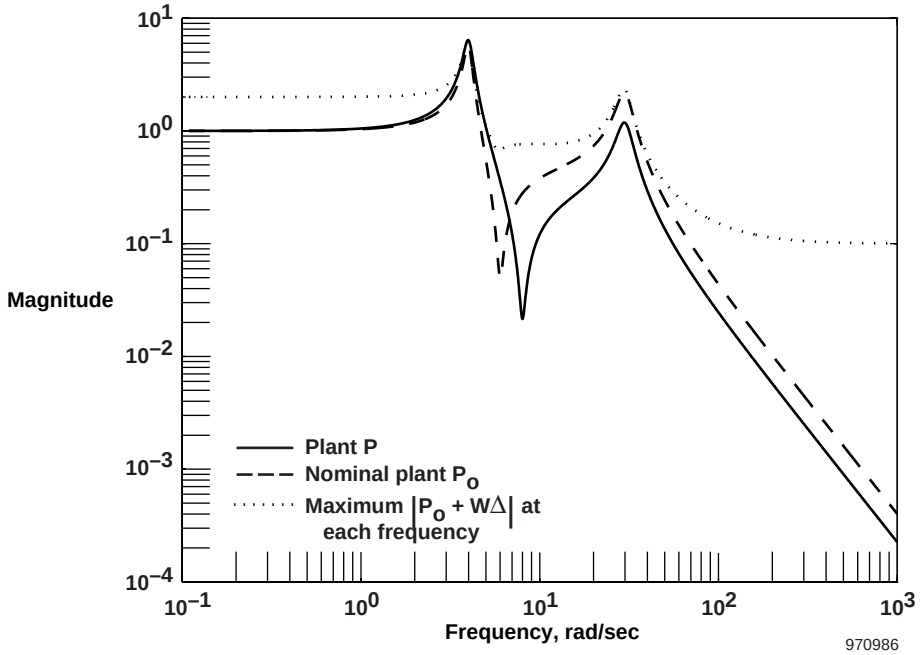

Figure 5.7. Transfer functions for example system with additive uncertainty.

These multiplicative and additive uncertainties are particularly important when comparing an analytical transfer function with experimental transfer functions derived from flight data. Analytical models are often computed for a low range of frequencies because the high frequencies add complexity to the model but do not always affect the stability margins of the aircraft. The experimental data may indicate a high-frequency mode that is not included in the analytical model, so a frequency-weighted dynamic multiplicative uncertainty can be associated with the model.

The issue of mode shape uncertainty is often encountered when comparing low-frequency-predicted dynamical responses with flight data because sensor measurements are directly affected by the mode shapes. Both multiplicative and additive uncertainties may be required to accurately model mode shape errors and account for inaccurate response levels (which may be higher than predicted at some frequencies but lower than predicted at others) and inaccurate frequencies associated with poles and zeros.

5.4 Uncertainty Associated with Nonlinearities

The μ framework described uses linear operators to represent dynamical models and associated uncertainties but does not admit nonlinear operators. The μ framework is useful for analyzing aircraft stability despite the constraints of linearity because physical systems, which are always nonlinear, can often be approximated by linear models to a high degree of accuracy. A classic example of this situation notes the linearized dynamics are often an acceptable representation of an aircraft operating near trim flight conditions, so linear models work well in practice for control synthesis and stability analysis.[39]

Nonlinear dynamics cannot always be accurately described by a linearized dynamics model, so the stability analysis should consider the effects of these nonlinearities.[40] The μ framework can associate linear uncertainty operators with linear models to describe the errors resulting from some types of unmodeled nonlinear dynamics. The uncertainty does not actually represent the nonlinearity; rather, the uncertainty allows the linear system responses to vary with sufficient magnitude to bound a range of nonlinear system responses.

Separating the nonlinear dynamics that cannot be linearized from the nonlinear dynamics that can be accurately represented by linear models is useful. Separate uncertainty descriptions can be formulated for each dynamical block, and the resulting operators can be combined using the LFT framework to formulate a single, linear, plant model with a structured uncertainty description. Figure 5.8 shows an example LFT system representation for a nominal plant P_o and associated uncertainty Δ, and a nominal linear model N_o and associated uncertainty Δ_N representing a system element with nonlinear dynamics.

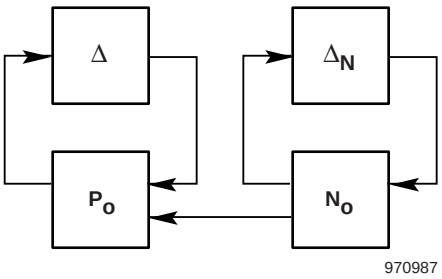

Figure 5.8. Linear fractional transformation system with nominal models and associated uncertainty operators.

The system shown in figure 5.8 is commonly used to describe the coupling between the aeroelastic dynamics and actuators affecting an aircraft through control surfaces. Actuators can display many types of nonlinear behaviors and should be considered in the aeroelastic stability analysis, because pilot and autopilot commands that maintain trim during flight ensure the control surfaces are continuously moving.[41] The errors in linear models resulting from unmodeled actuator dynamics such as nonlinear stiffness parameters or hysteresis functions can sometimes be described by a linear uncertainty operator.

Consider the response y of a nonlinear system N that models a system that has a nonlinear stiffness corresponding to a hardening spring that is valid for the bounded input signal $u \in [-10, 10]$. Such a system can represent an element of an actuator model or a nonlinear structural model.

$$y = Nu = 2u + 0.02u^2 + 0.0082u^3 \tag{82}$$

Define a linear nominal model N_o such that $y = N_o u$ approximates the response of N.

$$N_o = 2 \tag{83}$$

Associate an additive weighting operator Δ_N with N_o such that stability analysis considers the set of plants $\mathcal{N}$.

$$\mathcal{N} = \{N_o + \Delta_N : \|\Delta_N\|_\infty \le 1\} \tag{84}$$

Figure 5.9 shows that the maximum and minimum magnitudes of the responses of the set $\mathcal{N}$ are able to bound the response of the nonlinear system N for the range $u \in [-10, 10]$. These bounds are overly conservative throughout this operating range, but they achieve the desired goal of describing errors in the linear system response resulting from the unmodeled nonlinearity.

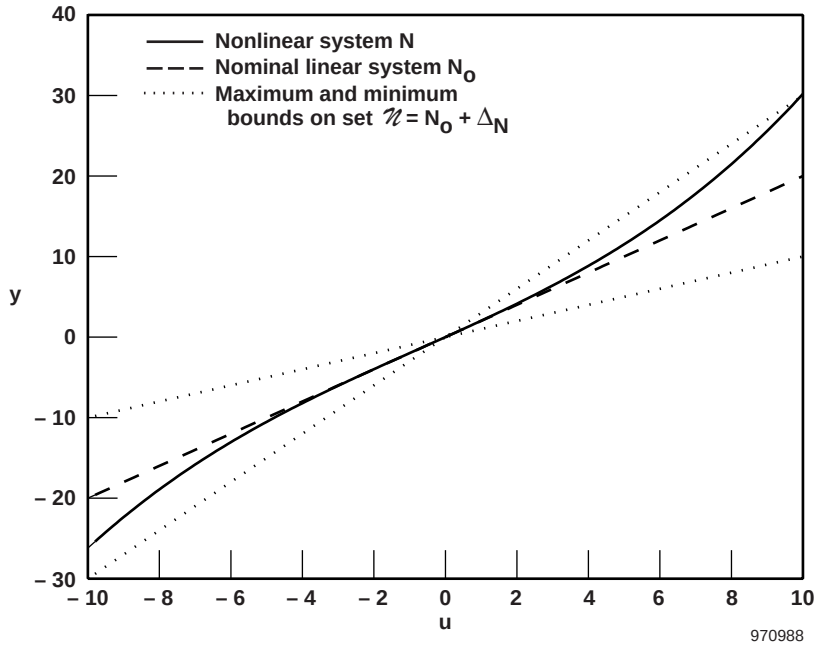

Figure 5.9. System responses for hardening spring example.

A similar procedure can be used to describe error caused by an unmodeled nonlinear softening spring. Consider the response y of a system represented by N that is valid for an input signal $u \in [-10, 10]$.

$$y = Nu = 2u + 0.005u^2 - 0.005u^3 \tag{85}$$

Define a linear nominal model N_o such that $y = N_o u$ approximates the response of N.

$$N_o = 2 \tag{86}$$

Associate an additive weighting operator Δ_N with N_o such that stability analysis considers the set of plants $\mathcal{N}$.

$$\mathcal{N} = \{N_o + \Delta_N : \|\Delta_N\|_\infty \le 1\} \tag{87}$$

Figure 5.10 shows that the maximum and minimum magnitudes of the responses of the set $\mathcal{N}$ are able to bound the response of the nonlinear system N for the range $u \in [-10, 10]$. These bounds are also overly conservative throughout this operating range, but they achieve the desired goal of describing errors in the linear system response resulting from the unmodeled nonlinearity.

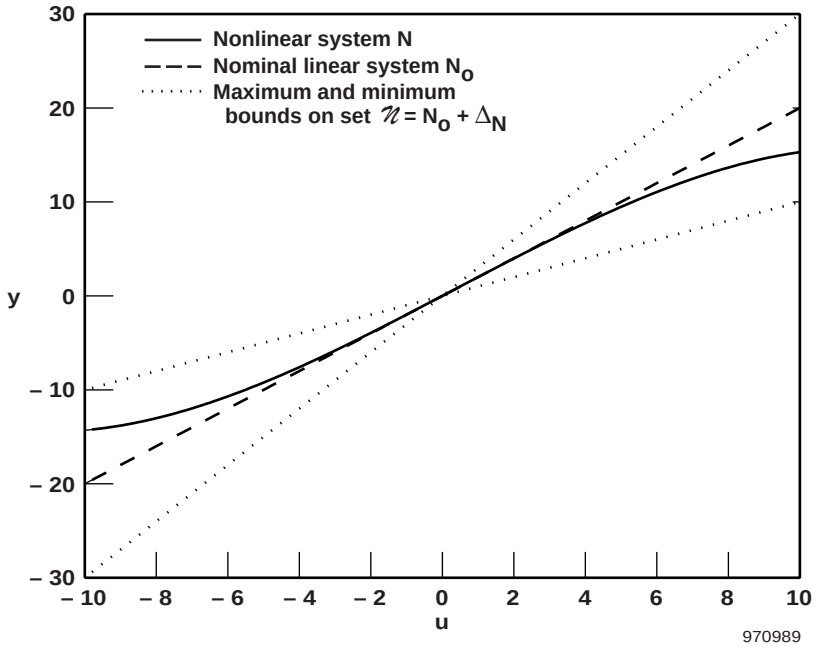

Figure 5.10. System responses for softening spring example.

Another nonlinearity that commonly affects aeroelastic systems is hysteresis. The response of a hysteretic system depends on the trend of the input signal such that an increasing input signal generates a certain response, but a decreasing input signal generates a different response. Such hysteresis dynamics are difficult to express as a simple mathematical formula, so for illustrative purposes, assume N is a nonlinear hysteresis function whose response y depends on the trend of the input signal. Define a linear nominal model N_o whose response $y = N_o u$ approximates the response of the hysteretic N.

$$N_o = 2 \tag{88}$$

Associate an additive weighting operator Δ_N with N_o such that stability analysis considers the set of plants $\mathcal{N}$.

$$\mathcal{N} = \{ N_o + \Delta_N \ : \ \|\Delta_N\|_\infty \leq 1 \} \tag{89}$$

Figure 5.11 shows that the maximum and minimum magnitudes of the responses of the set $\mathcal{N}$ are able to bound the response of the nonlinear system N with the hysteresis for the range $u \in [-10, 10]$. Again, the bounds resulting from a linear uncertainty description are overly conservative throughout this operating range, but they achieve the desired goal of describing errors caused by the unmodeled hysteresis nonlinearity.

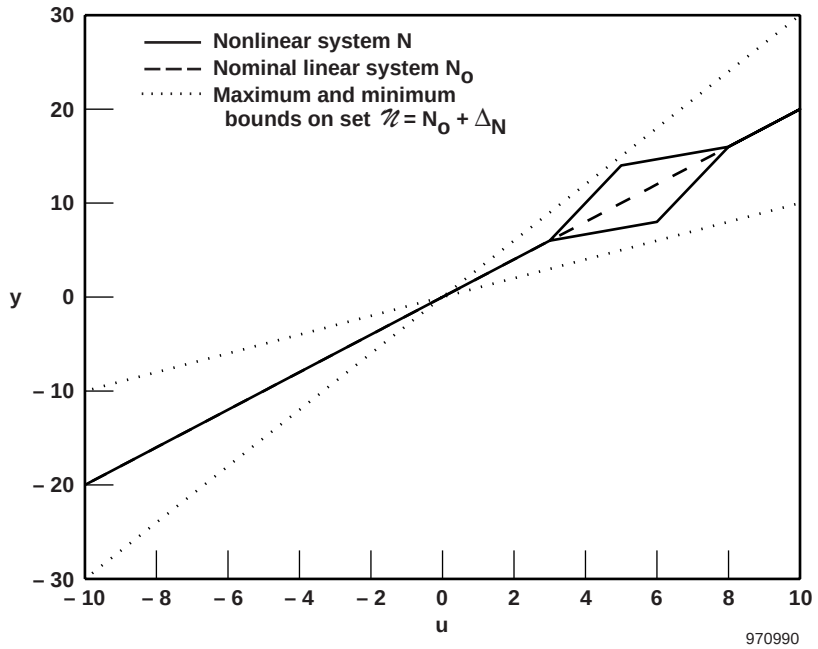

Figure 5.11. System responses for hysteresis example.

Explicitly constraining the operating region of the input signal $u \in [-10, 10]$ can be important to developing reasonable uncertainties to describe errors resulting from unmodeled nonlinearities. The errors in the linear model can grow excessively large when considering a large range of inputs, so the uncertainty magnitude would need to also grow excessively large. The conservatism resulting from such a large uncertainty description may be unacceptable and require the input range to be constrained to more reasonable limits.

The uncertainty description, even for a constrained operating region, will usually be overly conservative when describing modeling errors for certain parts of the operating region. The uncertainty is able to bound the errors in figures 5.9, 5.10, and 5.11, but the maximum and minimum bound are clearly not optimal. Some amount of conservatism is expected when describing errors resulting from unmodeled nonlinearities because a linear model, whether a single plant or a set of plants, will usually not be an accurate representation of a nonlinear system that cannot be linearized.

Also, several types of unmodeled nonlinearities exist that are frequently encountered in aircraft systems but are not easily described by linear uncertainty operators associated with the linear models. Examples of these types of nonlinearities include free play, dead-band responses, friction, and rate limiting of actuators.

The robust stability margins computed from μ with respect to the linear uncertainty operators describing unmodeled nonlinear dynamics will always be somewhat suspect, because this approach cannot consider stability properties unique to nonlinear systems such as bifurcation points and limit-cycle behaviors.[42, 43] This approach limits the usefulness of the μ method to systems for which the nonlinearities have small effects on the response and do not introduce nonlinear instabilities to the critical flutter mechanism.

5.5 Uncertainty Associated With Flight Data

A theoretical model with an associated uncertainty description can be an accurate representation of the aeroelastic dynamics of an aircraft, but responses from that model may not identically match flight data. Additional uncertainties can be associated with the model to describe errors that are observed between the predicted responses and the measured responses from a commanded excitation to the aircraft. These uncertainties do not necessarily indicate errors in the model; rather, these uncertainties indicate errors in the process used to generate aeroelastic responses and measure flight data.

One source of error is an incorrect assumption of excitation force used to generate the predicted and measured responses. The measured excitation force associated with the flight data may not correctly account for poor hardware performance and nonuniform spectral distribution of the force. Also, inexactly phased excitation between multiple force mechanisms can excite modes that are not anticipated by a theoretical analysis. A frequency-varying dynamic uncertainty can be associated with the force input of the analytical model to describe errors in the excitation.

The phenomenon of nonrepeatibility can cause discrepancies between predicted and measured responses from multiple occurrences of excitation signals. Nonrepeatibility affects flight data by introducing slight variations in responses, even for data recorded at identical flight conditions with identical excitation signals. This unexplained behavior may result from some unmodeled nonlinear dynamic or inexact excitation that is not correctly measured. External disturbances such as wind gusts or turbulence can introduce an unmodeled dynamic that inconsistently affects the aircraft responses. A frequency-varying dynamic uncertainty can be associated with the model to describe nonrepeatible data variations.

Another source of error between predicted and measured responses is an incorrect assumption of flight condition. Flight data sets are sometimes generated at test points that attempt to maintain a constant flight condition to match the data sets predicted from a model describing the aeroelastic dynamics at that same flight condition. Slight variations in flight conditions while the experimental response is measured may cause some discrepancy between the predicted response and the flight data. Parametric uncertainty associated with the unsteady aerodynamic model can be used to account for these errors because flight condition variations only affect the aerodynamic model and not the structural model.

The model may accurately represent the mode shapes of the aircraft but have a poor representation of the sensor locations. The responses measured by sensors are inherently dependent on sensor location, with respect to mode shapes, to determine the magnitude and phase of the signal. Additional errors in magnitude and phase are introduced when considering transfer-function estimates generated by signals that violate assumptions used in computational algorithms. A frequency-varying dynamic uncertainty can

be associated with the output of the plant model to describe errors in both mode shape and sensor location predictions.

The choice of signal-processing algorithms can also introduce errors between predicted and measured responses. The Fourier transform, which is the traditional tool for signal processing, assumes several characteristics of the data that may be violated with transient-response aeroelastic data.[44] Filtering and wavelet-based algorithms may be used to reduce errors introduced by signal processing and reduce conservatism in the resulting stability margins.[45, 46] Parameter uncertainty associated with the modal parameters of the linear model may be used to describe some errors in the natural frequencies and dampings observed using flight data analyzed by incorrect algorithms. Dynamic uncertainty may also be required to describe errors introduced by leakage and aliasing effects.

CHAPTER 6
MODEL VALIDATION OF UNCERTAINTY

6.1 Model Validation Using the Structured Singular Value

Robust stability analysis considers the stability of a system subject to a set of modeling errors and perturbations represented by a norm-bounded $\mathbf{\Delta}$. A logical question that arises is how to reasonably determine this set. This issue is important for computing robust flutter margins because μ can be overly conservative if the uncertainty is excessive beyond the true modeling errors and can be overly optimistic if the uncertainty does not sufficiently account for the true modeling errors.

Model validation algorithms can be used to indicate if an uncertainty description is reasonable with respect to flight data.[47] These algorithms consider whether or not a set of data measurements could have been generated by a proposed model that includes the nominal dynamics and associated uncertainty operators and noise and disturbance signals.

Uncertainty operators associated with the nominal plant model specifically in the LFT framework can be considered by validation algorithms.[48] Frequency-domain algorithms are generated that consider the model validation problem in the context of control design.[49] Time-domain approaches are also developed that can be solved with convex optimization algorithms for certain uncertainty structures.[50]

A model validation procedure has been formulated that uses a μ condition to determine if an uncertainty model is invalidated.[51] This procedure uses frequency-domain transfer-function data to determine if some perturbation $\Delta \in \mathbf{\Delta}$ to the nominal plant could produce the measurements. Consider the block diagram for robust stability analysis of systems with measurement y and forcing u signals shown in figure 6.1. The model validation question, as applied to uncertainty models, is given in question 6.1.1.

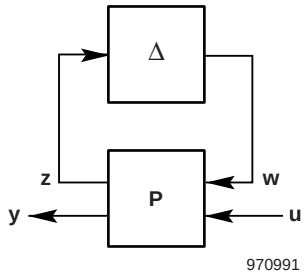

Figure 6.1. Linear fractional transformation system for robust stability analysis and model validation with forcing and measurement signals.

Question 6.1.1 (uncertainty validation): *Is there some frequency-varying* $\Delta \in \mathbf{\Delta}$ *for figure 6.1 such that* $F_u(P, \Delta)$ *could generate the set of observed data* y *and* u*?*

Define $P(s) \in \mathbf{C}^{n_o + n_z \times n_i + n_w}$ as a stable transfer-function system matrix such that $P \in \mathcal{RH}_\infty$. Partition this matrix into four elements such that $P_{11}(s) \in \mathbf{C}^{n_z \times n_w}$, $P_{22}(s) \in \mathbf{C}^{n_o \times n_i}$, and $P_{12}(s)$ and $P_{21}(s)$ are of appropriate size. $P_{22}(s)$ is the nominal-plant transfer function in the absence of uncertainty.

$$P = \begin{bmatrix} P_{11} & P_{12} \\ P_{21} & P_{22} \end{bmatrix} \tag{90}$$

Robust stability analysis of this system is determined using the transfer function P_{11}, which contains the feedback relationship between the plant dynamics and the uncertainty operator. The robust stability condition given by theorem 3.3.3 requires $\mu(P_{11}) < 1$.

The model validation condition uses these elements of P and the finite-energy frequency-domain signals y, $u \in \mathcal{H}_2$ where the measurements are scalar functions y, $u \in \mathbf{C}$. Formulate the following two matrices.

$$\begin{aligned} \bar{P}_{12} &= P_{12}u \\ \bar{P}_{22} &= P_{22}u - y \end{aligned} \tag{91}$$

The following theorem formulates the model validation test using μ.[51]

Theorem 6.1.2: *Given measurements* y *generated by inputs* u, *then the system* P *with associated uncertainty set* $\mathbf{\Delta}$ *is not invalidated if*

$$\mu(P_{11} - \bar{P}_{12}\bar{P}_{22}^{-1}P_{21}) > 1 \tag{92}$$

This condition may seem counterintuitive in that the desired condition for validation is μ greater than one, while the robust stability condition seeks a value less than one. This condition can be explained by considering the following relationship of $y = F_u(P, \Delta)\,u$ as shown in figure 6.1.

$$\begin{aligned} 0 &= [P_{22}u - y] + P_{21}\Delta(I - P_{11}\Delta)^{-1}[P_{12}u] \\ &= \bar{P}_{22} + P_{21}\Delta(I - P_{11}\Delta)^{-1}\bar{P}_{12} \end{aligned} \tag{93}$$

Define the plant $\bar{P} = \{P_{11}, \bar{P}_{12}, P_{21}, \bar{P}_{22}\}$. A value of $\mu(\bar{P}) < 1$ implies this system is robustly stable to all perturbations $\Delta \in \mathbf{\Delta}$. This robust stability of $\mu(\bar{P}) < 1$ also implies that the loop gain $F_u(\bar{P}, \Delta)$ is not singular for any value $\Delta \in \mathbf{\Delta}$. Thus, $\mu(\bar{P}) < 1$ would contradict the relationship shown in the above equations that requires $F_u(\bar{P}, \Delta)$ to be singular to satisfy the input-to-output relationship of the data. In this respect, the model validation test is actually an inverted robust stability test.

The phrase “model validation” may be misleading. No analytical model can ever be truly validated by considering a finite set of experimental data. A model may not be invalidated by the data, but no guarantee exists that a different data set could not be generated from the physical system that invalidates the model. The finite sets of measurement data cannot record the response of the system to an infinite number of input signals subject to an infinite number of initial conditions. Theorem 6.1.2 reflects this fact by explicitly stating the condition only determines if the model is invalidated by the data. The system is assumed to be nearly linear, and the data is assumed to sufficiently represent the behavior of the dynamics, so theorem 6.1.2 represents a model validation test.

6.2 Validating Norm Bounds for Uncertainty

The value of μ computed using theorem 6.1.2 can be interpreted as a measure of how reasonable the uncertainty description is. A value of $\mu = 2$ implies the uncertainty can be scaled by 2 before the model is invalidated. Alternatively, a value of $\mu = 0.5$ implies twice as much uncertainty is required for the model to not be invalidated. This interpretation of μ, as relating to the size of allowable perturbations, emphasizes the relationship of the model validation condition to a robust stability condition.

This model validation is used in practice to generate reasonable norm bounds for an uncertainty description. The following algorithm can be used to determine a sufficient level of uncertainty required such that the model is not invalidated by multiple data sets. A small scalar $\alpha > 1$ is chosen to scale the uncertainty set and increase the amount of allowable errors if the size of $\mathbf{\Delta}$ is not sufficient.

Algorithm 6.2.1 (Model Validation):

Given frequency-domain data sets $\{y_1, y_2, \ldots, y_n\}$ *and* $\{u_1, u_2, \ldots, u_n\}$:
Given frequency-domain transfer-function P *with elements* $P_{11}, P_{12}, P_{21}, P_{22}$:
Given uncertainty set $\mathbf{\Delta}$ *with initial norm bound:*
Given update scalar $\alpha > 1$:

valid = FALSE
while (valid == FALSE*)* {
    valid = TRUE
    for i = 1 : n {
        $\bar{P}_{12} = P_{12}u_i$
        $\bar{P}_{22} = P_{22}u_i - y_i$
        if $\mu\,(P_{11} - \bar{P}_{12}\bar{P}_{22}^{-1}P_{21}) < 1$ {
            valid = FALSE
        }
    }
    $P_{11} = \alpha P_{11}$ *(equivalent to* $\mathbf{\Delta} = \alpha\mathbf{\Delta}$*)*
}
$\mathbf{\Delta}$ *is the required norm-bounded uncertainty*

The norm bound on the uncertainty set $\mathbf{\Delta}$ is not actually increased with this method as denoted by the parentheses around the statement $\mathbf{\Delta} = \alpha\mathbf{\Delta}$. Scaling the uncertainty and retaining these scalings throughout the procedure would be difficult. The algorithm is simplified by always considering the uncertainty is scaled such that $\mu < 1$ is always the desired result. This scaling of the uncertainty is actually accomplished by the statement $P_{11} = \alpha P_{11}$, which scales the feedback signals between the plant and uncertainty operators. The norm bound for the uncertainty that is needed to ensure the uncertainty levels are not invalidated by the data is scaled into the plant by the parameter α. Robust flutter margins can be computed directly from the new scaled plant using algorithm 4.4.6 with a desired $\mu < 1$ condition.

Algorithm 6.2.1 is a straightforward implementation of the model validation test. The μ values are only compared with 1 to determine if the model is invalidated. More sophisticated algorithms could use the value of μ to determine the factor α to scale the uncertainty. Also, the values of μ across frequency could be exploited. Frequencies with low μ value indicate areas where the uncertainty set is least conservative; frequencies with high μ are overly conservative. The scaling α could vary with frequency to reflect this information.

The situation may arise when the initial value chosen for the norm bound of the uncertainty set may be overly conservative. In this situation, the model validation condition will pass for each data set during the first processing of the outer loop. The initial norm bound can simply be decreased by some level consistent with the lowest μ value computed during the validation checks, and algorithm 6.2.1 can be run again to compute a less conservative uncertainty description that does not invalidate the model.

Theorem 6.1.2 is only valid for scalar data signals generated by systems with a single input and single output. Multiple data signals can be considered by applying theorem 6.1.2 to each combination of single-input and -output signals. Algorithm 6.2.1 can still be used by simply including outer loops to cycle over the number of input and measurement signals.

The model validation algorithm using theorem 6.1.2 is a departure from traditional methods of analyzing flight data to assess accuracy of an analytical model. The most widely used algorithms for analyzing flight data estimate natural frequencies and modal damping. The model validation procedure using μ considers the response dynamics at each frequency without explicitly comparing modal properties. This procedure enhances the ability of the μ method to analyze flutter stability without requiring damping estimates.

Another interpretation of algorithm 6.2.1 uses the uncertainty $\mathbf{\Delta}$ to bound the magnitude and phase of the possible transfer functions generated by the family of plants $F_u(P, \mathbf{\Delta})$. The structured singular value ensures the experimental data transfer function lies within these analytical bounds at every frequency.

CHAPTER 7
PROCEDURE FOR THE μ METHOD

7.1 Model Updating

Generating a model by analyzing flight data is essential for computing a confident stability analysis. A nominal model generated purely from analytical equations of the predicted aircraft dynamics may not accurately describe the true aircraft. A model must be generated that accounts for the flight data to ensure the predicted dynamics represent the true dynamics.

The most direct method of generating a model from the flight data is to identify a system model entirely from the data measurements. Many system identification algorithms exist that have become standard tools for systems and control engineers.[52] Direct application of these methods to aeroelastic systems rarely produces an accurate model that accounts for the dynamics of the aircraft.[2] Aeroelastic response data is typically of poor quality relative to ground vibration test data because of the low signal-to-noise ratio and unobserved dynamics in the response measurements that may drastically lower the effectiveness of system identification algorithms.[2]

An alternative method is to use the nominal aircraft dynamical model as an initial estimate to model the true aircraft. The flight data are then used to update the elements of this model. Several methods have been devised to update an analytical structural model using experimental data.[53] Model updating can be performed on the full stress model or a subset computed with Guyan reduction.[54] Generally, considering the full model is preferable because the reduction may distribute local errors throughout the entire model if an orthogonality condition is violated.[55]

Two basic methods are proposed to update the full structural model using comparisons between experimental and predicted data. One method updates the mass and stiffness matrices of the finite-element model.[56] This method suffers from lack of physical interpretation of the matrix updates and possible numerical conditioning. Another method updates specific parameters in the model. This method is accurate for small systems but may require an excessive computational cost for large systems.

Aeroelastic models have the additional freedom of updating the aerodynamic and the structural elements. A method of updating the linear model in a modern control framework has been developed.[32] This method may be overly conservative for describing nonlinearities, and the corresponding stability margins are only accurate for flight conditions near the instability. A parametric identification algorithm has been developed that uses flight data to update specific terms in the aerodynamic model through a nonlinear optimization.[57] This method suffers with flight data because of unobserved dynamics and the low signal-to-noise ratio in the measurements.

The approach taken in this paper is to update only the uncertainty operators of the robust aeroelastic model, using the flight data, and leave the nominal dynamics model unchanged. The model validation condition of theorem 6.1.2 is used with the nominal plant P to generate a reasonable uncertainty description Δ to associate with P. Figure 7.1 shows the flow of information through the μ method.

Algorithm 6.2.1 presents a procedure to implement the μ method in a manner corresponding to figure 7.1. The model update procedure based on algorithm 6.2.1 actually scales the plant but has the equivalent effect of scaling the norm bound of the uncertainty description. The algorithm loops over the model validation procedure until an uncertainty description is determined that is not invalidated by the flight data. The final step is to compute a robust flutter margin from the scaled plant by using a $\mu < 1$ condition as in algorithm 4.4.6.

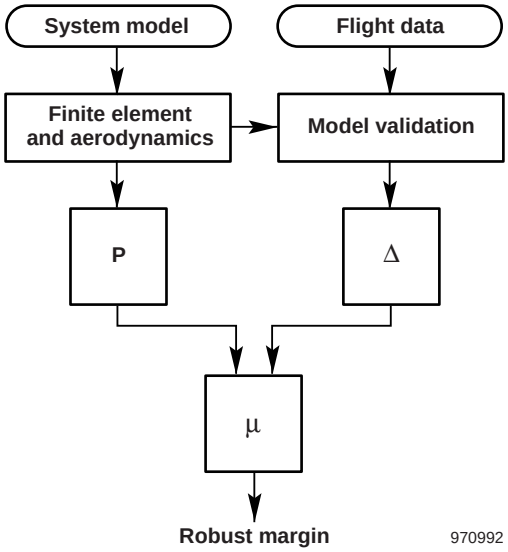

Figure 7.1. Information flowchart to generate plant and uncertainty operators from a system model and flight data with the μ method.

Algorithm 7.1.1 (robust flutter margins with model updating):

Given nominal plant P:
Given uncertainty set **Δ** *associated with* P:
Given input excitation data u:
Given output response measurement data y:
Define $W \geq I$ *as the scaling update for* Δ

while ($F_u(P, \Delta)$ *is invalidated by* u, y *using algorithm 6.2.1*) {
Δ = W**Δ**
}
$\delta_{flutter}^{rob}$ *is flutter margin computed from algorithm 4.4.6*

Several advantages exist to using this method as compared to traditional model updating methods. The typically poor quality of flight data, in association with aircraft dynamics consisting of many modes, makes updating a nominal model difficult. Traditional methods of norm-based update algorithms often generate a nonunique set of model updates that have no way to determine which update has the most logical physical interpretation. The method of updating the uncertainty operators based on a worst-case magnitude avoids this problem.

Also, this method can work with flight data of varying quality. The updated uncertainty description is highly accurate if the data show a high signal-to-noise ratio and much of the dynamics are observed by the sensors. If the data do not have these desired characteristics, however, the method can still compute a flutter margin. An uncertainty description may be difficult to compute if the data do not indicate the aircraft dynamics well, so the model validation procedure will not require a large magnitude for the uncertainty operators. The robust model in this situation will closely resemble the nominal model. In this way, the μ method will always generate a more accurate flutter margin, and at worst, the robust μ flutter margin will be equivalent to the nominal flutter margin.

7.2 Approaches to Use Flight Data

A flight test generally consists of maneuvers at several test points that may be at identical or different flight conditions. The entire flight test program will use many flight tests to measure response data at test points throughout the flight envelope. The model-updating method that generates uncertainty operators can use the entire set of flight data from the different test points.

Several approaches are formulated to use multiple flight data sets to update the uncertainty description associated with a nominal plant model. The uncertainty description may be different for each approach, and the resulting flutter margin will be different for each approach because of the dependence of μ on the uncertainty set. Two approaches discussed here are denoted as local and global.

A local approach uses flight data from test points at identical flight conditions. These data are used to generate an uncertainty description for the nominal model at the particular flight condition associated with the data. The magnitude of the uncertainty operators is chosen such that a robust model at the single flight condition is not invalidated by any of the flight data sets measured at that same flight condition with no consideration of data from other flight conditions.

The local approach shows the benefit of independently computing uncertainty descriptions for models at different flight conditions. This approach allows each uncertainty description to be more accurate because, for example, the flight data may indicate much smaller uncertainty operators are required for subsonic plant models even though large uncertainty operators are required for transonic plant models. The resulting worst-case flutter margins will be less conservative because less uncertainty is required for the model.

Algorithm 7.2.1 outlines the local approach to use flight data and compute flutter margins.

Algorithm 7.2.1 (local approach):

Define scalar n_f *as the number of flight conditions.*

Define scalar n_i *as the number of data sets at flight condition* i.

Define vectors $\left\{ u_i^1, u_i^2, \ldots, u_i^{n_i} \right\}$ *as input excitations at flight condition* i.

Define vectors $\left\{ y_i^1, y_i^2, \ldots, y_i^{n_i} \right\}$ *as response measurements at flight condition* i.

Define matrices $\{P_1, P_2, \ldots, P_{n_f}\}$ *as plant models at flight condition* i.

for i = 1 : n_f {
    Choose initial Δ_i
    for $j = 1 : n_i$ {
        validate $F_u(P_i, \Delta_i)$ *using* y_i^j *and* u_i^j
        increase size of Δ_i *if necessary to validate*
    }
    compute flutter margin $\delta_{flutter}^i$ *from* $\mu(F_u(P_i, \Delta_i))$
}

A global approach uses the entire set of flight data from test points throughout the flight envelope to generate a single uncertainty description for all nominal aircraft models. The magnitudes of the uncertainty operators are chosen such that all nominal models with the associated uncertainty description are not invalidated by any of the flight data sets.

Several advantages and disadvantages exist to using the global approach instead of the local approach. One disadvantage is a possible large increase in conservatism of the flutter margin because the uncertainty description is not minimized at each flight condition. A single particularly inaccurate plant model will require large uncertainty operators that may be highly conservative for plant models at flight conditions that are better representations of the true dynamics.

One advantage to this approach, however, is that the uncertainty description is truly worst-case with respect to the entire flight envelope. The worst-case errors from the worst-case flight condition are used to generate the uncertainty description for all conditions. Also, this approach is not very sensitive to poorly measured flight data. A poorly modeled modal response may only appear in certain data sets. The local approach would not include uncertainty for these dynamics at conditions that did not clearly observe this modal response, so the resulting flutter margin would not account for the true level of modeling errors. The flutter margin generated with the global approach may be more conservative than the local approach, but this approach introduces a corresponding higher margin of safety.

Algorithm 7.2.2 outlines the global approach to use flight data and compute flutter margins.

Algorithm 7.2.2 (global approach):
Define scalar n_f *as the number of flight conditions.*

Define scalar n_i *as the number of data sets at flight condition* i.

Define vectors $\left\{ u_i^1, u_i^2, \ldots, u_i^{n_i} \right\}$ *as input excitations at flight condition* i.

Define vectors $\left\{ y_i^1, y_i^2, \ldots, y_i^{n_i} \right\}$ *as response measurements at flight condition* i.

Define matrices $\{ P_1, P_2, \ldots, P_{n_f} \}$ *as plant models at flight condition* i.

Choose initial Δ
for $i = 1 : n_f$ {
    for $j = 1 : n_i$ {
        validate $F_u(P_i, \Delta)$ *using* y_i^j *and* u_i^j
        increase size of Δ *if necessary to validate*
    }
}
for $i = 1 : n_f$ {
    compute flutter margin $\delta_{flutter}^i$ *from* $\mu(F_u(P_i, \Delta))$
}

Hybrid approaches have also been formulated that mix the local and global approaches. One straightforward hybrid approach is to generate an uncertainty description using all data from a small range of flight conditions. This approach can be useful for separately considering sets of plant models that are generated using different techniques. For example, the model-generating package used for this paper computes all subsonic plant models with a doublet-lattice algorithm and the supersonic models are generated with constant-panel algorithms. A hybrid approach could be used to reflect this knowledge and consider groups of subsonic, supersonic, and transonic plants independently.

The approaches outlined here are certainly not exhaustive. A weighted-norm approach can be formulated that uses flight data from the entire flight envelope but depends heavily on a particular subset of that data. Other approaches could concentrate on particular dynamics through modal filtering techniques to generate separate uncertainty descriptions for individual modes.[58]

CHAPTER 8
ROBUST FLUTTER MARGINS OF THE F/A-18 SYSTEMS RESEARCH AIRCRAFT

8.1 Aircraft Flight Test

Robust flutter margins are computed for the F/A-18 Systems Research Aircraft (SRA) that is flown at NASA Dryden Flight Research Center as Ship 845.[59] The SRA is a standard two-seat F/A-18 with production engines. This aircraft is being used as a test bed for flutter testing, advanced actuator concepts, smart structures, optical sensors, and avionics systems.[59] Figure 8.1 shows the SRA in flight over the Mojave desert near Edwards, California.

Figure 8.1 F/A-18 systems research aircraft.

Flutter testing was initiated on the SRA because of a major left-wing structural modification that allows testing of several hydraulic and electromechanical aileron actuator concepts. The increased size and weight of these actuators required large and heavy items to be installed, replacing a fitting called a hinge-half that supports the aileron hinge, actuator, and a fairing. These structural modifications changed stiffness and damping properties and added approximately 20 lbm to the wing. Dependency of the aileron aeroelastic behavior on actuator dynamics warranted the flutter tests.

The results presented in this paper are associated with the F/A-18 SRA with the left-wing structural modification. More than 30 flight tests were conducted in two sessions, one session between September 1994 and February 1995 and one session between June 1995 and July 1995. A total of 260 data sets are measured from test points at various conditions throughout the flight envelope.

The flight flutter test program used a wingtip excitation system developed by Dynamic Engineering Incorporated (DEI). This exciter is a modification of an excitation system used for F-16 XL flutter

research.[60] The system consists of a wingtip exciter, an avionics box mounted in the instrumentation bay, and a cockpit controller.

Aerodynamic forces are generated by the wingtip exciter. This exciter consists of a small, fixed, aerodynamic vane forward of a rotating, slotted, hollow cylinder. Rotating the cylinder varies the pressure distribution on the vane and results in a wingtip force changing at two times the cylinder rotation frequency. The magnitude of the resulting force is determined by the amount of opening in the slot. Figure 8.2 shows the F/A-18 aircraft with a left-side wingtip exciter in the aft position.

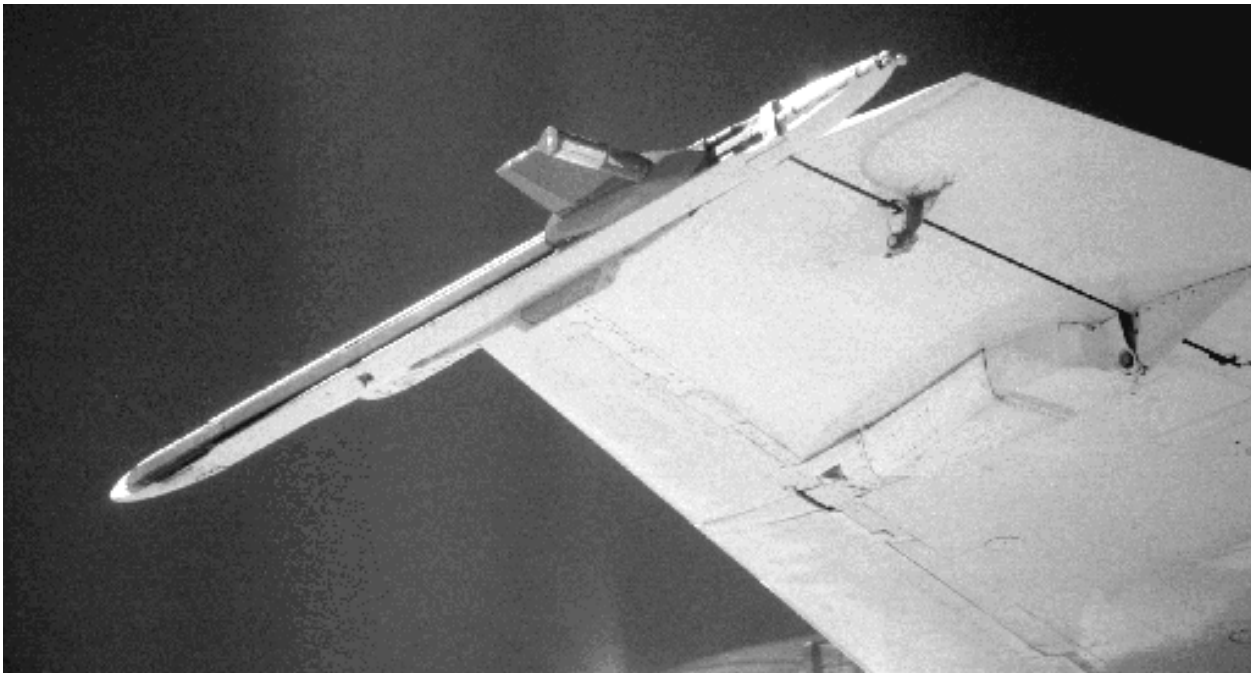

Figure 8.2 Left wing of the F/A-18 systems research aircraft with wingtip excitation system.

The cockpit controller commands a frequency range, duration, and magnitude for the wingtip excitation signal. Frequency-varying excitation is generated by changing the cylinder rotation frequency with sine sweeps. Each wingtip exciter is commanded to act in phase (0°) or out of phase (180°) with each other. Ideally, the in-phase data excite the symmetric modes of the aircraft, and the out-of-phase data excite the antisymmetric modes. In reality, nonideal phasing of the exciters often caused a mixture of symmetric and antisymmetric modes to be excited.

Flight data sets were recorded by activating the exciter system at a given flight condition. The aircraft attempted to remain at the flight condition throughout the series of sine sweeps desired by the controller. The sine sweeps were restricted to within 3 Hz and 35 Hz, and smaller ranges were sometimes used to concentrate on a specific set of modal responses. Multiple sets of either linear or logarithmic sweeps were used with the sweep frequency increasing or decreasing. Table 8.1 shows the flight test matrix of excitation parameters and flight conditions for the F/A-18 SRA flutter program.

Accelerometers are available at several points on the aircraft to record modal responses. Each wing has a sensor on the aileron and at the forward and aft position on the wingtip. Additional accelerometers are located on each vertical tail and horizontal stabilator.

Table 8.1. Operating and flight conditions for the F/A-18 SRA flight flutter test.

Mach	0.54, 0.65, 0.70, 0.80, 0.85, 0.90, 0.95, 1.05, 1.2, 1.4, 1.6
Altitude, ft	10K, 30K, and 40K
Exciter configuration	Symmetric, antisymmetric, and independent
Exciter position	Both forward, both aft, and left aft/right forward
Exciter force level	Low and high
Sweep type	Linear and logarithmic
Sweep duration, sec	15, 30, and 60
Sweep range, Hz	3–35, 3–12, 3–25, 25–35, 35–3, 3–40
Sweep multiples	1, 2, and 4 sweeps for each maneuver

8.2 Aeroelastic Data Analysis

Aeroelastic flight data generated with the exciter system are analyzed by generating transfer functions from the excitation force to the sensor measurements. These transfer functions are generated using standard Fourier transform algorithms. Several inherent assumptions associated with Fourier analysis exist that are violated with the flight data. The assumptions of time-invariant stationary data composed of sums of infinite sinusoids are not met by this transient-response data.[44, 61] The amount of uncertainty required to validate the model can be reduced by using wavelets to accurately process the data but are not considered in this paper.

Figure 8.3 shows an example of dynamical variations that are observed during flight testing. Two transfer functions generated from different data sets clearly show some variation. The natural frequency

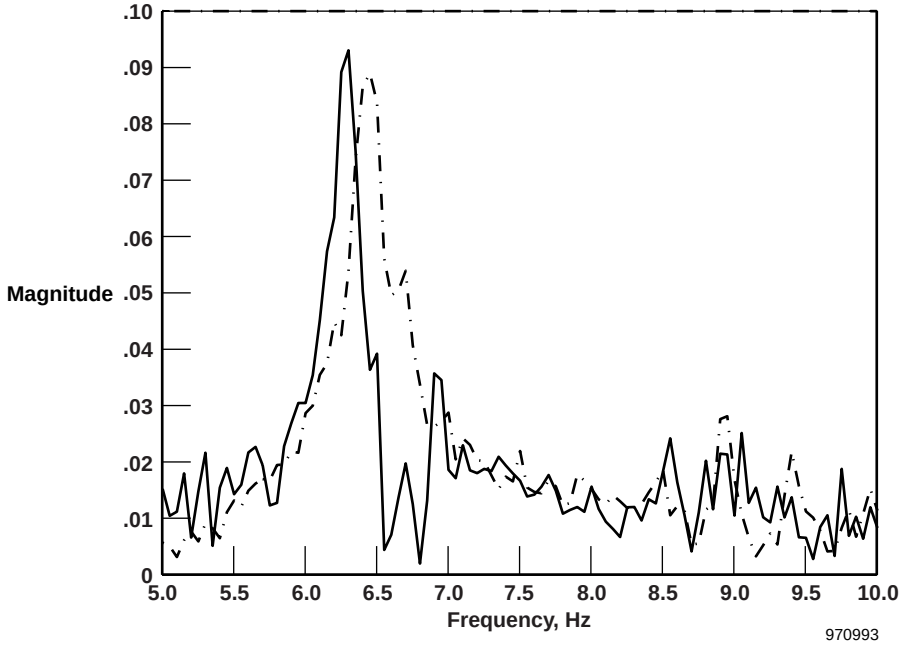

Figure 8.3. Flight data transfer functions from symmetric excitation to left wing forward accelerometer for Mach = 0.8 and 30,000 ft demonstrating variation in modal frequency and damping.

and modal response are different as observed by these two data sets, although each test point used the same sweep procedure at identical flight conditions of Mach 0.8 and an altitude of 30,000 ft. One possibility to account for such variations is the change in mass, a maximum of 10 percent, between the heavyweight and lightweight conditions caused by fuel consumption. Another possibility is the nonideal phasing between the exciters causing excitation that is not purely symmetric.

The deviations between the modal responses in figure 8.3 are used to generate uncertainty for the symmetric wing first-bending mode. Similar deviations observed in modal responses are used to generate uncertainty for each mode. Uncertainty levels in modes that are not observed are assumed to be similar to those of the observed modes.

Figure 8.3 shows modeling uncertainty caused by variations between the analytical model and the aircraft dynamics that change during a flight test. Additional uncertainty is introduced because of improper operation of the exciters. Several behaviors are observed because of these improper operations.

The most noticeable of these improper behaviors occurs as a function of dynamic pressure. The motors and rotating cylinder assemblies bind at high dynamic pressures, causing erratic phase relationships between the individual exciters on opposite wingtips. Figure 8.4 shows a representative plot of the phase difference in degrees between the left and right exciters operating in symmetric mode for a sweep taken at a test point with $\bar{q}$ = 356 lbf/ft^2. This phase plot, which does not maintain the desired 0° phase difference but is relatively constant and well-behaved, is in direct contrast to the phase difference at a test point of $\bar{q}$ = 825 lbf/ft^2 (fig. 8.5).

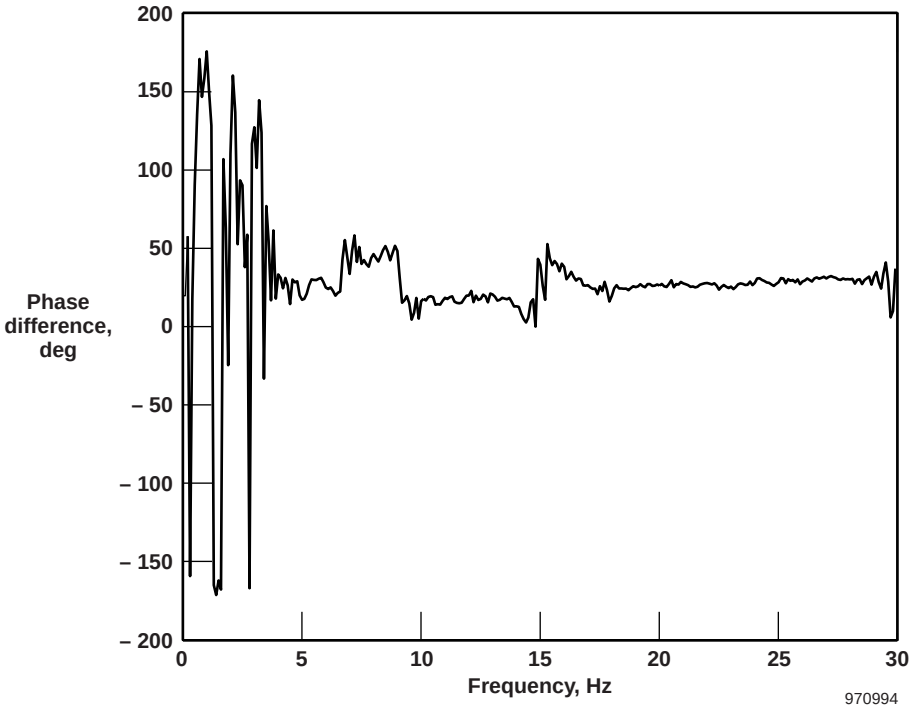

Figure 8.4. Phase difference in degrees between left and right exciters for sweep range 3–30 Hz at Mach = 0.90 and 30,000 ft at $\bar{q}$ = 356 lb/ft^2.

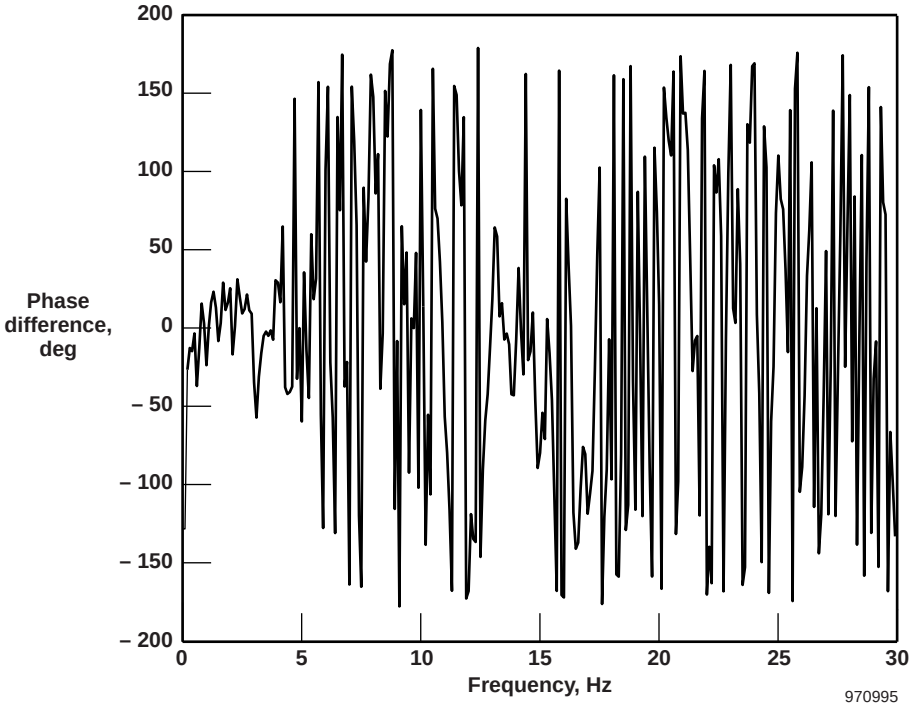

Figure 8.5. Phase difference in degrees between left and right exciters for sweep range 3–30 Hz at Mach = 0.90 and 10,000 ft at $\bar{q}$ = 825 lb/ft^2.

Another improper behavior is the nonrepeatibility observed with the data because of variations in transfer functions using different data sets recorded at identical flight conditions. Figures 8.6 and 8.7 show an example of such a variation observed for frequency-increasing and -decreasing sweeps. The μ method can use the data despite these nonrepeatabilities that would adversely affect traditional system identification approaches.

The data analysis process is further degraded by a poor measurement of the excitation force used to generate the modal responses. The excitation force is not directly measured, but a strain-gage measurement is used to approximate this force. The strain gage records lateral shear strain at the exciter vane root. This measurement is assumed to be representative of the vertical shear and spanwise-moment load at the wingtip rib. Time-frequency analysis using wavelets clearly shows this strain-gage signal to have some harmonic resonances from the structural response.[44]

The effect of the poor approximation of input force and the erratic behavior of the exciters is to reduce the quality of the flight data. Methods relying on system identification fail to accurately use the data to predict a flutter boundary.[57] The μ method is able to account for the data anomalies by including greater levels of uncertainty.

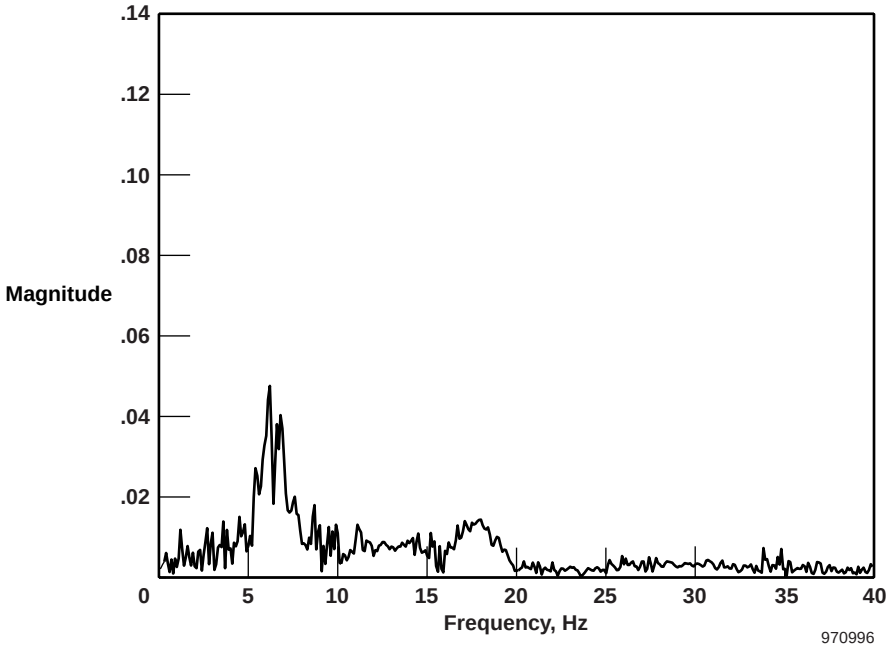

Figure 8.6. Flight data transfer function from symmetric excitation to left wing forward accelerometer for Mach = 0.8 and 30,000 ft with frequency increasing sweep from 3–35 Hz.

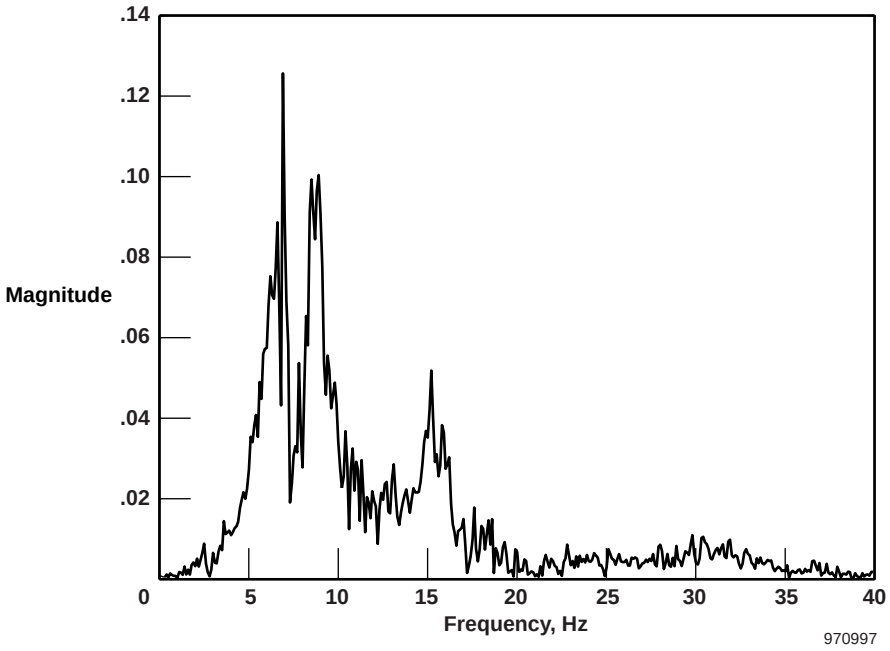

Figure 8.7. Flight data transfer function from symmetric excitation to left wing forward accelerometer for Mach = 0.8 and 30,000 ft with frequency decreasing sweep from 35–3 Hz.

8.3 Analytical Model

A finite-element model of the SRA is used to compute the aeroelastic dynamics and modal characteristics of the aircraft. The generalized equations of motion are used to derive a linear, finite-dimensional state-space model of the aircraft. This model contains 14 symmetric structural modes, 14 antisymmetric structural modes, and 6 rigid-body dynamic modes. The control surfaces are not active, and no control modes are included in the model. Table 8.2 shows natural frequencies of the elastic structural modes. These modal frequencies are computed for the aircraft with no aerodynamics considered.

Table 8.2. Elastic natural frequencies of the structural finite-element model of the fully fueled F/A-18 SRA with left-wing modifications and no wingtip excitation system.

Mode	Symmetric, Hz	Antisymmetric, Hz
Wing first bending	5.59	8.84
Fuselage first bending	9.30	8.15
Stabilator first bending	13.21	12.98
Wing first torsion	13.98	14.85
Vertical tail first bending	16.83	15.61
Wing second bending	16.95	16.79
Wing outboard torsion	17.22	–
Fuselage second bending	19.81	18.62
Trailing-edge flap rotation	23.70	23.47
Fuselage torsion	–	24.19
Launcher rail lateral	–	24.35
Stabilator fore and aft	28.31	28.58
Wing second torsion	29.88	29.93
Aileron rotation	33.44	–
Aft fuselage torsion	–	37.80
Aileron torsion	38.60	–
Wing pitch	–	39.18
Wing third bending	43.17	–

The predicted flutter results for this aircraft are computed from the finite-element model using the p-k method. A detailed explanation of the F/A-18 SRA modeling process and flutter analysis using traditional methods has previously been published.

The doublet-lattice and constant-panel methods are used to compute the frequency-varying unsteady aerodynamic forces for several subsonic, transonic, and supersonic Mach numbers. Force matrices for Mach 0.80, 0.90, 0.95, 1.10, 1.20, 1.40, and 1.60, are available. The unsteady aerodynamic forces are computed as a function of reduced frequency, k.

$$k = \omega \frac{\bar{c}}{2V} \tag{94}$$

The reduced frequency is a function of the true frequency (ω), the true velocity (V), and the mean aerodynamic chord ($\bar{c}$). Aerodynamic forces generated for ten reduced-frequency points between $k = 0.0001$ and $k = 4.0000$ are sufficient for flutter margin computation for this aircraft. Figure 8.8 shows the magnitude and phase of a sample calculation of the unsteady aerodynamic forces as a function of reduced frequency. An additional ten points computed between $k = 0.01$ and $k = 1.00$ demonstrate the function is smooth across frequency, so the original set of ten points is sufficient to describe the behavior of unsteady aerodynamic forces.

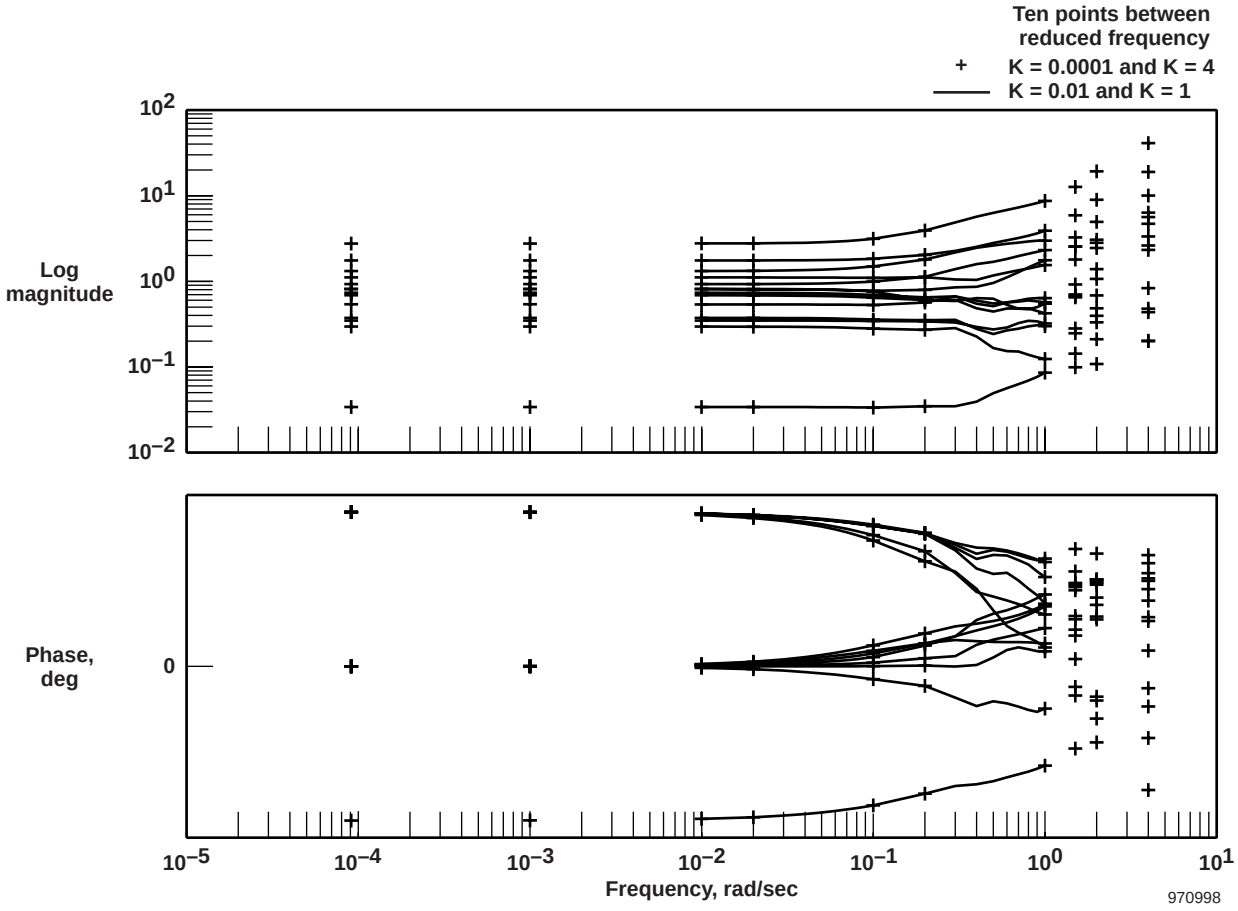

Figure 8.8. Magnitude and phase of the frequency-varying unsteady aerodynamic forces.

The unsteady aerodynamic forces are fit to a finite-dimensional state-space system. The system identification algorithm is a frequency-domain curve-fitting algorithm based on a least-squares minimization.[62] A separate system is identified for each column of the unsteady forces transfer-function matrix. Fourth-order state-space systems are used for each column of the symmetric forces, and second-order state-space systems are used for each column of the antisymmetric forces. These systems are combined to form a single multiple-input and multiple-output state-space model of the unsteady aerodynamics forces, previously designated Q(s). This model has 56 states for the symmetric modes and 28 states for the antisymmetric modes.

The analytical aeroelastic model has inputs for symmetric and antisymmetric excitation forces. The excitation force is assumed to be purely symmetric or antisymmetric. Ten outputs exist that correspond to the sensor locations on the aircraft.

8.4 Uncertainty Description

Noise and uncertainty operators are introduced to the linear aeroelastic model to account for variations between the analytical model and the actual aircraft. Standard analysis of the linear model is used to determine the framework for how uncertainty operators enter the system. Two uncertainty operators and a single noise input are used to describe the modeling uncertainty in the linear aeroelastic model. The magnitude of each uncertainty operator and the noise level is determined from both reasoning of the modeling process and analysis of the flight data.[63]

An uncertainty operator, Δ_A, is associated with the state matrix of the F/A-18 linear model. This uncertainty models variations in the natural frequency and damping values for each mode.[64] State-matrix uncertainty can account for errors in coefficients of the equations of motion and changes in the aircraft dynamics caused by parameter variations such as mass consumption during flight.

The Δ_A is a structured, diagonal matrix with real, scalar parameters as elements. Separate elements are used to affect each modal response and time lag in the state matrix. The modal response uncertainty parameters are each repeated two times, and each time-lag uncertainty appears once on the diagonal.

Each repeated modal uncertainty parameter affects natural frequency and damping by allowing variation in the state matrix elements. Consider formulating the state matrix as a block diagonal with a 2-by-2 block representing each mode. The real component of a modal eigenvalue, e_r, is the diagonal component of each block, and the imaginary part, e_i, is arranged on the off-diagonal positions. Define A_i as the block determining the natural frequency, w_i, and damping, ζ_i, of the i^{th} mode.

$$A_i = \begin{bmatrix} e_r & e_i \\ -e_i & e_r \end{bmatrix} \quad \Rightarrow \quad \begin{aligned} w_i &= \sqrt{e_r^2 + e_i^2} \\ \zeta_i &= -e_r / \omega_i \end{aligned} \tag{95}$$

Scalar weightings, w_r and w_i, are used to affect the amount of uncertainty in each matrix element. The amount of variation in the matrix elements and, correspondingly, the amount of variation in the natural frequency and damping, are determined by the magnitude of these scalar weightings. Define $\bar{e}_r$ and $\bar{e}_i$ as elements of the state matrix affected by an uncertainty parameter δ.

$$\begin{aligned} \bar{e}_r &= e_r (1 \pm w_r \delta) \\ \bar{e}_i &= e_r (1 \pm w_i \delta) \end{aligned} \tag{96}$$

Aeroelastic modes typically show low damping values caused by the real component being smaller than the imaginary component. Because linear modeling techniques often identify the natural frequency better than the damping value, the weighting for the real component is expected to be larger than that for the imaginary component. This weighting is reflected by the observed modal parameters in the flight data. The natural frequencies show variations of ±5 percent from the theoretical model, but the uncertainty in

the damping needs variations of approximately ±15 percent to validate all the flight data. The scalar weightings are chosen accordingly.

$$\begin{aligned} w_r &= 0.15 \\ w_i &= 0.05 \end{aligned} \tag{97}$$

The flight data are only able to determine uncertainty levels for the modal parameters of the experimentally observed modes. The uncertainty levels in the unobserved modes are assumed to be consistent with these values. Parametric uncertainty is introduced for each modal block in the state matrix, affecting observed and unobserved modes, using the weighting values given above.

The single scalar blocks of Δ_A are normalized to one by weighting their effect on the time lags of the state matrix. Variations observed in the flight data are used to determine that a weighting of $w_{lag} = 0.15$ is required to admit 15-percent variation in the time lags.

The second uncertainty operator, Δ_{in}, is a multiplicative uncertainty on the force input to the linear model. This uncertainty is used to cover nonlinearities and unmodeled dynamics. The linear model contains no dynamics at greater than 40 Hz, so the high-frequency component of this operator will reflect this uncertainty. This operator is also used to model the excitation uncertainty caused by the exciter system. Analysis of the flight data indicates the input excitation signals rarely had the desired magnitude and phase characteristics that they were designed to achieve. The low-frequency component of the input uncertainty reflects the uncertainty associated with the excitation system used to generate the flight data. The frequency-varying transfer function for weighting the input uncertainty is given as W_{in}.

$$W_{in} = 5\frac{s + 100}{s + 5000} \tag{98}$$

A noise signal is included with the sensor measurements. Knowledge of the aircraft sensors is used to determine that a level of 10-percent noise is possible in the measured flight data. An additional noise may be included on the force input caused by the excitation system, but the input multiplicative uncertainty is sufficient to describe this noise. Figure 8.9 shows the block diagram for the aeroelastic model with the uncertainty operators.

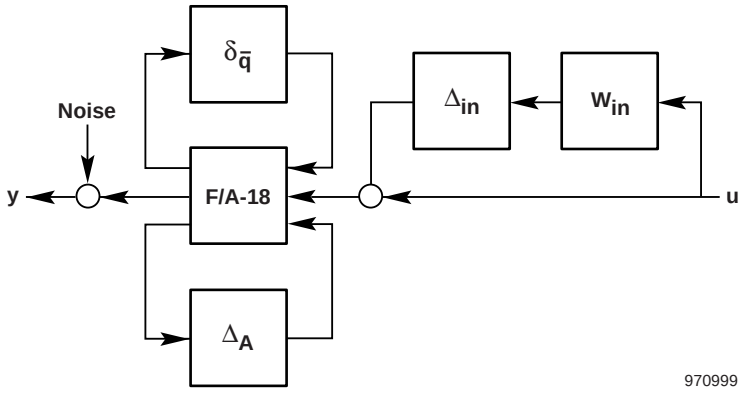

Figure 8.9. F/A-18 robust stability block diagram.

The flight data used to validate this uncertainty structure cover a large range of flight points. The entire set of 260 flight maneuvers throughout the flight envelope is considered. Using a single uncertainty description over the entire flight envelope may be conservative. Certainly assuming the linear models are more accurate at subsonic and supersonic speeds than at transonic speeds because of flow irregularities caused by shock formation is reasonable. Additionally, the flight data from the exciter system should be better at subsonic speeds than at supersonic speeds because of the degraded performance at high dynamic pressures. However, the analysis process is simplified by considering a single set of uncertainty operators. This process is equivalent to formulating the worst-case uncertainty levels at the worst-case flight condition and assuming that amount of uncertainty is possible for the remaining flight conditions.

8.5 Nominal and Robust Flutter Pressures

Flutter pressures are computed for a linear model with the associated modeling uncertainty structure using the μ analysis method.[65] Linear systems for symmetric and antisymmetric structural modes are separated for ease of analysis. These systems can easily be combined and analyzed as a single system; however, eigenvector analysis would be required to distinguish which critical flutter modes are symmetric and which are antisymmetric. Each system contains the same number of structural modes (14), and the uncertainty descriptions are identical for each linear model.

The system shown in figure 8.9 contains three uncertainty blocks. The parametric uncertainty covering variations caused by dynamic pressure, $\delta_{\bar{q}}$, is a scalar parameter repeated 14 times, once for each elastic mode. The parametric uncertainty block affecting the modal parameters, Δ_A, is a diagonal matrix with dimension equal to the number of states. Separate scalars along the diagonal represent uncertainty in each elastic mode, each mode in the aerodynamic force approximation, and each lag term. The uncertainty parameters for the modes are repeated two times; the parameters for the lag terms are single scalars. Define δ_i as the i^{th} uncertainty parameter for the system using n_m modes and n_l lag terms. The input-multiplicative uncertainty block, Δ_{in}, is a scalar for this single-input plant model because symmetric excitation is analyzed separately from antisymmetric excitation.

The parametric uncertainty parameters represent changes in elements of the state-space model. The variation of $\delta_{\bar{q}}$ between ± 1 admits dynamic pressures between $0 \le \bar{q} \le 2\bar{q}_o$. Allowing the modal uncertainty parameters, $\delta_1, \ldots, \delta_{n_m}$, to vary between ± 1 allows 5-percent variation in the imaginary part of the natural frequency and 15-percent variation in the real part. This variation corresponds to approximately 5-percent variation in the natural frequency and 15-percent variation in the damping value of each mode. These parameters are real quantities. The input-multiplicative uncertainty contains magnitude and phase information and is treated as a complex linear time-invariant uncertainty.

Nominal flutter pressures are initially computed by ignoring the modal and input uncertainties. The structured singular value is computed only with respect to the parametric uncertainty, allowing a range of dynamic pressures to be considered. Robust flutter pressures are computed with respect to the structured uncertainty set, Δ, described above using the structured singular value. Table 8.3 shows traditional flutter pressures computed using the p-k method and nominal and robust flutter pressures computed with μ.

Table 8.3 Nominal and robust flutter pressures computed with p-k and μ methods.

	Symmetric, lbf/ft^2			Antisymmetric, lbf/ft^2		
Mach	$\bar{q}_{\text{p-k}}$	$\bar{q}_{nom}$	$\bar{q}_{rob}$	$\bar{q}_{\text{p-k}}$	$\bar{q}_{nom}$	$\bar{q}_{rob}$
0.80	3360	3168	2909	4600	4593	3648
0.90	2700	2706	2575	3150	3057	2944
0.95	2430	2388	2329	2600	2751	2572
1.10	5400	5676	4120	5500	3265	2827
1.20	2469	2454	2327	2850	2893	2653
1.40	3528	3432	3034	4600	4439	4191
1.60	4470	4487	3996	5700	5870	4536

The nominal flutter dynamic pressures computed using the μ method can be directly compared with those computed using the traditional p-k method. Each of these flutter solutions is based on an analytical model that has no consideration of modeling uncertainty.

The nominal flutter points for the symmetric modes match closely with the p-k method throughout the flight envelope. The subsonic and supersonic cases show an especially good correlation with the p-k flutter points. For each of these flight regions, the μ analysis flutter dynamic pressures are nearly identical (within 1 percent) to the p-k method flutter dynamic pressures. The transonic case at Mach 1.1, however, shows a slight difference between the two methods. The μ method computes a flutter point that is greater than the p-k method. In each Mach regime (subsonic, supersonic, or transonic), the nominal flutter points are within 5 percent for the two methods.

The antisymmetric modes show a similar relationship between the flutter pressures computed with the μ and p-k methods. The subsonic and supersonic flutter points are within 5 percent for the two methods, but a greater deviation exists at the transonic condition. The μ computes a flutter pressure at Mach 1.1 that is 40 percent lower than the p-k method indicates.

The nominal flutter points for the μ and p-k methods show the greatest difference for both the symmetric and antisymmetric modes at the transonic case. The aerodynamics at Mach 1.1 are more difficult to accurately model than at either subsonic or supersonic speeds. Numerical sensitivity to representations of the unsteady aerodynamic forces causes differences in the nominal flutter pressure.

The robust flutter pressures computed using the μ method have lower dynamic pressures than the nominal pressures, which indicates the expected conservative nature of the robust computation. These new flutter points are worst-case values for the entire range of allowed uncertainty. The subsonic and supersonic flutter boundaries are not greatly affected by the uncertainty set. In each of these cases, the robust flutter point is within 10 percent of the nominal flutter point.

The flutter boundary at the transonic case, Mach 1.1, demonstrates significant sensitivity to the modeling uncertainty. The robust flutter dynamic pressures are approximately 70 percent of the nominal flutter pressures. This difference is explained by considering the rapid transition of critical flutter boundaries near this region. The critical flutter frequencies and the flutter dynamic pressure widely vary

between Mach numbers slightly lower and higher than transonic. The small amount of modeling uncertainty is enough to cause the worst-case flutter mechanism to shift, and the plant assumes characteristics more consistent with a nontransonic regime.

Table 8.4 shows the modal natural frequencies for the critical flutter modes. The frequencies computed using the p-k method and the μ analysis method are close throughout the flight envelope for both the symmetric and antisymmetric modes. Frequencies for the robust flutter solutions are slightly different than the nominal flutter frequencies because of the modeling uncertainty that allowed 5-percent variation in the modal natural frequencies.

Table 8.4. Frequencies of unstable modes associated with nominal and robust flutter pressures computed with p-k and μ methods.

	Symmetric, Hz			Antisymmetric, Hz		
Mach	$\omega_{\text{p-k}}$	ω_{nom}	ω_{rob}	$\omega_{\text{p-k}}$	ω_{nom}	ω_{rob}
0.80	8.2	7.6	7.7	9.0	9.1	9.1
0.90	7.4	7.3	7.3	9.2	9.1	9.2
0.95	6.8	6.9	6.9	9.1	9.2	9.2
1.10	12.1	13.2	13.0	28.6	28.0	28.3
1.20	26.5	27.4	27.4	26.9	28.9	28.9
1.40	28.1	28.1	28.1	30.4	31.7	31.8
1.60	28.9	30.1	30.1	32.8	32.3	32.1

Table 8.5 shows subcritical flutter pressures computed with the μ and p-k methods. Only nominal subcritical pressures are detected with μ, because the robust pressures are always worst-case critical pressures.

Table 8.5. Subcritical nominal flutter pressures computed with p-k and μ methods.

	Symmetric, lbf/ft^2		Antisymmetric, lbf/ft^2	
Mach	$\bar{q}_{\text{p-k}}$	$\bar{q}_{nom}$	$\bar{q}_{\text{p-k}}$	$\bar{q}_{nom}$
0.90			4700 5300	4583 5093
0.95	7450	6919		
1.10			6050	6001
1.20	5400	5003	8400	7943
1.40	8970	8959		
1.60	8400	8843		

The μ analysis computes subcritical flutter pressures within 10 percent of the p-k method for both the symmetric and antisymmetric modes. The μ method is even able to detect the subcritical flutter hump mode occurring for antisymmetric excitation at Mach 0.9.

8.6 Nominal and Robust Flutter Margins for a Flight Envelope

The nominal and robust flutter pressures shown in table 8.3 are used to compute flutter margins for a flight envelope. These flutter margins are determined by the distance between the flutter pressure and the dynamic pressure at the edge of the flight envelope at a particular Mach number.

Table 8.6 shows the flight conditions for several points at greater than Mach 0.8, which have the highest dynamic pressures in the defined flight envelope and the nominal and robust flutter margins. All of these flutter margins have positive values, indicating the envelope is free of flutter instabilities. The critical flutter pressures are simply the sum of the flight envelope dynamic pressures and the flutter margins.

Table 8.6. Nominal and robust flutter margins for a flight envelope expressed as allowable increase in dynamic pressure computed with p-k and μ methods for symmetric and antisymmetric modes.

Flight envelope		Symmetric, lbf/ft^2			Antisymmetric, lbf/ft^2		
Mach	$\bar{q}$	$\Gamma_{\text{p-k}}$	Γ_{nom}	Γ_{rob}	$\Gamma_{\text{p-k}}$	Γ_{nom}	Γ_{rob}
0.80	948	2412	2220	1961	3652	3645	2700
0.90	1200	1500	1506	1375	1950	1857	1744
0.95	1337	1093	1051	992	1263	1414	1235
1.10	1491	3909	4185	2629	4009	1774	1336
1.20	1438	1031	1016	889	1412	1455	1215
1.40	1252	2276	2180	1782	3348	3187	2939
1.60	1027	3443	3460	2969	4673	4843	3509

The flutter margins are often expressed in terms of the percent change, Π, in knots of equivalent airspeed, *KEAS*, between the flight envelope and the flight condition corresponding to the critical flutter pressure. Table 8.7 shows these percentage values.

Table 8.7. Nominal and robust flutter margins for a flight envelope expressed as percent of allowable increase in *KEAS* computed with p-k and μ methods for symmetric and antisymmetric modes.

Flight envelope		Symmetric			Antisymmetric		
Mach	*KEAS*	$\Pi_{\text{p-k}}$	Π_{nom}	Π_{rob}	$\Pi_{\text{p-k}}$	Π_{nom}	$\Pi_{\text{p-k}}$
0.80	529	88	82	75	120	120	96
0.90	595	50	50	46	62	59	56
0.95	628	35	33	31	39	43	38
1.10	663	90	95	66	92	48	37
1.20	652	31	31	26	41	41	35
1.40	608	67	65	55	91	88	82
1.60	550	108	109	97	135	139	109

A flutter margin yielding a percentage $\Pi = 15$ for allowable increase in *KEAS* is commonly used to determine an operable flight envelope. The flutter margins shown in table 8.7 demonstrate the indicated flight envelope for the F/A-18 SRA is acceptable because the nominal and robust flutter margins are all greater than 15 percent for symmetric and antisymmetric modes. The smallest flutter margin occurs for the symmetric mode dynamics at Mach 1.2, which presents a robust flutter margin of only 26 percent; however, even this condition is greater than the desired 15-percent margin.

The dynamic pressures at which flutter occurs are converted into altitudes, commonly known as matched-point solutions, using standard atmospheric equations. Figure 8.10 shows these altitudes plotted for the symmetric modes, and figure 8.11 shows them for the antisymmetric modes. The flight envelope of the F/A-18 airplane is shown on these plots, along with the required 15-percent flutter boundary for military aircraft.

Figures 8.10 and 8.11 show several short solid lines to indicate the p-k flutter solutions throughout the flight regime. Each of these short solid lines represents the flutter points caused by a specific mode. Flutter points for the symmetric modes shown in figure 8.10 show four solid lines indicating three different critical flutter modes for the considered range of Mach numbers and a subcritical flutter mode occurring at supersonic Mach numbers. In figure 8.11, the antisymmetric modes show the onset of flutter from three different critical modes and three subcritical flutter modes throughout the flight envelope. Table 8.4 shows the frequencies of the critical flutter modes.

The subsonic flutter altitudes for symmetric and antisymmetric modes demonstrate a similar characteristic. The nominal flutter boundary shows a significant variation from Mach 0.80 to Mach 0.95 that is caused by sensitivity to Mach number for the dynamics associated with the critical flutter mode. The robust flutter boundary indicates the sensitivity of the plant to errors and the worst-case perturbation. The higher altitude for the nominal flutter boundary at Mach 0.81 than for Mach 0.80 is reflected in the large conservatism associated with the robust flutter boundary. Similarly, slight variation of Mach number near Mach 0.95 is not expected to decrease the nominal flutter margin, so less conservatism is associated with the robust flutter boundary.

An interesting trend is noticeable for the symmetric mode robust flutter points in figure 8.10 at the supersonic Mach numbers. The flutter mechanism results from the same modes from Mach 1.2 to Mach 1.6 with some increase in frequency. Similarly, the altitudes of the nominal flutter margins show little change for these Mach numbers. The aeroelastic dynamics associated with the critical flutter mode are relatively unaffected by the variation of Mach over this range, and consequently, each flutter boundary has the same sensitivity to modeling errors.

The robust flutter margins for the antisymmetric modes at supersonic Mach numbers show a slightly different behavior than the symmetric mode flutter margins. The flutter instability is again caused by a single mechanism from Mach 1.2 to Mach 1.6, with similar frequency variation for the symmetric modes. The robust flutter margins demonstrate a similar sensitivity to modeling errors at Mach 1.2 and Mach 1.4, but at Mach 1.6, a greater sensitivity is shown. The greater conservatism at Mach 1.6 may indicate impending transition in flutter mechanism to the subcritical mode at slightly higher Mach number.

Figures 8.10 and 8.11 show dark solid lines representing the required boundary for flutter points. All nominal and robust flutter points lie outside this region, indicating the flight envelope should be safe from flutter instabilities. The robust flutter boundaries computed with μ indicate more danger of encountering flutter exists than was previously estimated with the p-k method. In particular, the robust flutter margin for symmetric excitation at Mach 1.2 lies considerably closer to the boundary than the p-k method indicates.

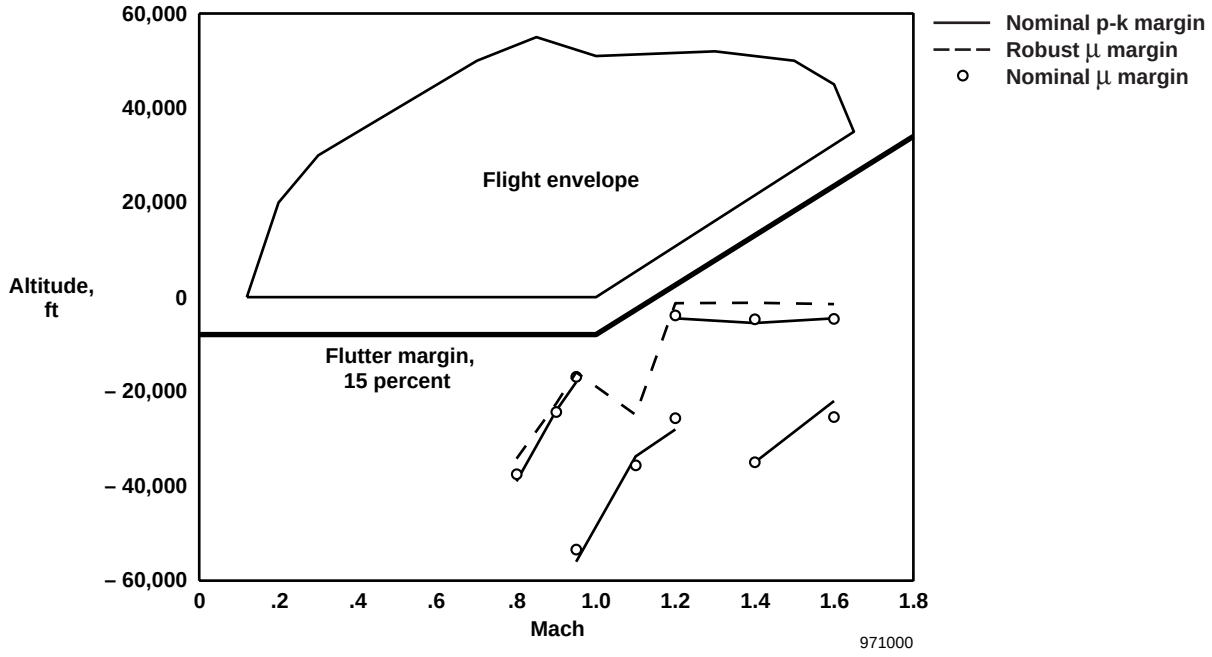

Figure 8.10. Nominal and robust flutter points for symmetric modes.

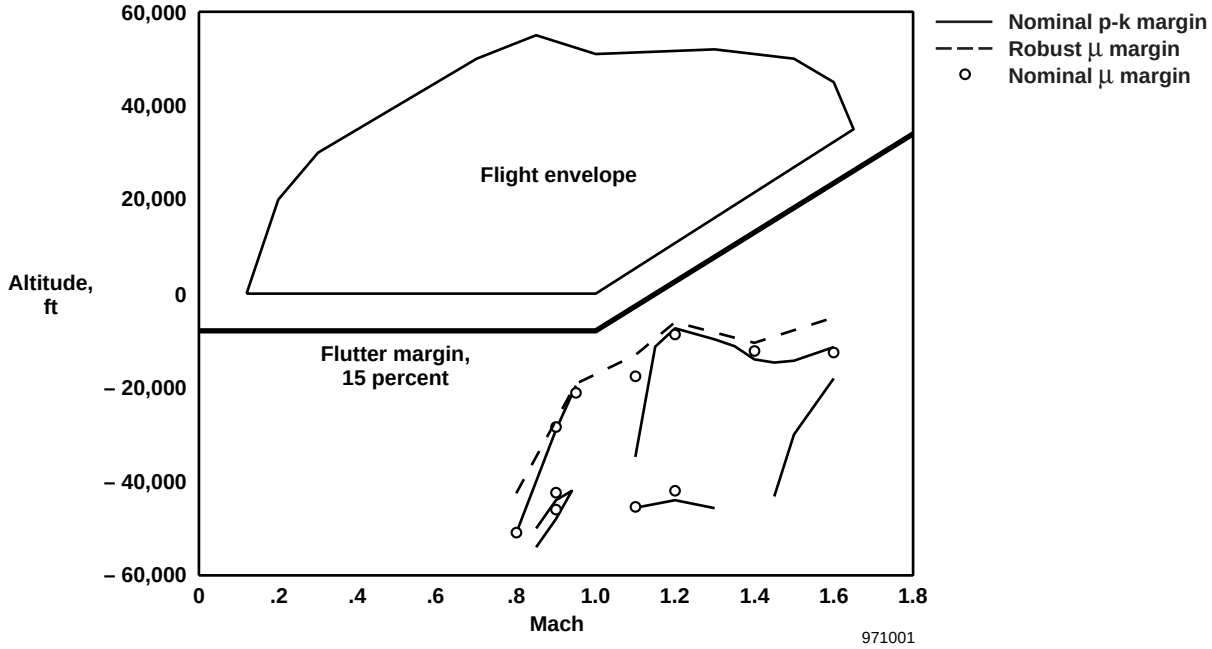

Figure 8.11. Nominal and robust flutter points for antisymmetric modes.

8.7 Computational Analysis

The μ analysis method of computing flutter margins presents significant analytical advantages because of the robustness of the resulting flutter margin, but the method also has several computational advantages over the p-k method. The μ algorithm requires a single, linear, aeroelastic, plant model at a given Mach number to compute critical and subcritical flutter margins. An entire set of flutter margins

can be easily generated in a few minutes using a standard engineering workstation and commercially available software packages.[15]

The p-k method is an iterative procedure that requires finding a matched-point solution. The aircraft is analyzed at a particular Mach number and air density. The airspeed at these conditions resulting in a flutter instability is computed. This airspeed, however, often does not correspond to the unique airspeed determined by that Mach number and air density for a standard atmosphere. Various air densities are used to compute flutter solutions, and the corresponding airspeeds are plotted. Figure 8.12 shows an example of an airspeed plot for flutter.

Figure 8.12 shows vertical lines representing two antisymmetric modes that may flutter at Mach 1.4. The p-k method computes a flutter solution at the airspeed indicated where the modal line crosses the standard-atmosphere curve. This flutter solution is difficult to compute from only a few air density computations. Typically, several air densities are used to compute airspeed flutter solutions, and a line is extrapolated between the points to determine the matched-point solution at the standard-atmosphere crossing point. The nonlinear behavior shown for mode 1 near the standard-atmosphere crossing point indicates an accurate flutter boundary would be extremely hard to predict unless many solutions are computed near the true matched-point solution.

The p-k method can also have difficulty predicting the subcritical flutter margins. The second mode in figure 8.12 may or may not intersect the standard-atmosphere curve. More computational analysis is required to determine the behavior of this mode at high airspeeds. The μ analysis method accurately detects the critical and subcritical flutter margins without requiring expensive iterations.

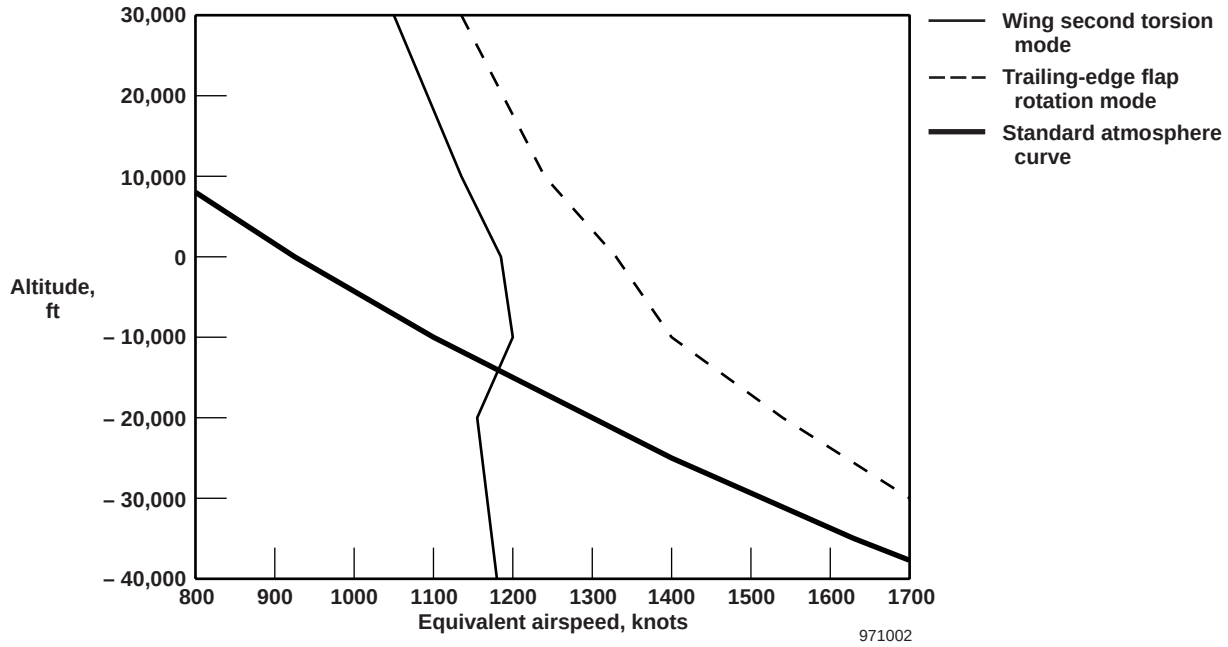

Figure 8.12. Antisymmetric p-k flutter solutions for Mach 1.4.

CHAPTER 9
RESEARCH EXTENSIONS

9.1 Sensitivity Analysis

Stability margins, especially for high-performance aircraft, may be extremely sensitive to the aircraft dynamics and flight conditions. Analytical models must be accurate to ensure the estimated stability properties represent the true aircraft stability properties. Such accuracy is difficult to achieve for complex modern aircraft designs because components such as flexible structural elements and flight regimes such as high angles of attack are complex to model. The sensitivity of the stability margins to changes in the model indicates some degree of confidence in the predicted aircraft stability properties. Margins with low sensitivity are relatively trustworthy; margins with high sensitivity may be inaccurate in the presence of modeling errors.

Sensitivity of flutter margins with respect to aeroelastic dynamics is traditionally considered using statistical approaches. Elements of an analytical model are subjected to random perturbations with known statistical properties, and changes in stability margins are monitored. A state-space model is used to compute sensitivity to modal variations with a first-order approach.[12] A finite-element model is used to estimate sensitivity to higher-order perturbations.[16] These methods are based on Monte Carlo simulations that can be extremely time-consuming and provide no guarantees of sensitivity to perturbations not explicitly used in the simulation.

The μ method can be directly applied to compute a measure of the sensitivity of the stability properties to variations in the analytical model. The conservatism introduced by the worst-case stability margin is exactly a measure of the sensitivity to variations on the order of the uncertainty operators. Similarity between nominal and robust margins indicates low sensitivity with respect to perturbations included in $\mathbf{\Delta}$.

Definite advantages exist to computing sensitivity with μ instead of statistical approaches. The exceedingly high number of perturbations needed for Monte Carlo simulations of complex systems is replaced by a single calculation because operator theory ensures μ considers all perturbations $\Delta \in \mathbf{\Delta}$. Also, the sensitivity is guaranteed to be worst-case with respect to these perturbations.

9.2 On-Line Stability Tracking

Flight flutter testing incurs dramatic time and costs for safely expanding the flight envelope to ensure no aeroelastic instabilities are encountered. Traditional flight test methods for determining flutter margins that track estimates of modal damping obtained from flight data are inefficient and dangerous.[2] Multiple data sets must be taken at each test point to ensure sufficient excitation of critical modal dynamics. Also, the envelope must be expanded in small increments because damping only indicates stability at the current test point and cannot be reliably extrapolated to consider other flight conditions. Several proposed on-line methods use modal filtering, parameter identification, and envelope analysis to increase confidence in the flutter boundary.[66] These methods, like damping tracking, compute stability indicators rather than predictors.

The μ method is extended to compute stability estimates on-line during a flight test. The procedure uses flight data from the current test point to update the uncertainty description and compute a new flutter

margin.[67] Local and global approaches are formulated to reflect different degrees of confidence in the model and flight data.

The concept of a flutterometer is introduced as a flight test tool to indicate the proximity of a flutter condition.[38] The on-line application of μ is a suitable algorithm for such a tool because μ is a stability predictor and not merely a stability indicator. The flutterometer is anticipated to greatly improve the efficiency of flight flutter programs. The time and cost can be reduced because the analysis time at each test point is reduced, and because the predictive nature of μ allows greater distance in flight conditions between test points because the flutter boundary is indicated. Also, flight test safety is increased because the worst-case nature of μ introduces conservatism to the predicted flutter boundary.

9.3 Robust Aeroservoelastic Stability Analysis

Aeroservoelastic dynamics couple structural dynamics, control dynamics, sensing, aerodynamics, and actuation.[68] Stability analysis must account for the flutter dynamics and any unstable interactions caused by the control system. More uncertainties inherently exist in an aeroservoelastic model because of poor actuator modeling, nonlinear effectiveness of control surfaces, and noisy feedback measurements. Incorrect margins of aeroservoelastic stability may result from analysis that does not account for these model uncertainties.[69]

Several traditional approaches are used to analyze aeroservoelastic stability. Gain and phase margins can be computed for single-input and single-output transfer functions.[21] This approach does not characterize robustness and does not easily extend to multiple-input and multiple-output systems. An approach using singular values associated with loop-sensitivity functions has also been developed.[41] This method considers robustness but does not provide necessary and sufficient conditions for robust stability.

The μ method can be immediately used to compute aeroservoelastic stability margins.[36] The closed-loop system, including the controller and all uncertainty operators, is formulated in the LFT framework, and μ computes a worst-case stability margin. This framework allows flutter and aeroservoelastic stability margins to be easily computed from the same model.

9.4 Nonlinear Limit-Cycle Oscillation Analysis

The flutter phenomenon analyzed in this paper is a destructive instability associated with linear operators. Another phenomenon known as a limit-cycle oscillation is a potentially destructive instability associated with nonlinear systems. The nonlinearities can arise from structural dynamics, such as nonlinear stiffness functions and freeplay, and from the aerodynamics caused by flow separation and shock movement.[70, 71]

The μ method as described in this paper is not immediately well-suited to analyze highly nonlinear systems. Linear operators can be used to bound uncertainty for small amounts of nonlinearity, but this formulation will be overly conservative when the nonlinearities are significant. The μ method will not even detect or characterize many limit-cycle oscillations because these phenomena, which can be destructive to the aircraft, are actually stable in the sense of Lyapunov.

An approach to extend the μ method to include nonlinear limit-cycle dynamics has been developed. The nominal model for this approach is the linear model that represents the best approximation to the aircraft dynamics. The flight data are used to generate a nonlinear operator to associate with the linear

operator through feedback that allows the closed-loop system to model the observed nonlinear behavior of the aircraft. Uncertainty descriptions are also generated for the linear and nonlinear operators, and robust stability theory is used to compute a worst-case stability margin.

Two approaches are investigated to analyze a nonlinear aeroelastic system.[72, 73] The first approach uses multiresolution wavelets to identify nonlinear behavior in the flight data.[74] These wavelets present time and frequency information that allow a more accurate representation of the observed dynamics.[75] Another approach is based on nonlinear system identification in the LFT framework.[76] This approach will simultaneously generate a nonlinear operator and an uncertainty description for use with robust stability analysis.

CHAPTER 10
CONCLUSION

A structured singular value (μ) analysis method of computing flutter margins has been introduced. This method analyzes robust stability of a linear aeroelastic model with uncertainty operators. Flight data can be used to formulate the uncertainty operators to accurately account for errors in the model and the observed range of aircraft dynamics caused by time-varying aircraft parameters, nonlinearities, and flight anomalies such as test nonrepeatibility. The μ-based approach computes flutter margins that are robust or worst-case, with respect to the modeling uncertainty.

Nominal and robust flutter margins have been computed for the F/A-18 Systems Research Aircraft (SRA) using μ and p-k methods. The similarity of the nominal flutter margins demonstrates the μ method is a valid tool for computing flutter instability points and is computationally advantageous. Robust flutter margins have been generated with respect to an uncertainty set generated by analysis of extensive flight data. These margins are accepted with a great deal more confidence than previous estimates because these margins directly account for modeling uncertainty in the analysis process. The robust flutter margins indicate the desired F/A-18 SRA flight envelope should be safe from aeroelastic flutter instabilities; however, the flutter margins may lie noticeably closer to the flight envelope than previously estimated.

This method introduces μ as a flutter margin parameter that presents several advantages over tracking damping trends as a measure of a tendency to instability from available flight data. The μ extends to provide information about model sensitivity and is equally suitable for aeroelastic and aeroservoelastic analysis. The predictive nature of μ makes it particularly attractive for flight test programs because a robust stability margin can be computed using data from a stable test point.

Dryden Flight Research Center
National Aeronautics and Space Administration
Edwards, California, October 20, 1997

APPENDIX A
UPPER BOUND FOR THE STRUCTURED SINGULAR VALUE

The structured singular value, μ, is a difficult quantity to compute and appears to be a nonpolynomial-hard (NP-hard) problem.[77] Upper and lower bounds have been derived that can easily be computed. The lower bound can be solved by a power iteration that extracts the smallest destabilizing perturbation.[20] The upper bound can be posed as an optimization problem to present a conservative bound on the worst-case stability properties of the system. This paper is primarily concerned with computing a worst-case stability analysis, so this appendix concentrates on the optimization formulation to compute a μ upper bound.

Question A.0.1: *What is an upper bound for* μ *with respect to a general structured uncertainty description that can be computed?*

A simple upper bound for μ is immediately obvious from definition 3.3.1.

$$\mu(P) \leq \bar{\sigma}(P) \tag{A1}$$

This upper bound is essentially the robustness as measured by the small gain theorem and can be highly conservative when the uncertainty operator is structured. The conservatism in this upper bound can be reduced by considering two properties of singular values.

Property A.0.2: *The maximum singular value has a multiplicative property.*

$$\bar{\sigma}(P)\bar{\sigma}(P^{-1}) = 1 \tag{A2}$$

Property A.0.3: *The maximum singular value has a triangle-inequality property.*

$$\bar{\sigma}(DP) \leq \bar{\sigma}(D)\bar{\sigma}(P) \tag{A3}$$

These properties demonstrate the maximum singular value of a scaled matrix is less than or equal to that of an unscaled matrix.

Lemma A.0.4: *Given matrix* $P \in \mathbf{C}^{n \times n}$ *and invertible* $D \in \mathbf{C}^{n \times n}$, *then*

$$\bar{\sigma}(DPD^{-1}) \leq \bar{\sigma}(P) \tag{A4}$$

Recall the definition of the uncertainty structure given in section 3.2.

$$\mathbf{\Delta} = \left\{ \Delta = \mathrm{diag}\left(\delta_1^R I_{R_1}, \ldots, \delta_m^R I_{R_m}, \delta_1^C I_{C_1}, \ldots, \delta_n^C I_{C_n}, \Delta_1, \ldots, \Delta_p \right) : \delta_i^R \in \mathbf{R}, \delta_i^C \in \mathbf{C}, \Delta_i \in \mathbf{C}^{c_i \times c_i} \right\} \tag{A5}$$

A set of scaling matrices is defined with structure similar to the uncertainty structure. The set $\mathcal{D}$ contains blocks to scale with every complex and real uncertainty block.[20]

$$\mathcal{D} = \left\{ D = \text{diag}\left(D_1^R, \ldots, D_m^R, D_1^C, \ldots, D_n^C, d_1^c I_{c_1}, \ldots, d_p^c I_{c_p} \right) : D_i^R \in \mathbf{C}^{R_i \times R_i}, D_i^C \in \mathbf{C}^{c_i \times c_i}, d_i \in \mathbf{C}, D = D^* > 0 \right\} \tag{A6}$$

The set of scalings $\mathcal{G}$ affect only the real parametric uncertainty blocks.[78]

$$\mathcal{G} = \left\{ G = \text{diag}\,(G_1, \ldots, G_m, 0, \ldots, 0) : G_i \in \mathbf{C}^{R_i \times R_i}, G = G^* \right\} \tag{A7}$$

Several advantageous properties of these scalings exist.

Property A.0.5: *Symmetric factors and inverses of scalings are valid scalings.*

$$D^{-1}, D^{-\frac{1}{2}}, D^{\frac{1}{2}} \in \mathcal{D} \text{ for every } D \in \mathcal{D} \tag{A8}$$

Property A.0.6: *Every scaling* $D \in \mathcal{D}$ *and* $G \in \mathcal{G}$ *commutes with every uncertainty* $\Delta \in \mathbf{\Delta}$.

$$\begin{aligned} D\Delta &= \Delta D \\ G\Delta &= \Delta G \end{aligned} \tag{A9}$$

The μ is shown to be invariant under transformations using the scaling matrices $\mathcal{D}$. [20] This invariance arises as a direct consequence of Properties A.0.5 and A.0.6, which demonstrate $\mathbf{\Delta} = \mathcal{D}\mathbf{\Delta}\mathcal{D}^{-1}$. Thus, computing μ with respect to $\mathbf{\Delta}$ is equivalent to computing μ with respect to $D\mathbf{\Delta}D^{-1}$ for all $D \in \mathcal{D}$. A new upper bound for μ is formulated using these scaling matrices.

$$\mu(P) \le \inf_{D \in \mathcal{D}} \bar{\sigma}(DPD^{-1}) \le \bar{\sigma}(P) \tag{A10}$$

This upper bound is less conservative than the unscaled upper bound because of the final inequality that is a consequence of lemma A.0.4. This upper bound uses a search over all valid scaling matrices to find the optimal scaling matrix that reduces the conservatism in the robustness computation. This upper bound can be formulated as a maximum eigenvalue condition as demonstrated in lemma A.0.7.

Lemma A.0.7: *The constant matrix* P *is robustly stable and* $\mu(P) < 1$ *with respect to the set* $\mathbf{\Delta}$ *if*

$$\inf_{D \in \mathcal{D}} \left\| D^{\frac{1}{2}} P D^{-\frac{1}{2}} \right\|_\infty < 1 \tag{A11}$$

or equivalently

$$\inf_{D \in \mathcal{D}} \bar{\lambda}(P^* DP - D) < 0 \tag{A12}$$

This upper bound allows scalar uncertainty parameters to lie within a norm-bounded disk centered in the complex plane that can be conservative if these parameters are real. The conservatism can be reduced

by introducing the second set of scaling matrices, $\mathcal{G}$, that affect only the real parametric uncertainty blocks. These scalings restrict the uncertainty set to lie within a norm-bounded disk covering the real axis between 1 and –1, but that disk is allowed to be centered off the origin. A new upper bound is formulated with both $\mathcal{D}$ and $\mathcal{G}$ scalings.[78, 79]

$$\mu(P) \le \sqrt{max(0, \alpha_*)}$$

$$\alpha_* = \inf_{\substack{D\in\mathcal{D} \\ G\in\mathcal{G}}} \min_{\alpha\in\mathbf{R}} \{\alpha : P^*DP + j(GP - P^*G) - \alpha D \le 0\} \tag{A13}$$

This upper bound is presented as an optimization in lemma A.0.8.

Lemma A.0.8: *The constant matrix* P *is robustly stable, and* $\mu(P) < 1$ *with respect to the set* $\mathbf{\Delta}$*, if*

$$\inf_{\substack{D\in\mathcal{D} \\ G\in\mathcal{G}}} \{\alpha : \bar{\lambda}(P^*DP + j(GP - P^*G) - \alpha D) \le 0\} < 1 \tag{A14}$$

The $\mathcal{G}$ matrices are zero if no real parameter uncertainty blocks exist in the system, so the condition in lemma A.0.8 reverts to the condition in lemma A.0.7. When the $\mathcal{G}$ matrices are nonzero, the additional terms in the new upper-bound condition arise by using an additional constraint on the signals in the system.[78] Consider a signal in the closed-loop system relating an uncertainty signal. The system equation takes on the following form if the system is well-posed, ignoring the extraneous error and disturbance signals.

$$\Delta P x = x \tag{A15}$$

Allow the uncertainty to be a single repeated real parameter, $\Delta = \delta I$ with $\delta \in \mathbf{R}$, and take the complex conjugate transpose of the entire equation.

$$\delta x^* P^* = x^* \tag{A16}$$

Combining this formula with a scaling $G \in \mathcal{G}$ leads to the following.

$$x^*GPx = \delta x^*P^*GPx = x^*P^*G(\delta Px) = x^*P^*Gx \tag{A17}$$

The following matrix is derived from the right and left sides of this equation.

$$x^*(GP - P^*G)x = 0 \tag{A18}$$

Consider the matrix term of the complex uncertainty robustness upper bound scaled by x.

$$x^*(P^*DP - \alpha D)x < 0 \tag{A19}$$

Combining the two equations leads to the new upper-bound condition.

$$x^*(P^*DP + j(GP - P^*G) - \alpha D)x < 0 \tag{A20}$$

This μ upper bound is directly related to robust stability analysis resulting from the small gain theorem.[78] The $\mathcal{D}$ scaling matrices use structure in the uncertainty; the $\mathcal{G}$ matrices use additional phase information provided by real, parametric, uncertainty blocks.[79] This robustness condition is also related to a stability criterion used in absolute stability theory where the scaling matrices enter as Popov multipliers.[80]

The μ upper-bound conditions in lemma A.0.7 and lemma A.0.8 compute the robustness of a constant matrix to simplify the equations without carrying ω terms throughout the derivations. In practice, the robustness must be computed for physical systems described by linear, time-invariant transfer functions, $G \in \mathcal{RH}_\infty$, which are complex-valued matrix functions of frequency. The upper-bound conditions are computed for these transfer functions by including an additional search over frequency to find the worst-case upper bound.

Lemma A.0.9: *The transfer-function matrix* $P(j\omega) \in \mathcal{RH}_\infty$ *is robustly stable and* $\mu(P) < 1$ *with respect to the* set $\mathbf{\Delta}$ *if*

$$\max_{\omega} \inf_{\substack{D \in \mathcal{D} \\ G \in \mathcal{G}}} \{\alpha : \bar{\lambda}(P(j\omega)^* D P(j\omega) + j(G P(j\omega) - P^*(j\omega) G) - \alpha D) \le 0\} < 1 \tag{A21}$$

Established software packages compute the μ upper bound by finding optimal scaling matrices at distinct frequency points.[15] Frequency-varying scalings commute with linear time-invariant (LTI) uncertainty that may not accurately capture the nature of the modeling errors. Restricting the scaling matrices to be constant with no frequency variation allows consideration of uncertainty operators with linear time-varying (LTV) behavior. The μ upper bound for complex uncertainty is a necessary and sufficient condition for robust stability of an LTI plant with complex LTV uncertainty for any block structure.[81] Computing robustness measures for LTI systems with complex LTV uncertainty has been addressed for finite-energy signals[82] and for finite-gain signals.[83] Related papers have studies of robustness conditions for systems with some type of rate bounds on the LTV uncertainty.[84]

In general, a system will require both LTI and LTV uncertainties blocks to accurately describe the modeling errors. Parametric uncertainties are associated with physical elements of the system that are necessarily real and often time-varying. Dynamic uncertainties are used to introduce magnitude and phase variations in uncertain signals and should be considered time-invariant. Introduce two sets of structured uncertainty operators.

$$\mathbf{\Delta}_{TV}(t)\left\{\Delta(t) = \operatorname{diag}\left(\delta_1^R I_{R_1}, \ldots, \delta_m^R I_{R_m}, \delta_1^C I_{C_1}, \ldots, \delta_n^C I_{C_n}, \Delta_1, \ldots, \Delta_p\right) : \delta_i^R(t) \in \mathbf{R},\ \delta_i^C(t) \in \mathbf{C},\ \Delta_i(t) \in \mathbf{C}^{c_i \times c_i}\right\} \tag{A22}$$

$$\mathbf{\Delta}_{TI}(\omega)\left\{\Delta(\omega) = \operatorname{diag}\left(\delta_1^R I_{R_1}, \ldots, \delta_m^R I_{R_m}, \delta_1^C I_{C_1}, \ldots, \delta_n^C I_{C_n}, \Delta_1, \ldots, \Delta_p\right) : \delta_i^R(\omega) \in \mathbf{R},\ \delta_i^C(\omega) \in \mathbf{C},\ \Delta_i(\omega) \in \mathbf{C}^{c_i \times c_i}\right\} \tag{A23}$$

The set $\mathbf{\Delta}_{TV}$ contains all LTV uncertainty operators that are allowed to change infinitely fast as a function of time. Other researchers have investigated limits on the rate variation of complex time-varying

parameters that are not addressed in this paper.[84] Correspondingly, the set $\mathbf{\Delta}_{TI}$ contains all LTI uncertainty operators that are allowed to vary with frequency. These sets are allowed to enter the problem as shown in figure A.1.

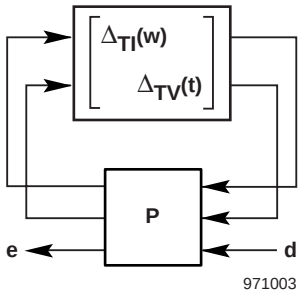

Figure A.1. Block diagram with LTI and LTV uncertainty.

Associated with these uncertainty descriptions are scaling matrices. Constant scaling matrices, $\mathcal{D}_{TV}$, are structured like $\mathcal{D}$ to associate with the time-varying uncertainty, $\mathbf{\Delta}_{TV}$. Frequency-dependent scalings, $\mathcal{D}_{TI}(\omega)$, are associated with the time-invariant uncertainty, $\mathbf{\Delta}_{TI}$. The block structure of each of these sets matches the block structure of the corresponding uncertainty set.

The uncertainty and scaling matrix sets can be combined into single sets for ease of notation.

$$\begin{aligned} \bar{\mathbf{\Delta}} &= \mathrm{diag}\{\Delta_{TI}(\omega), \Delta_{TV}(t)\} \\ \bar{\mathcal{D}} &= \mathrm{diag}\{D_{TI}(\omega), D_{TV}\} \\ \bar{\mathcal{G}} &= \mathrm{diag}\{G_{TI}(\omega), G_{TV}\} \end{aligned} \tag{A24}$$

Lemma A.0.10 describes the robustness upper-bound condition.

Lemma A.0.10: *Given some* $\alpha > 0$ *and norm-bounded uncertainty* $\bar{\mathbf{\Delta}}$ *such that*

$$\max_{\omega} \bar{\sigma}(\Delta_{TI}(\omega)) \le \frac{1}{\alpha} \qquad \max_{t} \bar{\sigma}(\Delta_{TV}(t)) \le \frac{1}{\alpha} \tag{A25}$$

then the system described by transfer function $P(j\omega)$ *is robustly stable with respect to* $\bar{\mathbf{\Delta}}$ *if scaling matrices* $D \in \bar{\mathcal{D}}$ *and* $G \in \bar{\mathcal{G}}$ *exist such that*:

$$\max_{\omega} \bar{\lambda}(P(j\omega)^{*}D(\omega)P(j\omega) + j(G(j\omega)P(j\omega) - P(j\omega)^{*}G(\omega)) - \alpha^{2}D(\omega)) < 0 \tag{A26}$$

The search for optimal scaling matrices that achieve the lowest robustness value possible can be formulated as an optimization to minimize α subject to a constraint function associated with an eigenvalue condition. An additional constraint arises from restricting the $\mathcal{D}$ scaling matrices to be positive definite.

$$\min_{\omega} \alpha$$

$$\textit{subject to} \qquad -M^{*}DM - j\,(GM - M^{*}G) + \alpha^{2}D > 0 \qquad (A27)$$

$$D > 0$$

This upper-bound condition is written in this format to ease understanding of the function and develop solution algorithms. Specifically, the minimization problem as shown above with the eigenvalue constraints is a linear matrix inequality (LMI). The LMI is a convenient framework to use because common properties global to all LMI problems exist.[85] The main property states an LMI is a convex function of the variables that allows solutions to be computed using standard convex optimization algorithms. The ellipsoid method and the interior point algorithm of the method of centers are shown to be efficient for LMI solutions.[86–88]

This optimization involves a search over frequency. Only a finite set of frequency points are used in practice, and engineering judgment must be used in choosing the set of frequency points. Testing the robustness condition at more frequency points will increase the accuracy of the upper bound, but the number of free parameters will rise accordingly and increase computational time.[89]

APPENDIX B
NOMINAL AEROELASTIC MODELS IN THE STRUCTURED SINGULAR VALUE FRAMEWORK WITH KNOWN AERODYNAMIC STIFFNESS AND DAMPING

This paper presents an aeroelastic model formulated by approximating the unsteady aerodynamics as a state-space system. The unsteady aerodynamic forces are treated as an unknown system with no specialized structure. This appendix considers formulating a state-space system to the unsteady aerodynamics with a specified structure. The resulting aeroelastic model is parameterized around dynamic pressure, and the structured elements of the aerodynamic forces appear in the model.

The general formulation shown in section 4.1 approximates the unsteady aerodynamic forces as a state-space system. This unstructured formulation does not explicitly include additional information regarding the aerodynamics that can be obtained from sources other than the computational model. In particular, the steady aerodynamics and first-order derivatives are often measured from wind-tunnel testing. Two matrix terms are introduced to the unsteady aerodynamic formulation to include this information.

$$Q(s) = A_0 + sA_1 + \begin{bmatrix} A_Q & B_Q \\ C_Q & D_Q \end{bmatrix} = A_0 + sA_1 + D_Q + C_Q(sI - A_Q)^{-1}B_Q \tag{B1}$$

This system is quite similar to Karpel's form.[29] The main difference is the absence of an additional s^2A_2 term. This term is typically not available from experimental data and is not explicitly represented in this formulation.

The state-space elements, $\{A_Q, B_Q, C_Q, D_Q\}$, are computed using standard system identification algorithms. The known matrix elements are subtracted from the unsteady aerodynamic force data, and the resulting system, $Q_{ss}(s)$, is approximated by the state-space elements.

$$Q_{ss}(s) = Q(s) - A_0 - sA_1 = \begin{bmatrix} A_Q & B_Q \\ C_Q & D_Q \end{bmatrix} \tag{B2}$$

Given the number of generalized states, n, such that $A_0, A_1 \in \mathbf{R}^{n \times n}$ and the number of aerodynamic states, n_Q, define $A_Q \in \mathbf{R}^{n_Q \times n_Q}$, $B_Q \in \mathbf{R}^{n_Q \times n}$, $C_Q \in \mathbf{R}^{n \times n_Q}$, and $D_Q \in \mathbf{R}^{n \times n}$ as the elements of the state-space system approximating $Q_{ss}(s)$.

The aeroelastic model is extended to include the additional A_0 and A_1 terms. Consider the signal, y, generated by an input to the state-space portion of force matrix. Define the signal, $x \in \mathbf{R}^{n_Q}$, as the vector of aerodynamic states.

$$y = Q_{ss}(s)\eta \quad \Leftrightarrow \begin{bmatrix} \dot{x} \\ y \end{bmatrix} = \begin{bmatrix} A_Q & B_Q \\ C_Q & D_Q \end{bmatrix} \begin{bmatrix} x \\ \eta \end{bmatrix} \tag{B3}$$

Formulate the aeroelastic differential equation using x.

$$
\begin{aligned}
0 &= M\ddot{\eta} + C\dot{\eta} + K\eta + \bar{q}Q(s)\eta \\
&= M\ddot{\eta} + C\dot{\eta} + K\eta + \bar{q}(A_0 + sA_1 + D_Q + C_Q(sI - A_Q)^{-1}B_Q)\eta \\
&= M\ddot{\eta} + (C + \bar{q}A_1)\dot{\eta} + (K + \bar{q}A_0)\eta + \bar{q}Q_{ss}(s)\eta \\
&= M\ddot{\eta} + (C + \bar{q}A_1)\dot{\eta} + (K + \bar{q}A_0)\eta + \bar{q}y \\
&= M\ddot{\eta} + (C + \bar{q}A_1)\dot{\eta} + (K + \bar{q}A_0)\eta + \bar{q}(C_Q x + D_Q \eta) \\
&= M\ddot{\eta} + (C + \bar{q}A_1)\dot{\eta} + (K + \bar{q}A_0 + \bar{q}D_Q)\eta + \bar{q}C_Q x
\end{aligned}
\tag{B4}
$$

A state-space system is formulated using the generalized states, η and $\dot{\eta}$, and the unsteady aerodynamic states, x. The state-update matrix is determined by the following three differential equations.

$$
\begin{bmatrix} \dot{\eta} \\ \ddot{\eta} \\ \dot{x} \end{bmatrix} = \begin{bmatrix} 0 & I & 0 \\ -M^{-1}(K + \bar{q}A_0 + \bar{q}D_Q) & -M^{-1}(C + \bar{q}A_1) & -\bar{q}M^{-1}C_Q \\ B_Q & 0 & A_Q \end{bmatrix} \begin{bmatrix} \eta \\ \dot{\eta} \\ x \end{bmatrix} \tag{B5}
$$

This state-space aeroelastic can be parameterized around dynamic pressure. Consider an additive perturbation to dynamic pressure, $\delta_{\bar{q}} \in \mathbf{R}$.

$$
\bar{q} = \bar{q}_o + \delta_{\bar{q}} \tag{B6}
$$

Separate terms in the system dynamics that involve $\delta_{\bar{q}}$.

$$
\begin{aligned}
0 &= M\ddot{\eta} + (C + \bar{q}A_1)\dot{\eta} + (K + \bar{q}A_0 + \bar{q}D_Q)\eta + \bar{q}C_Q x \\
&= M\ddot{\eta} + [(C + \bar{q}_o A_1)\dot{\eta} + (K + \bar{q}_o A_0 + \bar{q}D_Q)\eta + \bar{q}_o C_Q x] \\
&\qquad + \delta_{\bar{q}}[A_1\dot{\eta} + A_0\eta + D_Q\eta + C_Q x] \\
&= \ddot{\eta} + [M^{-1}(C + \bar{q}_o A_1)\dot{\eta} + M^{-1}(K + \bar{q}_o A_0 + \bar{q}_o D_Q)\eta + \bar{q}_o M^{-1}C_Q x] \\
&\qquad + \delta_{\bar{q}}[M^{-1}A_1\dot{\eta} + M^{-1}A_0\eta + M^{-1}D_Q\eta + M^{-1}C_Q x] \\
&= \ddot{\eta} + [M^{-1}(C + \bar{q}_o A_1)\dot{\eta} + M^{-1}(K + \bar{q}_o A_0 + \bar{q}_o D_Q)\eta + \bar{q}_o M^{-1}C_Q x] + \delta_{\bar{q}} z \\
&= \ddot{\eta} + [M^{-1}(C + \bar{q}_o A_1)\dot{\eta} + M^{-1}(K + \bar{q}_o A_0 + \bar{q}_o D_Q)\eta + \bar{q}_o M^{-1}C_Q x] + w
\end{aligned}
\tag{B7}
$$

The signals z and w are introduced into this formulation to associate the perturbation in dynamic pressure to the nominal dynamics in a feedback manner. The signal z can be generated as an output of the plant because it is a linear combination of states.

$$
z = M^{-1}A_1\dot{\eta} + M^{-1}A_0\eta + M^{-1}D_Q\eta + M^{-1}C_Q x \tag{B8}
$$

The signal w is related to z by the dynamic pressure perturbation.

$$w = \delta_{\bar{q}}\, z \tag{B9}$$

The state-space aeroelastic model for nominal stability analysis in the μ framework is formulated using the state-update matrix. The matrix is determined by the dynamics at the nominal dynamic pressure and the additional input and output signals used to introduce perturbations to the dynamic pressure. That perturbation, $\delta_{\bar{q}}$, is not an explicit parameter in the state-space model because the perturbation only affects the plant through a feedback relationship as determined by the signals z and w. Define the transfer function P(s) generated by state-space matrices such that z = P(s)w.

$$\left[\begin{array}{c} \dot{\eta} \\ \ddot{\eta} \\ \dot{x} \\ \hline z \end{array}\right] = \left[\begin{array}{ccc|c} 0 & I & 0 & 0 \\ -M^{-1}(K + \bar{q}_o A_0 + \bar{q}_o D_Q) & -M^{-1}(C + \bar{q}_o A_1) & -\bar{q}M^{-1}C_Q & -I \\ B_Q & 0 & A_Q & 0 \\ \hline M^{-1}(A_0 + D_Q) & M^{-1}A_1 & M^{-1}C_Q & 0 \end{array}\right] \left[\begin{array}{c} \eta \\ \dot{\eta} \\ x \\ \hline w \end{array}\right] \tag{B10}$$

Figure 4.1 shows the feedback interconnection between the perturbation in dynamic pressure and the nominal plant model parameterized around that perturbation. This interconnection is a linear fractional transformation, and the small gain condition of lemma 2.4.1 or the structured singular value condition of theorem 3.3.3 can be directly applied to analyze stability with respect to a variation in the flight condition $\bar{q}$. This system reduces to the parameterized model presented in section 4.2 if $A_0 = A_1 = 0$.

REFERENCES

[1]Bisplinghoff, Raymond L., Holt Ashley, and Robert L. Halfman, *Aeroelasticity*, Dover Publications, Inc., Mineola, NY, 1996.

[2]Kehoe, Michael W., "A Historical Overview of Flight Flutter Testing," *Advanced Aeroservoelastic Testing and Data Analysis*, AGARD-CP-566, Nov. 1995, pp. 1-1–1-15.

[3]Hassig, H. J., "An Approximate True Damping Solution of the Flutter Equation by Determinant Iteration," *AIAA Journal of Aircraft*, vol. 8, no. 11, Nov. 1971, pp. 885–889.

[4]Cooper, Jonathan E. and Thomas E. Noll, "Technical Evaluation Report on the 1995 Specialists' Meeting on Advanced Aeroservoelastic Testing and Data Analysis," *Advanced Aeroservoelastic Testing and Data Analysis*, AGARD-CP-566, Nov. 1995, pp. T-1–T-10.

[5]Gaukroger, D. R., C. W. Skingle, and K. H. Heron, "An Application of System Identification to Flutter Testing," *Journal of Sound and Vibration*, vol. 72, no. 2, Sept. 1980, pp. 141–150.

[6]Nissim, E. and Glenn B. Gilyard, *Method for Experimental Determination of Flutter Speed by Parameter Identification*, NASA TP-2923, 1989.

[7]Shelley, S. J., L. C. Freudinger, and R. J. Allemang, "Development of an On-Line Parameter Estimation System Using the Discrete Modal Filter," *Proceedings of the 10th International Modal Analysis Conference*, vol. 1, Feb. 1992, pp. 173–183.

[8]Shelley, Stuart J. and Charles R. Pickrel, "New Concepts for Flight Flutter Parameter Estimation," *Proceedings of the 15th International Modal Analysis Conference*, vol. 1, Feb. 1997, pp. 490–496.

[9]Bécus, G. A., "Automated Search for the Most Critical Flutter Configuration in Models with Uncertainty," *Mathematical and Computer Modelling*, vol. 14, 1990, pp. 977–982.

[10]Bécus, Georges A. and Corey Rekow, "Robust Control Theory Methods in Flutter Analysis," *International Forum on Aeroelasticity and Structural Dynamics 1991*, DGLR–Bericht 91-06, June 1991, pp. 464–468.

[11]Bécus, Georges A., "Stability Robustness of Aeroelastic Systems: A Perturbation Approach," *International Forum on Aeroelasticity and Structural Dynamics*, vol. 1, June 1997, pp. 425–432.

[12]Poirion, F., "Impact of Random Uncertainties on Aircraft Aeroelastic Stability," unpublished paper presented at the Conference on Stochastic Structural Dynamics, San Juan, Puerto Rico, Jan. 1995.

[13]Ray, Laura Ryan and Robert F. Stengel, "Application of Stochastic Robustness to Aircraft Control Systems," *AIAA Journal of Guidance, Control, and Dynamics*, vol. 14, no. 6, Nov.–Dec. 1991, pp. 1251–1259.

[14]Lind, R. and M. Brenner, "Robust Flutter Margins of an F/A-18 Aircraft from Aeroelastic Flight Data," *AIAA Journal of Guidance, Control, and Dynamics*, vol. 20, no. 3, May–June 1997, pp. 597–604.

[15]Balas, Gary J., et al, *μ-Analysis and Synthesis Toolbox*, Musyn Inc. and The MathWorks Inc., Minneapolis, MN and Natick, MA, 1995.

[16]Hutin, P. M., “State of the Art and Open Problems in Aeroelasticity,” unpublished paper presented at the annual meeting of the International Forum on Aeroelasticity and Structural Dynamics, Rome, Italy, June 1997.

[17]Maciejowski, J. M., *Multivariable Feedback Design*, Addison-Wesley Publishers Ltd, Wokingham, England, 1989.

[18]Green, Michael and David J. N. Limebeer, *Linear Robust Control*, Prentice-Hall, Inc., Englewood Cliffs, NJ, 1995.

[19]Doyle, John C., Bruce A. Francis, and Allen R. Tannenbaum, *Feedback Control Theory*, MacMillan Publishing Company, New York, NY, 1992.

[20]Packard, A. and J. Doyle, “The Complex Structured Singular Value,” *Automatica*, vol. 29, no. 1, 1993, pp. 71–109.

[21]Gupta, K. K., M. J. Brenner, and L. S. Voelker, *Development of an Integrated Aeroservoelastic Analysis Program and Correlation with Test Data*, NASA TP-3120, 1991.

[22]Gupta, K. K., *STARS—A General-Purpose Finite Element Computer Program for Analysis of Engineering Structures*, NASA RP-1129, 1984.

[23]Gupta, K. K., *STARS—An Integrated General-Purpose Finite Element Structural, Aeroelastic, and Aeroservoelastic Analysis Computer Program*, NASA TM-101709, 1991.

[24]Blair, Max, *A Compilation of the Mathematics Leading to the Doublet Lattice Method*, Air Force Wright Laboratory, WL-TR-92-3028, Mar. 1992.

[25]Giesing, J. P., *Subsonic Unsteady Aerodynamics for General Configurations, Part 1, Vol. 1: Direct Application of the Nonplanar Doublet-Lattice Method*, AFFDL-TR-71-5-PT-1-VOL-1, Nov. 1971.

[26]Appa, K., “Constant Pressure Panel Method for Supersonic Unsteady Airload Analysis,” *AIAA Journal of Aircraft*, vol. 24, no. 10, Oct. 1987, pp. 696–702.

[27]Roger, Kenneth L., “Airplane Math Modeling Methods for Active Control Design,” *Structural Aspects of Active Controls*, AGARD-CP-228, Aug. 1977, pp. 4-1–4-11.

[28]Karpel, M., “Design for Active Flutter Suppression and Gust Alleviation Using State-Space Aeroelastic Modeling,” *AIAA Journal of Aircraft*, vol. 19, no. 3, Mar. 1982, pp. 221–227.

[29]Morino, L., F. Mastroddi, R. De Troia, G. L. Ghiringhelli, and P. Mantegazza, “Matrix Fraction Approach for Finite-State Aerodynamic Modeling,” *AIAA Journal*, vol. 33, no. 4, Apr. 1995, pp. 703–711.

[30]Morino, L., F. Mastroddi, R. De Troia, and M. Pecora, “On Finite-State Aerodynamic Modeling With Applications to Aeroservoelasticity,” unpublished paper presented at the of Forum International Aeroelasticite et Dynamique de Structures, Association Aeronautique et Astronautique de France, 1993.

[31]Nissim, E., "Reduction of Aerodynamic Augmented States in Active Flutter Suppression Systems," *AIAA Journal of Aircraft*, vol. 28, no. 1, Jan. 1991, pp. 82–93.

[32]Gondoly, Karen Denise, *Application of Advanced Robustness Analysis to Experimental Flutter*, Masters of Science in Aeronautics and Astronautics Thesis, Massachusetts Institute of Technology, June 1995.

[33]Poirion, Fabrice, "Multi Mach State Space Modeling," *International Forum on Aeroelasticity and Structural Dynamics*, vol. 2, June 1997, pp. 307–311.

[34]Feron, Eric, "A More Reliable Robust Stability Indicator for Linear Systems Subject to Parametric Uncertainties," *IEEE Transactions on Automatic Control*, vol. 42, no. 9, Sept. 1997, pp. 1326–1330.

[35]Feron, Eric, "Robustness of Linear Systems Against Parametric Uncertainties: Towards Consistent Stability Indicators," *34th IEEE Conference on Decision and Control Proceedings*, vol. 3, Dec. 1995, pp. 1425–1430.

[36]Lind, Rick and Marty Brenner, "Analyzing Aeroservoelastic Stability Margins Using the μ Method," AIAA-98-1895, Apr. 1998.

[37]Zimmerman, Norman H. and Jason T. Weissenburger, "Prediction of Flutter Onset Speed Based on Flight Testing at Subcritical Speeds," *AIAA Journal of Aircraft*, vol. 1, no. 4, July–Aug. 1964, pp. 190–202.

[38]Lind, Rick C. and Martin J. Brenner, "A Worst-Case Approach for On-Line Flutter Prediction," *International Forum on Aeroelasticity and Structural Dynamics*, vol. 2, June 1997, pp. 79–86.

[39]Adams, Richard J., James M. Buffington, Andrew G. Sparks, and Siva S. Banda, *Robust Multivariable Flight Control*, Advances in Industrial Control Series, Springer-Verlag, London, 1994.

[40]Gelb, Arthur and Wallace E. Vander Velde, *Multiple-Input Describing Functions and Nonlinear System Design*, McGraw-Hill Book Company, New York, 1968.

[41]Brenner, Martin J., *Aeroservoelastic Modeling and Validation of a Thrust-Vectoring F/A-18 Aircraft*, NASA TP-3647, 1996.

[42]Thompson, J. M. T. and H. B. Steward, *Nonlinear Dynamics and Chaos*, John Wiley and Sons, Ltd., Great Britain, 1986.

[43]Wiggins, S., *Introduction to Applied Nonlinear Dynamical Systems and Chaos*, Springer-Verlag, New York, NY, 1990.

[44]Brenner, Martin J., Richard C. Lind, and David F. Voracek, "Overview of Recent Flight Flutter Testing Research at NASA Dryden," AIAA-97-1023, Apr. 1997.

[45]Brenner, Marty and Rick Lind, "Wavelet Filtering to Reduce Conservatism in Aeroservoelastic Robust Stability Margins," AIAA-98-1896, Apr. 1998.

[46]Freudinger, Lawrence C., Rick Lind, and Martin J. Brenner, "Correlation Filtering of Modal Dynamics Using the Laplace Wavelet," *Proceedings of the 16th International Modal Analysis Conference*, Feb. 1998, pp. 868–877.

[47]Ljung, Lennart and Lei Guo, "The Role of Model Validation for Assessing the Size of the Unmodeled Dynamics," *IEEE Transactions on Automatic Control*, vol. 42, no. 9, Sept. 1997, pp. 1230–1239.

[48]Chen, Jie, "Frequency-Domain Tests for Validation of Linear Fractional Uncertain Models," *IEEE Transactions on Automatic Control*, vol. 42, no. 6, June 1997, pp. 748–760.

[49]Smith, R. S. and J. C. Doyle, "Model Validation: A Connection Between Robust Control and Identification," *IEEE Transactions on Automatic Control*, vol. 37, no. 7, May 1992, pp. 942–952.

[50]Poolla, K., P. Khargonekar, A. Tikku, J. Krause, and K. Nagpal, "A Time-Domain Approach to Model Validation," *IEEE Transactions on Automatic Control*, vol. 39, no. 5, May 1994, pp. 951–959.

[51]Kumar, Arun and Gary J. Balas, "An Approach to Model Validation in the μ Framework," *Proceedings of the American Control Conference*, June 1994, pp. 3021–3026.

[52]Ljung, Lennart, *System Identification: Theory for the User*, Prentice-Hall, Inc., Englewood Cliffs, NJ, 1987.

[53]de Boer, A. and M. H. M. Ellenbroek, "A Study on Methods to Compare Measured and Calculated Modal Data," National Aerospace Laboratory NLR, The Netherlands, NLR-TP-93095-U, Mar. 12, 1993.

[54]He, J. and D. J. Ewins, "Compatibility of Measured and Predicted Vibration Modes in Model Improvement Studies," *AIAA Journal*, vol. 29, no. 5, May 1991, pp. 798–803.

[55]Lin, R. M. and M. K. Lim, "Analytical Model Updating and Model Reduction," *AIAA Journal*, vol. 34, no. 9, 1996, pp. 1966–1969.

[56]Berman, A. and E. J. Nagy, "Improvement of a Large Analytical Model Using Test Data," *AIAA Journal*, vol. 21, no. 8, Aug. 1983, pp. 1168–1173.

[57]Feron, Eric and James D. Paduano, *Advanced Techniques for Flutter Clearance*, Final Report for NASA Project DFRCU-95-025. (Contact NASA Center for Aerospace Information, Parkway Center, 7121 Standard Drive, Hanover, MD 21076-1320.)

[58]Zhang, Q., R. J. Allemang, and D. L. Brown, "Modal Filter: Concept and Applications," *Proceedings of the 8th International Modal Analysis Conference*, vol. 1., Jan. 1990, pp. 487–496.

[59]Sitz, Joel R., *The F-18 Systems Research Aircraft Facility*, NASA TM-4433, 1992.

[60]Vernon, Lura, *In-Flight Investigation of a Rotating Cylinder-Based Structural Excitation System for Flutter Testing*, NASA TM-4512, 1993.

[61]Lind, Rick C., Martin J. Brenner, and Lawrence C. Freudinger, "Improved Flight Test Procedures for Flutter Clearance," *International Forum on Aeroelasticity and Structural Dynamics*, vol. 3, June 1997, pp. 291–298.

[62]Nalbantoğlu, V., G. Balas, and P. Thompson, “The Role of Performance Criteria Selection in the Control of Flexible Structures,” AIAA-96-3841, July 1996.

[63]Lind, R., and M. Brenner, “Incorporating Flight Data into a Robust Aeroelastic Model,” *AIAA Journal of Aircraft*, vol. 35, no.2, Mar.–Apr. 1998.

[64]Balas, Gary J. and Peter M. Young, “Control Design for Variations in Structural Natural Frequencies,” *AIAA Journal of Guidance, Control, and Dynamics*, vol. 18, no. 2, Mar.–Apr. 1995, pp. 325–332.

[65]Lind, Rick and Marty Brenner, “Worst-Case Flutter Margins From F/A-18 Aircraft Aeroelastic Data,” AIAA-97-1266, Apr. 1997.

[66]Cooper, J. E., M. J. Desforges, P. R. Emmett, and J. R. Wright, “Advances in the Analysis of Flight Flutter Test Data,” *Advanced Aeroservoelastic Testing and Data Analysis*, AGARD-CP-566, Nov. 1995, pp. 13-1–13-12.

[67]Lind, R. and M. Brenner, “Utilizing Flight Data to Update Aeroelastic Stability Estimates,” AIAA-97-3714, Aug. 1997.

[68]Livne, Eli, “Integrated Aeroservoelastic Optimization: Status and Direction,” AIAA-97-1409, Apr. 1997.

[69]Roberts, Richard Peter, *Rational Function Approximations to Unsteady Aerodynamics*, Doctor of Philosophy in Aerospace Engineering Thesis, University of Bristol, Oct. 1996.

[70]Dowell, Earl H., “Nonlinear Aeroelasticity,” *AIAA Structures, Structural Dynamics, and Materials Conference*, AIAA-90-1031-CP, Apr. 1990, pp. 1497–1509.

[71]Dowell, Earl H. and Marat Ilgamov, *Studies in Nonlinear Aeroelasticity*, Springer-Verlag, New York, 1988.

[72]Ko, J., A. Kurdila, and T. Strganac, “Nonlinear Control Theory for a Class of Structural Nonlinearities in a Prototypical Wing Section,” AIAA-97-0580, Jan. 1997.

[73]O’Neil, T., H. Gilliat, and T. Strganac, “Investigations of Aeroelastic Response for a System with Continuous Structural Nonlinearities,” AIAA-96-1390, Apr. 1996.

[74]Benveniste, Albert, Ramine Nikoukhah, and Alan S. Willsky, “Multiscale System Theory,” *IEEE Transactions on Circuits and Systems—I: Fundamental Theory and Applications*,” vol. 41, no. 1, Jan. 1994, pp. 2–15.

[75]Lind, Rick, Kyle Snyder, and Marty Brenner, “Investigating Transient and Limit Cycle Behaviors of a Nonlinear Structure By Wavelet Transforms,” AIAA-98-1808, Apr. 1998.

[76]Wolodkin, Gregory Jon, *System Identification Methods for a Class of Structured Nonlinear Systems*, Doctor of Philosophy in Engineering, Electrical Engineering and Computer Sciences Dissertation, University of California at Berkeley, 1996.

[77]Braatz, R. P., P. M. Young, J. C. Doyle, and M. Morari, “Computational Complexity of μ Calculation,” *IEEE Transactions on Automatic Control*, vol. 39, no. 5, May 1994, pp. 1000–1002.

[78]Fan, M. K. H., A. L. Tits, and J. C. Doyle, "Robustness in the Presence of Mixed Parametric Uncertainty and Unmodeled Dynamics," *IEEE Transactions on Automatic Control*, vol. 36, no. 1, Jan. 1991, pp. 25–38.

[79]Young, Peter M., Matthew P. Newlin, and John C. Doyle, "μ Analysis with Real Parametric Uncertainty," *Proceedings of the 30th IEEE Conference on Decision and Control*, Dec. 1991, pp. 1251–1256.

[80]How, Jonathan P. and Steven R. Hall, "Connections Between the Popov Stability Criterion and Bounds for Real Parameter Uncertainty," *Proceedings of the American Control Conference*, June 1993, pp. 1084–1089.

[81]Shamma, J. S., "Robust Stability with Time-Varying Structured Uncertainty," *IEEE Transactions on Automatic Control*, vol. 39, no. 4, Apr. 1994, pp. 714–724.

[82]Apkarian, P., J. P. Chretien, P. Gahinet, and J. M. Biannic, "μ Synthesis by D–K Iterations with Constant Scaling," *Proceedings of the American Control Conference*, June 1993, pp. 3192–3196.

[83]Iwasaki, Tetsuya, "Robust Performance Analysis for Systems with Norm-Bounded Time-Varying Structured Uncertainty," *Proceedings of the American Control Conference*, Baltimore MD, June 1994, pp. 2343–2347.

[84]Rantzer, Anders, "Uncertainties with Bounded Rates of Variations," *Proceedings of the American Control Conference*, June 1993, pp. 29–30.

[85]Boyd, Stephen, Laurent El Ghaoui, Eric Feron, and Venkataramanan Balakrishnan, *Linear Matrix Inequalities in System and Control Theory*, Studies in Applied Mathematics, Society for Industrial and Applied Mathematics, Philadelphia, PA, 1994.

[86]Bland, Robert G., Donald Goldfarb, and Michael J. Todd, "The Ellipsoid Method: A Survey," Operations Research, vol. 28, no. 6, Nov.–Dec. 1981, pp. 1039–1091.

[87]Boyd, S. and L. El Ghaoui, "Method of Centers for Minimizing Generalized Eigenvalues," *Linear Algebra and Applications: Special Issue on Numerical Linear Methods in Control*, vol. 188, July 1993, pp. 63–111.

[88]Gahinet, Pascal, Arkadi Nemirovski, Alan J. Laub, and Mahmoud Chilali, *LMI Control Toolbox*, The MathWorks Inc., Natick, MA, 1995.

[89]Lind, Rick, Gary J. Balas, and Andy Packard, "Robustness Analysis With Linear Time-Invariant and Time-Varying Real Uncertainty," *AIAA Guidance, Navigation and Control Conference*, AIAA-95-3188-CP, Aug. 1995, pp. 132–140.

REPORT DOCUMENTATION PAGE

Form Approved
OMB No. 0704-0188

1. AGENCY USE ONLY (Leave blank)	2. REPORT DATE	3. REPORT TYPE AND DATES COVERED
	March 1998	Technical Paper

4. TITLE AND SUBTITLE

Robust Flutter Margin Analysis That Incorporates Flight Data

5. FUNDING NUMBERS

WU 529 31 14

6. AUTHOR(S)

Rick Lind and Martin J. Brenner

7. PERFORMING ORGANIZATION NAME(S) AND ADDRESS(ES)

NASA Dryden Flight Research Center
P.O. Box 273
Edwards, California 93523-0273

8. PERFORMING ORGANIZATION REPORT NUMBER

H-2209

9. SPONSORING/MONITORING AGENCY NAME(S) AND ADDRESS(ES)

National Aeronautics and Space Administration
Washington, DC 20546-0001

10. SPONSORING/MONITORING AGENCY REPORT NUMBER

NASA/TP-1998-206543

11. SUPPLEMENTARY NOTES

Rick Lind is a National Research Council research associate.

12a. DISTRIBUTION/AVAILABILITY STATEMENT

Unclassified—Unlimited
Subject Category 08

12b. DISTRIBUTION CODE

13. ABSTRACT (Maximum 200 words)

An approach for computing worst-case flutter margins has been formulated in a robust stability framework. Uncertainty operators are included with a linear model to describe modeling errors and flight variations. The structured singular value, μ, computes a stability margin that directly accounts for these uncertainties. This approach introduces a new method of computing flutter margins and an associated new parameter for describing these margins. The μ margins are robust margins that indicate worst-case stability estimates with respect to the defined uncertainty. Worst-case flutter margins are computed for the F/A-18 Systems Research Aircraft using uncertainty sets generated by flight data analysis. The robust margins demonstrate flight conditions for flutter may lie closer to the flight envelope than previously estimated by p-k analysis.

14. SUBJECT TERMS

Aeroelasticity, Flight data analysis, Flutter, Robust stability, Structural dynamics, Structured singular value

15. NUMBER OF PAGES

105

16. PRICE CODE

A06

17. SECURITY CLASSIFICATION OF REPORT	18. SECURITY CLASSIFICATION OF THIS PAGE	19. SECURITY CLASSIFICATION OF ABSTRACT	20. LIMITATION OF ABSTRACT
Unclassified	Unclassified	Unclassified	Unlimited

Available from the NASA Center for AeroSpace Information, 800 Elkridge Landing Road, Linthicum Heights, MD 21090; (301)621-0390